IntechOpen

Environmental Risks

Edited by Florin-Constantin Mihai and Adrian Grozavu

ENVIRONMENTAL RISKS

Edited by **Florin-Constantin Mihai**
and **Adrian Grozavu**

Environmental Risks
http://dx.doi.org/10.5772/intechopen.72155
Edited by Florin-Constantin Mihai and Adrian Grozavu

Contributors

Hans J. Scheel, Ssu-Yao Yang, Chyan-Deng Jan, Ji-Shang Wang, Matthew Thompson, Yu Wei, Zhiwei Liu, Michael Caggiano, Jabulani Gumbo, M.J. Mokgoebo, T.A. Kabanda, Florin-Constantin Mihai

Notice

Statements and opinions expressed in the chapters are these of the individual contributors and not necessarily those of the editors or publisher. No responsibility is accepted for the accuracy of information contained in the published chapters. The publisher assumes no responsibility for any damage or injury to persons or property arising out of the use of any materials, instructions, methods or ideas contained in the book.

First published in London, United Kingdom, 2018 by IntechOpen
IntechOpen is the global imprint of INTECHOPEN LIMITED, registered in England and Wales, registration number: 11086078, The Shard, 25th floor, 32 London Bridge Street
London, SE19SG – United Kingdom
Printed in Croatia

British Library Cataloguing-in-Publication Data
A catalogue record for this book is available from the British Library

Additional hard copies can be obtained from orders@intechopen.com

Environmental Risks, Edited by Florin-Constantin Mihai and Adrian Grozavu
p. cm.
Print ISBN 978-1-78984-223-4
Online ISBN 978-1-78984-224-1

Meet the editors

Florin-Constantin Mihai holds a PhD degree in Geography (2013) with maximum distinction from the Department of Geography, "Alexandru Ioan Cuza" University of Iasi (Romania), and BSc and MSc degrees in Environmental Science. He has published papers in local and international peer-reviewed journals, conference proceedings, and book chapters on various topics regarding environmental and waste management issues. His research aims to develop new methods and indicators to assess the key environmental issues across various geographical scales. His research interests include environmental geography, waste management, pollution, sanitation, sustainability, circular economy, public and environmental policies, spatial analysis, and rural and regional development. Previously edited books *E-waste in Transition: from Pollution to Resource* and *Solid Waste Management in Rural Areas* are available at https://www.intechopen.com/.

Adrian Grozavu is a full professor at the Department of Geography of the "Alexandru Ioan Cuza" University of Iasi (Romania). He teaches courses in the disciplines of natural and anthropogenic risks, physical geography, geomorphology, and cartography coordinating numerous graduation studies. He has published papers particularly in the fields of geomorphology, land use dynamics, natural and anthropogenic hazards, and risks to human communities. His research interests focus on the diagnostic analysis of hazards, but especially the exposure and vulnerability components of the risk equation, where such evaluations become essential in the research of any type of risk. Particular attention is paid to assessing the different dimensions of vulnerability (physical, environmental, economic, social) and the integration of new assessment methods and indicators.

Contents

Preface

Environmental risks are a multi- and interdisciplinary topic with a great interest in current society. This book examines issues of natural hazards (e.g., typhoons, landslides, wildfires), anthropogenic activities (construction of artificial dams, the operation of nuclear power plants), and their potential risks to the environment and/or quality of life at various scales, from local to regional and even at a global level.

The book contains five chapters from worldwide contributors, and discusses concepts related to environmental risks as evidenced by the literature in the field towards relevant case studies.

The first chapter (introductory chapter) performs a critical overview of risk concepts, research methodology, and local, regional, and global environmental threats for natural and socioeconomic systems.

The second chapter examines the impact of typhoon Morakot, which occurred in August 2009, on hillslope stability in Taiwan (catastrophic landslides, floods, changes in topographic and morphometric features), with significant repercussions on human settlements within the Cishan watershed, with a focus on the compound-disaster perspective and its domino effect.

The third chapter reveals the state of the art in wildfire suppression planning and illustrates the application of advanced planning tools on a fire-prone landscape in Colorado (USA) supported by relevant geospatial tools.

The fourth chapter assesses the impacts of five dams in Limpopo Province (South Africa) on downstream river ecosystems, using data from aerial photographs and orthophotos, supplemented by fieldwork.

The fifth chapter analyzes the nuclear accident of the Fukushima Daiichi reactors in 2011 (Japan) with significant impacts on the environment. The chapter performs a review of possible solutions concerning the radioactive cloud, soil and water contamination, rubble, and nuclear waste issues.

The book intends to discuss concepts, methods, and techniques to address environmental risks and vulnerabilities, revealing the complex interactions between nature and human communities and activities. Policies and practices for disaster risk management should be based on the best state-of-the-art methods and techniques, integration between natural and/or social approaches, interdisciplinary research, and multilevel cooperation.

Dr. Florin-Constantin Mihai and Prof. Dr. Adrian Grozavu
Faculty of Geography and Geology
"Alexandru Ioan Cuza" University
Iași, Romania

Chapter 1

Introductory Chapter: Environmental Risks between Conceptualization and Action

Adrian Grozavu and Florin-Constantin Mihai

Additional information is available at the end of the chapter

http://dx.doi.org/10.5772/intechopen.81072

1. Risk-related concepts

Changes in the contemporary world materialized in particular through population growth and mobility, urbanization, and economic expansion also result in an increased exposure of people and assets to extreme events and impose, implicitly, adequate management of induced risks.

The occurrence of natural and anthropogenic risk phenomena, known as hazards, puts a heavy tribute on disaster-sensitive human communities regardless of their level of development. The magnitude of the disasters and their increasing frequency and severity imply the need for their approach by the entire world community and for global action. It is, therefore, necessary to find answers to questions: Is the world really a more dangerous place? If so, what are the causes? Why is the dimension of disasters much higher in poor countries? What are the best ways to reduce the impact of hazards and disasters in the future?

In this context, knowledge of risks becomes a sine qua condition in carrying out impact studies, risk prevention plans, spatial planning plans, and, in general, a condition for effective management of natural resources or sustainable development projects. This explains a large number of specialized studies, the extent of research in the field, and the sustained efforts to achieve the transfer from theory to practice.

A multidisciplinary scientific field has emerged over the past decades, in which there is a specialized terminology that wants to be as precise as possible, eliminating the semantic ambiguities and the difficulties of communication between the theoreticians and practitioners. Within this multidisciplinary research field, the methodology, taken from different fundamental domains, gradually improved, new methods and models of integrated analysis

were imagined, and the possibilities of applying the research results were diversified. The necessity to develop conceptual models of risk, well-argued scientifically, derives from the complexity of the risk and the necessity of its holistic approach.

Frequently, the *risk* is defined as the product of the probability of a phenomenon occurrence and its negative consequences, thus associating two distinct elements: on the one hand, the hazard and, on the other hand, the sensitive element of destructive effects, which most of the times the man is considered. In other words, the risk arises from the spatial overlap of hazards and the elements at risk. Recently, United Nations General Assembly (2016) formulates the definition of risk as "the potential loss of life, injury, or destroyed or damaged assets which could occur to a system, society or a community in a specific period of time, determined probabilistically as a function of hazard, exposure, vulnerability and capacity" [1].

Regarding the concept of *hazard*, most often it is defined as a potential source of danger, being associated or identified with those natural or anthropogenic processes and phenomena that can cause material or human losses or impair the quality of the environment. The term brings together all those processes and phenomena with destructive potential and whose occurrence cannot be predicted with certainty. Hazards are associated with random processes and phenomena, at least in appearance, which can occur in a well-determined environment and whose mechanisms are known by the researcher but for which the moment and place of the next occurrence cannot be determined by simply knowing the prior states. They are characterized by a certain probability of occurrence and a certain intensity or magnitude, which refers to the impact force in time and space. The central idea of hazard is not the phenomenon itself but the likelihood of its occurrence; in other words, the hazard is a threat, not the event itself. It can manifest as a harmful event, and, when measured in terms of real damage, deaths, or injuries, it becomes a disastrous or catastrophic event.

The specific categorization is difficult and contentious, but it is generally considered that environmental hazards are "extreme geophysical events, biological processes and technological accidents that release concentrations of energy or materials into the environment on a sufficiently large scale to pose major threats to human life and economic assets" [2]. Natural events can be considered here (volcanic eruptions, tropical cyclones, drought, epidemic diseases, wildfires, etc.), but also major technological accidents (transport accidents, industrial explosions and fires, release of toxic or radioactive materials, public facilities structural collapse, storage, transport and improper use of hazardous materials) and the so-called context hazards that are driven by forces operating on mega-scales, hemispheric to planetary, and are able to produce environmental change (international air pollution that can lead to climate change and sea level rise, deforestation, desertification, loss of natural resources, land pressure, impact from near-earth objects, etc.).

Exposure is another component of risk that is considered, in simple terms, as the number of people and/or other elements at risk that may be affected by a particular event. The United Nations General Assembly (2016) defines exposure as "the situation of people, infrastructure,

housing, production capacities and other tangible human assets located in hazard-prone areas" [1]. Thus, exposure involves the overlapping of socioeconomic systems with hazard favorable factors, which is, in other words, a precondition for risk and disaster.

The main component of risk is *vulnerability*, a concept that has been progressively developed over the past decades, registering a great number of definitions and points of view. The United Nations General Assembly (2016) considers vulnerability as "the conditions determined by physical, social, economic and environmental factors or processes which increase the susceptibility of an individual, a community, assets or systems to the impacts of hazards" [1].

The peer-reviewed literature shows that the key element in defining and assessing vulnerability can differ from exposure, preparedness, and prevention, to coping ability, adaptive capacity, and recovery, and each approach identifies the essential peculiarities of human structures (from individual to societal) in their relation with different hazards [3].

Some authors provide conceptual comparative analysis of different vulnerability models putting in balance distinct conditions of vulnerability: multiple contexts, multiple dimensions, temporal variability, multiple scales, and scale interdependency [3–5].

2. Risks in the environment

The analysis of the risks that threaten today's human society highlights several characteristics: recrudescence, diversification, and organic link between risks and urban. The recrudescence of catastrophic events and the increase in their global costs can be attributed to global changes, especially climatic changes, and to the way in which man himself exhibits the risks through countless ways: the occupation of vulnerable zones and of exposed sites to hazards, increasing in urbanization and industrialization, pressure on resources, etc.

Risk diversification is also a feature of today's geographic systems, increasingly anthropized. Besides the risks already assumed by society, there are many others risks, either passive (which can be reactivated at any time) or unknown (technological or from the social sphere) risks.

The connection between the urban and the risks is also becoming increasingly obvious. By its basic feature, that of concentration of people and activities on narrow spaces, the city becomes a vulnerable place to any exogenous or endogenous disruptive agent. Urban risks have multiple causes and consequences. Urban fabrics in a continuous expansion, multiplication of uses, and close interdependence between the different systems and processess that ensure the functioning of urban settlements favor, in case of extreme events, the occurrence of chain effects (domino effects). It is possible that future disasters will occur on increasing scales, precisely not only of the concentration of the population in urban areas but also of the increasing complexity of human society.

In 2017, according to the EM-DAT database of the Center for Research on the Epidemiology of Disasters (CRED) in Louvain, 318 natural disasters occurred, affecting 122 countries (96

million people suffering in one way or another), causing the death of 9503 people and economic damages of US$314 billion [6]. If the number of deaths in the year 2017 was far below the average of the last 10 years, instead, in terms of costs, in the year 2017, it is ranked second, due to the impact of three hurricanes affecting the United States and the Caribbean: Harvey (US$95 billion), Irma (US$66 billion), and Maria (US$69 billion). The majority of losses were caused by weather-related disasters. Almost 90% of deaths were due to climatological, hydrological, or meteorological disasters; the floods were responsible for nearly 60% of affected people, while the storms (mainly hurricanes) have caused 85% of economic damages.

As far as the spatial distribution is concerned, the situation in 2017 reflects the trend of previous years when the Asian continent experienced the highest disaster occurrence (43% of the total). The most affected were China and India, followed by a number of Caribbean island states, affected by hurricanes, and Africa (in particular, Mauritania, where 88% of the population was affected by a drought). Overall, the high mortality and number of people affected correlated to the country's population, as well as economic losses correlated to GDP, highlighting the burden of disasters on small islands in 2017 [6].

Even the more localized and more reversible extreme events, like hurricanes, floods, droughts, technological accidents, etc., are of particular concern, mega-scale events capable of cutting across regional geographical units and existing socio-economic systems have to be considered. The most extreme adverse impacts could come from climate change (e.g., the worst 1 percent of scenarios) and may account for a large portion of expected losses [7]. In urban areas, this is projected to increase risks for economies and ecosystems, including risks from storms and extreme precipitation, inland and coastal flooding, landslides, etc. [8]. These risks are amplified for those lacking essential infrastructure and services or living in exposed areas.

It is considered that the mechanism through which climate change mega-catastrophe could arise is that of the climate's crossing a systemic threshold, referred to as abrupt climate change, developed in a few years or decades, due to atmospheric pollution, in particular to greenhouse gas (GHG) emissions. According to different scenarios, the global average temperature could increase by 2–4°C by the end of the twenty-first century [8]. Heating may be exacerbated by the faster melting of the snow cover and ice that reflects the heat but also the release of liquefied methane in the tundra or even from oceans.

One of the impacts of wide-scale climate change could be the global rise in sea level by collapse and melting of the Antarctic and Greenland ice sheets. The breakage, in July 2017, of a piece of a 2500-square-mile (about three billion tons) iceberg from the Larsen-C ice shelf, as well as numerous cracks and melting lakes, which continues to spread both in the west and east of Antarctica, may be signs of destabilizing the ice sheet, which could lead to an irreversible process of flowing and melting into the sea. Thus, given the continuing increase in population, infrastructure, and other facilities in coastal areas of the world, rising sea levels are becoming a serious threat.

Another category of risk scenarios involves weakening and other disturbances of ocean currents, assuming changes in precipitation and temperature models, severe disturbances of ocean ecosystems, and intensification of extreme phenomena, with severe effects on agriculture as

well as on other economic and social sectors. The unusually warm and dry weather in Western Europe in July 2018, with temperatures above 30°C and the numerous forest fires produced beyound the polar circle in the Scandinavian Peninsula or rains of extreme intensity in the Japanese archipelago that have generated the most severe flooding in the last 60 years, even if they are assigned to the oscillation of the jet streams system in the atmosphere, they also could confirm the scenario of ocean currents disturbance.

There is also the risk of changes in ecosystems, significant biodiversity loss due to climate variation, rainfall, and temperature changes. There is the prospect of very large ecosystem disruptions, of continuous and extensive vegetation, and also desertification or irreversible conversion of forests into pastures. IPCC (2014) specifies that "A large fraction of species faces increased extinction risk due to climate change during and beyond the twenty-first century, especially as climate change interacts with other stressors. Most plant species cannot naturally shift their geographical ranges sufficiently fast to keep up with current and high projected rates of climate change in most landscapes" [8].

Particular attention must be paid to the so-called cascading-event catastrophes, when a number of hazards can occur within a relatively short period of time, especially in the immediate vicinity, and can potentiate each other so as to result in a cascade of consequences of much greater severity (e.g., prolonged drought can result in a severe lack of food, which, in turn, can generate disputes breaking down the civil order, which can cause destabilization of the government and political disturbances, and which can further lead to large-scale migration for survival or even regional conflicts) and thus to overcome the resilience of certain socioeconomic systems.

As far as anthropic hazards are concerned, serious threats are improper industrial and agricultural activities and environmental pollution combined with poor environmental legislation enforcement. Poverty and rural migration toward urban areas concentrate the population in slum areas across developing and transition countries which frequently lack access to sanitation and proper hygiene conditions. The so-called informal settlements are predisposed to massive pollution, exposing their inhabitants to disease and infections.

Many cities and rural regions are facing the lack of sound public utilities such as improved drinking water and sanitation facilities, wastewater treatment or basic solid waste management services. At the global level, there are huge disparities between high-income countries and developing ones regarding the population access to such critical amenities broken down per urban and rural population [9].

The greatest short-term danger to humans from untreated excreta, wastewater, septage, and wastewater sludge is from pathogens, microorganisms that can cause severe diseases [10]. Diseases caused by pollution were responsible for an estimated 9 million premature deaths in 2015 approximately 16% of all deaths worldwide [11].

Furthermore, The Lancet Commission on Pollution and Health stipulates that "all forms of pollution combined were responsible for 21% of all deaths from cardiovascular disease, 26% of deaths due to ischemic heart disease, 23% of deaths due to stroke, 51% of deaths due to chronic obstructive pulmonary disease, and 43% of deaths due to lung cancer worldwide" [11].

An emerging environmental threat in the last decade is the plastic pollution, with a multilevel coverage from local water bodies (creeks, rivers, lakes) to the remote or deepest locations across the planet's oceans. River and marine ecosystems across the globe have been loaded with macro- and microplastics, and impact on wildlife is critically endangered.

Even rural communities may significantly contribute to river plastic pollution if there are no sound waste collection schemes. As an example, over 290 tons of plastic bottles were collected during 2005–2012 in the proximity of Izvoru Muntelui dam lake (Eastern Carpathians), most of them generated by the upstream villages [12].

Solid waste management is a critical sector of public health and environment; however, most of the transition and developing countries are facing real challenges concerning the collection efficiency and proper disposal of solid waste. It is also a major contributory factor to urban flooding across the globe with examples from Asia, Africa, and Latin America [13]. Poor waste management services lead to open dumping practices, blocked drainage and channels, and clogged rivers by waste which further favor the flood of surrounding communities. Floods and tropical storms favor the water stagnation within built-up areas among various debris which increases the epidemic outbreak risks.

Landfills are the main disposal option despite these sites are a source of complex pollution (air-soil-water nexus) if it is not updated to best available techniques. Conventional landfills or dumpsites pose serious risks for surroundings, particularly those sites who serve the mega-cities and larger cities across Africa, Asia, South and Central America, and South and Eastern Europe.

Landfills are an important source of anthropogenic methane contributing to GHG emissions being the main disposal option including for high-income countries. Due to methane accumulation, internal combustion may generate spontaneous, uncontrolled fires being dangerous for surrounding households and emitting toxic pollutants in the air. Landfills located in low-lying areas are also exposed to flash floods or those located in hilly regions to landslides or erosion. The collapse of landfills killed 130 people (including children) in Africa during 2017, the most devastating being the waste landslide of Koshe site in March (Addis Ababa, Ethiopia) with 115 deaths [14].

Frequently, informal settlements are located near large urban dumpsites where the people face numerous threats. Improper location of waste disposal sites increases the pollution and health risks for surrounding communities. Peripheral areas of cities are exposed to industrial pollution, poverty and poor connection to public utilities such as drinking water, sewage, sanitation, and waste management facilities. Rural areas are more vulnerable to the negative effects of industrial energy and agriculture systems which support urban areas [15].

In Africa, where drought and conflicts are dominant disasters, there is a migration of people toward neighboring regions and countries where refugee camps face improper sanitation and waste management facilities [14]. Similar poor housing conditions are encountered in other refugee camps of the Middle East (e.g., Syrian refugees in Lebanon, Jordan) or Europe. The conflict areas and refugee crisis is an emerging social and political crisis with repercussions on the environment. Refugee camps must have access to basic utilities and their environmental impact to be analyzed [16].

Closely with the limited waste management services and poor socioeconomic conditions is one of the widespread practices such as the open burning of household waste. It poses serious health risks because hazardous substances are released at a low burning temperature such as dioxins, polycyclic aromatic hydrocarbons (PAHs), or black carbon. These toxins are carcinogenic and powerful short-lived air pollutants, and the impact of open burning practices should be further investigated across transition and developing countries. Developed countries are facing the environmental issues associated with more expensive technologies such as municipal waste incineration plants or co-incineration facilities (e.g., cement industry).

Poorer households rely on solid fuels as a domestic energy source. Rudimentary household furnaces expose the inhabitants to dangerous indoor air pollution (carbon monoxide poising) or fire risk. Fossil fuel combustion in developed and transition countries and burning of biomass in developing countries account for 85% of airborne particulate pollution and for almost all pollution by oxides of sulfur and nitrogen [11].

Another widespread bad practice across the world is illegal dumping of waste, affecting water bodies, public lands, roadsides, forest, floodplains, and coastal areas. Improper disposal of hazardous wastes leads to severe public health issues at the regional level as shown in Southern Italy where 2000 toxic substance dumping sites were detected in Campania beside the illegal burning practices of wheels, plastics, textiles, and other industrial residuals [17]. In addition to risks caused by heavy metals, uncontrolled dumping of waste is a potential threat of pathogenic infections, chronic diseases, and the infestation of vermin [14].

Illegal traffic of e-waste and obsolete electronics from the EU and United States toward developing countries of Africa and Asia reveals the global interconnections of environmental crimes. In such destinations, the toxic wastes are frequently treated in rudimentary conditions using manual labor. Severe health issues are associated with exposure to e-waste recycling sites including vulnerable population such as pregnant women and children [18]. Notorious ewaste dumps such as Guiyu in China and Agbogbloshie in Ghana are worst-case scenarios where the environment is heavily polluted contaminating the soil, groundwater, rivers, crops, and livestock.

Other waste streams, such as medical wastes, animal waste, batteries and accumulators, used tires, obsolete vehicles, bulky items, construction and demolition waste, and sewage sludge need special attention for treatment and disposal in order to prevent the environmental contamination.

Obsolete pesticides and other agricultural chemicals are a serious environmental potential threat for most of the countries where agriculture still plays a key role in their economies. Chemical pollution is a severe global concern with a diverse range of contaminated sites by toxic chemicals, persistent organic pollutants, radionuclides, and heavy metals (e.g., mercury, lead, chromium, and cadmium) released into air, water, and soil by active and abandoned factories, smelters, mines, and hazardous waste sites [11].

Another critical environmental issue is found in sub-Saharan Africa and Asia, where 892 million people still practice open defecation [19]. In such regions, soil and water infestation with human excreta and solid waste is highly probably due to the lack of basic facilities. Furthermore, at the global level, rural households rely on outside toilets with a poor

connection to sewage systems or septic tanks. This fact leads to groundwater contamination with the critical impact on human health. Provision of safe drinking water facilities is challenging for rural population compared to urban areas as for sanitation sector. In 2015, 0.8 million deaths were estimated to be caused by unsafe sanitation and 1.3 million to unsafe water sources [11]. Almost 3 billion people lack sound waste collection services with a critical situation across rural areas of low- and middle-income countries [9].

In sub-Saharan Africa and parts of Asia and Central and South America, wastewater treatment systems, if they exist, are minimal or function poorly, while in eastern Europe, Turkey, the Russian Federation, Mexico, South America, and other areas, wastewater treatment has advanced, but wastewater sludge and biosolids management are emerging concerns, and complex regulatory structures are being developed [10]. The poor and the marginalized communities are most exposed to health pollution threats in every country of the globe. The Agenda 2030 aims to end open defecation and to provide universal access to basic utilities as part of sustainable development goals (SDGs).

Cross-border pollution issues via air, water bodies, or emerging transportation systems challenge the current international relations. Plastic pollution, oil spills, chemical pollution, industrial accidents, and other environmental threats raise several governance issues, and frequently, the local communities have few options to combat such events.

3. Addressing environmental risks

As previously mentioned, the possibilities of addressing the risk issue and of applying the research results have been continuously diversified. Different viewpoints or approaches can be framed either in a behavioral paradigm, a structural paradigm, or a complexity paradigm [2].

Behavioral paradigm is the hazard-based point of view that emphasizes the role of human adjustment to natural hazards through defensive technical measures, scientific acquirements, and emergency plans for disaster mitigation [3].

The structural paradigm is rather a cross-hazard and a disaster-based viewpoint that focuses on the characteristics of socioeconomic and political structures, the lack of resources or human exploitation of nature. Nowadays, these two approaches coexist, but it should be noted that physical scientists have a distinct preference for the behavioral perspective, while the social scientists and human geographers rather prefer the second one [3].

The complexity paradigm is built on the foundations of the two paradigms already mentioned, taking from each of them the most valuable aspects and pursuing a more comprehensive approach, considering that disasters are the result either of the interactions between the natural and social worlds and within each of them.

A recent addressing is the multi-hazard approach which is related to the complex nature of the interaction between the hazards [20]. For risk assessment, it is important to evaluate the widest possible range of impacts, including low-probability outcomes with large consequence [8]. Different methods for risk assessment can be applied: quantitative and qualitative

risk assessment methods, the event-tree analysis (very useful for analyzing complex chains of events and the associated probabilities), the risk matrix approach, the indicator-based approach, etc.).

Of great importance is the development of spatial decision support systems with the aim to analyze the effect of risk reduction planning alternatives and to support decision makers in selecting the best alternatives. They are composed of a number of integrated components such as risk assessment, risk reduction planning, temporal scenario, and communication and visualization components [20].

Important advances in addressing risks are due to new technology, including applications of satellite remote sensing, airborne laser scanning (ALS), global positioning systems (GPS), and geographical information systems (GIS). They provide strong support in all phases of the risk management process through monitoring, evaluation, warning, and mobilization of emergency aid.

There is currently a shift of efforts from post-disaster responses and measures to a more responsible, pre-disaster attitude and action. If the events themselves cannot be prevented from occurring, their disastrous consequences can be reduced by a well-established prior plan and by preparing emergency measures for the community at risk. Experience of past events, centralization of the results in disaster observation, and use of modern methods and techniques for evaluating vulnerable areas, can reduce the degree of unpredictability of destructive phenomena occurrence.

Thus, pre-disaster protection becomes a priority within the cycle of disaster management and includes risk assessment (hazard identification, probability and scenarios, exposure and vulnerability evaluation and mapping, loss estimation); mitigation (construction of engineering works and protective structure, insurance, land planning); preparedness (forecast systems, warning schemes, safe refuges, stockpile aid); and emergency plans (evacuation routes, practice drills, first aid supplies).

In the case of climate change mega-hazard, traditional responses to the risk are of limited value in mitigating risk, so different types of possible ex ante responses are considered [7]: global abatement to rapidly stabilize the concentration of GHGs in the atmosphere to a sufficiently low level; development and deployment of controlled geoengineering (e.g., technologies to reduce the amount of solar energy the planet absorb or to remove the CO_2 from the atmosphere); and large-scale adaptation measures to reduce the consequences of mega-catastrophes or short-circuit the cascading of more localized disasters.

The subject of environmental risks continues to be of great interest to various national and international institutions. Among the efforts of the United Nations, the Sendai Framework for Disaster Risk Reduction 2015–2030 underscores that disaster risk reduction is essential to achieve sustainable development. It strongly supports the integration of the disaster and climate risk reduction, at the global, regional, national, and local level, into the 2030 Agenda for Sustainable Development frame [21].

There are still a number of future needs in the field of environmental risks research, such as multilevel cooperation; interdisciplinary research; integration between natural and social

approaches; selection of relevant evaluation indicators, especially vulnerability indicators [22]; transferability of methods; the use of GIS techniques; and the existence of output maps, considering scale and hierarchy, etc. [23].

4. Conclusions

Environmental risks are associated with various natural phenomena and human activities which are potential threats to urban and rural communities and natural and seminatural ecosystems, creating disturbances from local to global level. Population growth, urbanization, resources depletion, pollution and climate change amplify the current risks and emerge new threats to natural and socioeconomic systems.

Risks are unevenly distributed and are generally greater for disadvantaged people and communities in countries at all levels of development [8]. Most vulnerable places, countries, and regions are those with poor socioeconomic conditions, lack or improper access to basic utilities (such as drinking water supply, sanitation, hygiene, sludge and solid waste management services), poor land use and agricultural management, and uncontrolled industrial activities. Usually, poor countries pay a higher tribute to death, while wealthy countries account for the highest levels of material losses.

Environmental policies must be continuously updated supported by relevant data and proper monitoring process to mitigate the environmental risks from local to international level. Multilevel cooperation is compulsory on this matter, and further mechanisms must be developed in the context of climate changes, urban expansion, and emerging economies of low- and middle-income countries.

Author details

Adrian Grozavu[1] and Florin-Constantin Mihai[2]*

*Address all correspondence to: mihai.florinconstantin@gmail.com

1 Department of Geography, Faculty of Geography and Geology, "Alexandru Ioan Cuza" University of Iasi, Iasi, Romania

2 Department of Research, Faculty of Geography and Geology, "Alexandru Ioan Cuza" University of Iasi, Iasi, Romania

References

[1] United Nations General Assembly. Report of the open-ended intergovernmental expert working group on indicators and terminology relating to disaster risk reduction.

December 2016. Available at: https://www.preventionweb.net/files/50683_oiewgreport-english.pdf [Accessed: June 28, 2018]

[2] Smith K, Petley DN. Environmental hazards. In: Assessing Risk and Reducing Disaster. 5th ed. New York, USA: Routledge; 2008

[3] Stângă IC, Grozavu A. Quantifying human vulnerability in rural areas: Case study of Tutova Hills (Eastern Romania). Natural Hazards and Earth System Sciences. 2012;**12**:1987-2001. DOI: 10.5194/nhess-12-1987-2012

[4] Hufschmidt G. A comparative analysis of several vulnerability concepts. Natural Hazards. 2011;**58**:621-643. DOI: 10.1007/s11069-011-9823-7

[5] Birkmann J, Kienberger S, Alexander DE, editors. Assessment of Vulnerability to Natural Hazards. A European Perspective. San Diego, USA: Elsevier; 2014

[6] Cred Crunch 50. EM-DAT The International Disaster Database. Center for Research on the Epidemiology of Disasters-CRED. Natural Disasters in 2017: Lower mortality, higher cost. 2018. Available at https://www.cred.be/sites/default/files/CredCrunch50.pdf [Accessed: June 26, 2018]

[7] Kousky C, Rostapshova O, Toman M, Zeckhauser R. Responding to Threats of Climate Change Mega-Catastrophes, Policy Research Working Paper 5127. The World Bank Development Research Group, Environment and Energy Team; November 2009. Available at: http://www.rff.org/files/sharepoint/WorkImages/Download/RFF-DP-09-45.pdf [Accessed: June 28, 2018]

[8] IPCC. Climate change 2014: Synthesis report. In: Pachauri RK, Meyer LA, editors. Contribution of Working Groups I, II and III to the Fifth Assessment Report of the Intergovernmental Panel on Climate Change. Geneva, Switzerland: IPCC; 2014: 151 pp. Available at: https://www.ipcc.ch/pdf/assessment-report/ar5/syr/SYR_AR5_FINAL_full.pdf [Accessed: June 26, 2018]

[9] Mihai FC. One global map but different worlds: Worldwide survey of human access to basic utilities. Human Ecology. 2017;**45**(3):425-429. DOI: 10.1007/s10745-017-9904-7

[10] UN-HABITAT. Global atlas of excreta, wastewater sludge, and biosolids management: Moving forward the sustainable and welcome uses of a global resource. 2008. Available at: https://esa.un.org/iys/docs/san_lib_docs/habitat2008.pdf [Accessed: June 26, 2018]

[11] Landrigan PJ et al. The Lancet Commission on pollution and health. The Lancet. 2018; **391**(10119):462-512). DOI: 10.1016/S0140-6736(17)32345-0

[12] Mihai F-C. Rural plastic emissions into the largest mountain lake of the Eastern Carpathians. Royal Society Open Science. 2018;**5**(5):172396. DOI: 10.1098/rsos.172396

[13] Lamond J, Bhattacharya N, Bloch R. The role of solid waste management as a response to urban flood risk In developing countries. A case study analysis. WIT Transactions on Ecology and the Environment. 2012;**159**:193-205. DOI: 10.2495/FRIAR120161

[14] UNEP. Africa Waste Management Outlook. Nairobi, Kenya: United Nations Environment Programme; 2018

[15] Kelly-Reif K, Wing S. Urban-rural exploitation: An underappreciated dimension of environmental injustice. Journal of Rural Studies. 2016;**47**:350-358. DOI: 10.1016/j.jrurstud.2016.03.010

[16] Price RA. Environmental impact assessments in refugee crises. K4D Helpdesk Report. Brighton, UK: Institute of Development Studies; 2017. Available from: https://assets.publishing.service.gov.uk/media/5a5f2cdbed915d7dfea66cd8/229-EIA-in-refugee-crises.pdf [Accessed: June 26, 2018]

[17] Mazza A, Piscitelli P, Neglia C, Rosa GD, Iannuzzi L. Illegal dumping of toxic waste and its effect on human health in Campania, Italy. International Journal of Environmental Research and Public Health. 2015;**12**(6):6818-6831. DOI: 10.3390/ijerph120606818

[18] Grant K et al. Health consequences of exposure to e-waste: A systematic review. The Lancet Global Health. 2013;**1**(6):e350-e361. DOI: 10.1016/S2214-109X(13)70101-3

[19] WHO Progress on Drinking Water, Sanitation, and Hygiene: 2017 Update and SDG Baselines. Geneva: World Health Organization (WHO) and the United Nations Children's Fund (UNICEF); 2017. License: CC BY-NC-SA 3.0 IGO

[20] van Westen CJ, Greiving S. Multi-hazard risk assessment and decision making. In: Dalezios NR, editor. Environmental Hazards Methodologies for Risk Assessment and Management. London: IWA Publishing; 2017. pp. 31-94

[21] UNISDR 2017. United nations plan of action on disaster risk reduction for resilience. Towards a Risk-informed and Integrated Approach to Sustainable Development. Available from: https://www.preventionweb.net/files/49076_unplanofaction.pdf [Accessed: June 26, 2018]

[22] Birkmann J. Indicators and criteria for measuring vulnerability: Theoretical bases and requirements. In: Birkmann J, editor. Measuring Vulnerability to Natural Hazards—Towards Disaster Resilient Societies. Tokyo: United Nations University Press; 2006. pp. 55-77

[23] Fuchs S, Birkmann J, Glade T. Vulnerability assessment in natural hazard and risk analysis: Current approaches and future challenges. Natural Hazards. 2012;**64**:1969-1975. DOI: 10.1007/s11069-012-0352-9

Chapter 2

Landslides Triggered by Typhoon Morakot in Taiwan

Ssu-Yao Yang, Chyan-Deng Jan and Ji-Shang Wang

Additional information is available at the end of the chapter

http://dx.doi.org/10.5772/intechopen.76930

Abstract

Landslides are general geomorphic erosion processes on hillslopes and can usually cause severe threats to human life and property due to their unexpected occurrence and fast traveling. Typhoon Morakot (in 2009) released more than 2000 mm rainfall during 6 days at the beginning of August 5 in Taiwan, leading to a large number of landslides, especially in southern Taiwan. Here we significantly devote this chapter to address the causes and effects of landslides in Cishan River watershed accompanied with the primary factors of landslide triggering such as the geologic and topographic settings and rainfall characteristics. We evaluate the devastation of landslides caused by Typhoon Morakot and its aftermath, and also assess the present status of landslide hazards mitigation strategies in Taiwan.

Keywords: landslide, river channel adjustment, Taiwan, Typhoon Morakot

1. Introduction

Landslides are general geomorphic erosion processes on hillslopes and can usually cause severe threats to human life and property due to their unexpected occurrence and fast traveling. Landslides can mobilize a cascades of loose materials from hillslopes into river channels, affecting the sediment yield of watersheds and its corresponding consequent evolution of river channels, habitats, deltas and coast lines in the downstream. Typically, this geomorphic erosion (i.e., landslides) occurs in mountainous landscapes with strong ground motion from earthquakes [1], snow-melt infiltration [2], and rainfall infiltration [3, 4].

Taiwan is an island of an area of 36,000 km^2, and two-thirds of its area are covered by rugged mountains and hills, steep topography, young (3 million years) and weak geological formulations, active earthquakes, and loose soils [5]. Earthquakes and heavy rains play a major role on contributing to the occurrence of landslides. Many landslides have been mainly triggered

by typhoons that usually brought heavy rains in Taiwan. In recently decades, the most severe landslides triggered by heavy rains in Taiwan are those by Typhoon Morakot in the period of August 5 to 10, 2009. Typhoon Morakot brought more than 2000 mm rainfall during 6 days, leading to a large number of landslides, especially in southern Taiwan. The understanding of landslide hazards has been still limited until Typhoon Morakot hit in Taiwan that caused a total of 45,125 of landslides and the catastrophic Hsiaolin landslide in the Cishan River watershed (CRW). The Hsiaolin landslide generated a huge debris dam that blocked the Cishan River and its consequent dam break caused more than 400 people dead and missing; also, the village itself no longer exists [44].

After Typhoon Morakot, the natural environmental conditions of watershed systems were significantly changed due to severe landslides and associated damages. For developing cost-effective landslide hazards mitigation strategies and measures, we should have better understanding on the causes and effects of landslides. Basing on the data taken from the study area of CRW, we devote this chapter to: (1) address the causes and effects of landslides in this watershed (i.e., CRW) accompanied with the primary factors of landslide triggering such as the geologic and topographic settings and rainfall characteristics; (2) evaluate the devastation of landslides caused by Typhoon Morakot and its aftermath; (3) assess the present status of landslide hazards mitigation strategies in Taiwan. Results from landslide research in this chapter lays the foundation and establishes the guidelines for developing possible effective landslide hazards mitigation strategies and measures.

2. General information of landslide triggers in Cishan River watershed, Taiwan

The island of Taiwan is located at the obliquely convergent boundary of the Eurasian continent and the Philippine Sea plate and separated from Eurasia continent by the 175 km wide Taiwan Strait. This collision of the Luzon arc results in two-thirds of its area being covered by rugged mountains and hills, steep topography, young (3 million years) and weak geological formulations, active earthquakes, and loose soils [5]. The average elevation is 765 m and about 31% of the total island area has an elevation of exceeding 1000 m. Most mountains are very steep with slope gradients of 25° and local relief of 1000 m or more.

Taiwan is periodically disturbed by typhoons and local storms and experiences a 2500 mm mean annual rainfall depth equivalent to a triple of global mean values. Majority of rainfall occurs between June and October when trade wind and typhoons strongly provide the sources of moisture. During the rainy seasons, the geological and climatic regimes usually combine to generate severe hillslope denudation by soil erosion, landslides, and debris flows.

Dadson et al. [6] indicates that the rivers of Taiwan transfer suspended sediment of 384 Mt/y to the ocean based on the data measured between 1970 and 1999. This represents 1.9% of estimated global river-borne suspended-sediment discharges but is only derived form 0.024% of Earth's subaerial surface. The Erosion rate were quite high in the eastern Central Range and southwestern region of Taiwan, especially on the Western Foothills with a rate of up to 60 mm/y [6].

2.1. Cishan River watershed and its lithologic complexes

Cishan River watershed lies on the Western Foothills of Taiwan and has an area of 842 km^2 and a mean gradient of 39.3%. Its maximum elevation of 3950 m is near the Southwestern Foothills of Jade Mountain, gradually decreasing from north to south to 31 m, with mean elevation of 473 m. Obviously, there is a significant difference between the maximum and minimum elevations in this long, narrow watershed (**Figure 1**). The geologic setting is underlain by sandstone, shale, slate, and phyllite, and drains geological ages between Eocene to Pleistocene distributed from the upper to lower regions. This is clear that the geological formation is young and weak (between 5.3 and 0.01 million years ago), leading to poorly lithologic resistance to erosion. The Cishan River is 118 km in length, flowing through the watershed. The geomorphic characteristics (i.e., elevation and slope) were obtained by digitizing a 5 × 5 m digital elevation model (provided by Water Resources Agency, Taiwan, WRA) using Geographic Information System (GIS).

Figure 2 shows a geological map of CRW (provided by the Geological Survey Center, MOEA, Taiwan). There are nine lithologic complexes and rock units in the Cishan River watershed:

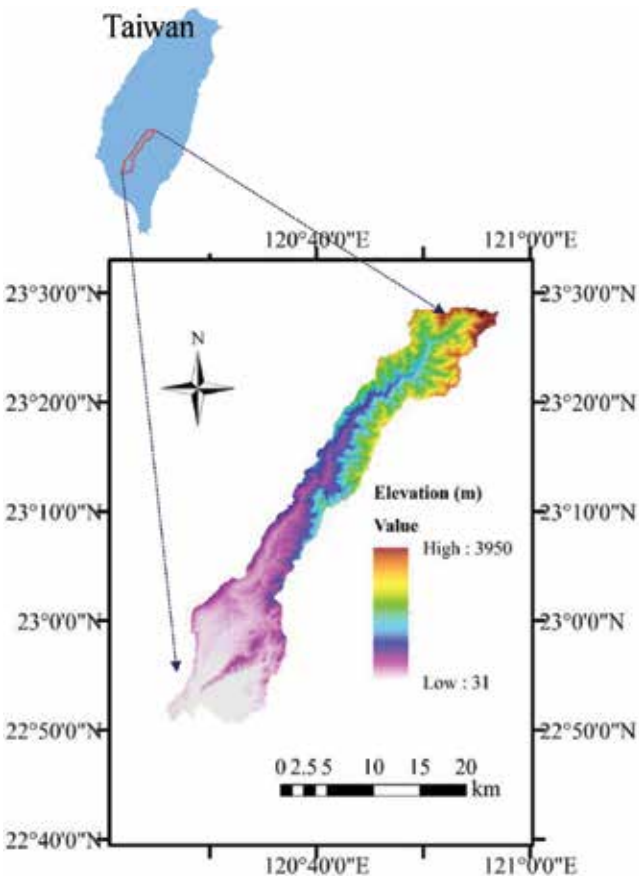

Figure 1. Locations and topography of Cishan River watershed (CRW).

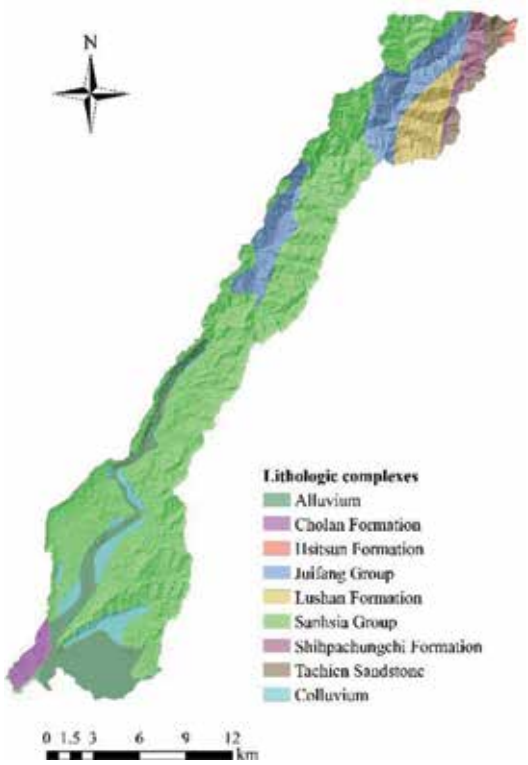

Figure 2. Map of lithologic complexes for the Cishan River watershed.

(a) Cholan Formation, Pliocene in age, (b) Hsitsun Formation, Eocene to Oligocene, (c) Juifang Group, Middle Miocene, (d) Lushan Formation, Miocene in age, (e) Sanhsia Formation, Late Miocene to Pliocene, (f) Shihpachungchi Formation, Eocene, (g) Tachien Sandstone, Eocene, (h) Colluvium, Pleistocene, and (i) Alluvium, Holocene. Each complex comprises different types of sedimentary rocks varying in strength. Interbedded sandstone, argillite, phyllite and slate dominate the rocks of Lushan Formation. Juifang Group, Cholan and Sanhsia Formations mainly comprise sandstone and shale. Hsitsun Formation includes the rocks of Slate, sandstone and phyllite. Shihpachungchi and Tachien Sandstone comprise sandstone, slate and shale. Alluvium and Colluvium contain weak sand, gravel and clay.

The CRW drains tropical monsoon climate zones. The mean annual rainfall is about 3267 mm and the mean annual temperature is 25.1°C. The relative atmospheric moisture averages 75.6%. In this region, the majority of rainfall occurs between June and October because periodic typhoons and trade wind can provide abundant moisture sources during wet season. Conversely, the Center Mountain usually blocks moisture brought by northwestern trade wind, leading to less rainfalls in other months during dry season.

Cishan River watershed drains the Western Foothills of Taiwan, which has a decadal erosion rate of ~30 mm/y. The Cishan River is a main tributary of the Kao-Pin River (the largest river of Taiwan for total river basin) that supplied 49 Mt./y during 1990 and 1999 and this value of

river-borne suspended-sediment discharge is only smaller than that supplied from the Beinan River (~88 Mt./y) in Taiwan [6]. The Water Resource Agency (WRA) of Taiwan continuously made stream gauging and a fortnight suspended-sediment sampling at the Shanlin Bridge station near the downstream from 1986 to 2005, restarting from 2010 till now. Based on the data recording at this gauging station, the Cishan River has a mean suspended-sediment concentration of about 696 ppm, annual sediment yield of about 1.06 Mt./y.

2.2. Catastrophic landslide in Hsiaolin Village

Hsiaolin village is a village on the foothill of Hsiendu Mountain in the Cishan River watershed. At 6:16 AM (local time) on 9 August in 2009, the catastrophic landslide was triggered on the hillslope of Hsiendu Mountain when rainfall reached 1676.5 mm equal to 72-hour accumulative rainfall obtained from the rainfall record of the Jiashan station, with the peak hourly rainfall intensity of 95 mm/h (**Figure 3**). This landslide is the largest landslide occurred during Typhoon Morakot, damming the near Cishan River channel and was break at about 7:40 AM on 9 August. This dam-break flood led to abrupt change in the water level of the Cishan River downstream area, and instrumental records on the downstream of the Hsiaolin Village indicated that 2.75 m drop during the period from 7:10 to 7:50 AM and 7.88 m rise during the period from 8:40 to 9:30 AM. Note that this evident water level changes in the Cishan River channel were observed at 27.8 km downstream of the Hsiaolin Village [44]. Total causality in Hsiaolin Village were more than 400 people dead and missing. The village itself no longer exists.

Figure 4 shows the Formosat-II image and aerial photos of the Hsiaolin landslide. According to the digital terrain models (DTMs) with a resolution of 5 m established by the aerial photos

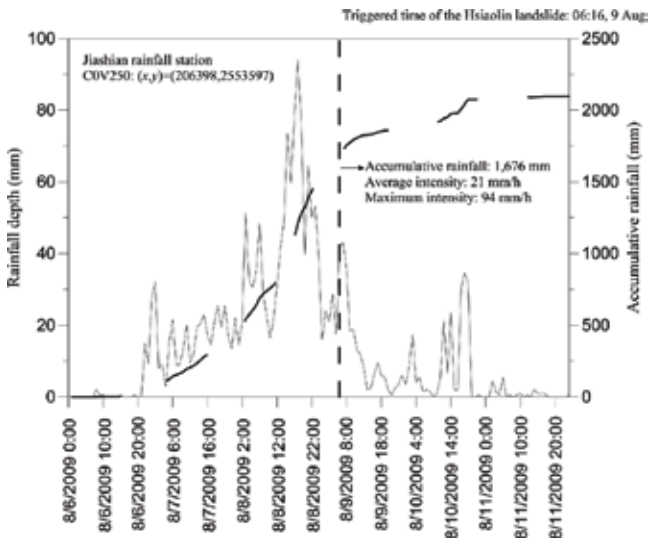

Figure 3. Hourly and accumulative rainfall for typhoon Morakot recorded by the Jiashan rainfall stations (11.4 km SSW of the Hsiaolin landslide) during the period from 6 Aug. to 11 Aug.

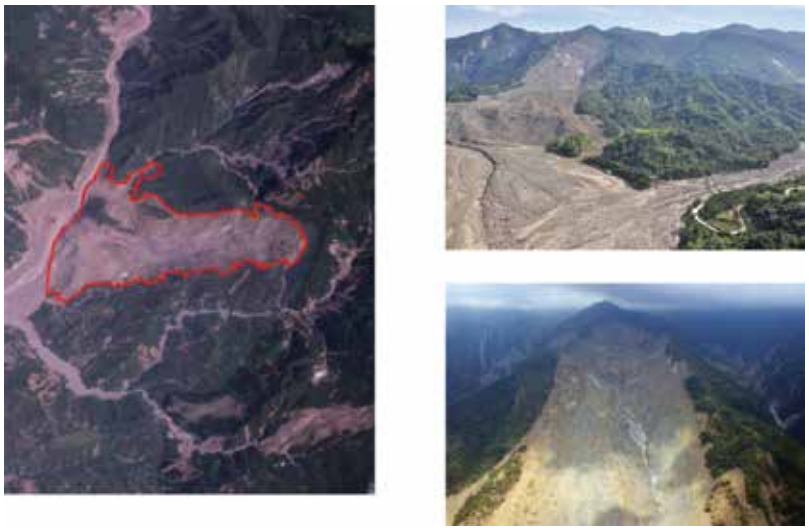

Figure 4. Formosat-II image and aerial photos of the Hsiaolin landslide in the Cishan River watershed, Taiwan.

provided by the Agricultural and Forestry Aerial Survey Institute of Taiwan, Kuo et al. [7] indicated that the major body of the Hsiaolin landslide had the extent of 57×10^4 m^2 and was estimated to have a volume about 24 ± 2 million m^3, distributed at an average depth of 42 ± 3 m. Moreover, it is 3.2 km long in an E–W direction and 0.8 to 1.5 km wide. The total fall height was 830 m from the top of the head scarp, at an elevation of 1280 m, to the toe of the landslide deposit at 450 m [8]. Comparing the Hsiaolin landslide with the 1:25000 geologic map (provided by CGS, MOEA) shows that this landslide crops the late Miocene to early Pliocene Yenshuikeng Formation composed of mudstone, sandstone, and shale. Strength of sandstone is much greater than mudstone and shale, and its corresponding uniaxial compressive strength is about 15 Mpa [9]. The source area of the Hsiaolin landslide was the dip slope of the east limb of the syncline that could exhibits simple traces of strata on a horizontal cross-section, however, because the strata and slopes on the east region of the Cishan River shows the similar characteristics, the bedding traces have rather complicated patterns [8].

A cascade of loose sediment produced by the Hsiaolin landslide deposited on the Cishan River and generated the barrier lake that was suddenly broken about 1 to 2 hours after its generation. The landslide dam was estimated to have a volume of 15.4 million m^3. This is clear that only half of the total sliding mass contributed to the main body of the landslide dam [10]. The maximum elevation produced by this catastrophic landslide is about 475 m, on the west bank of the Cishan River and the maximum water level that can overtop the dam crest is about an elevation of 413 m. The height of the dam was about 44 m and the deepest deposit was a thick of 60 m. Moreover, this dam drained about 354 km^2 watershed area and trapped about 9.9 million m^3 water before overtopping occurred [10]. On the basis of data recorded by continuous river stream gauging from Shanlin Bridge station, the water level of the Cishan river dropped to 118 m nearly at 08:00 AM after the landslide dam formation and rapidly rise up to 126 m at about 9:40 AM [11]. Hence, we can infer that the landslide dam was suddenly flushed out by river water after the dam formation during the period of only 2 hours.

http://dx.doi.org/10.5772/intechopen.76930

3. Methodology and results

3.1. Rainfall brought by typhoon Morakot

On August 8, 2009, Typhoon Morakot was "born" at approximately 22.4°N and 133.8°E in the North Pacific Ocean, about 1000 km far from Northeastern Philippines, moving west at a speed of 10–30 km/h towards Taiwan. In retrospect, Typhoon Morakot had not been considered a serious threat before striking Taiwan. However, contrary to the prediction, after landing Taiwan, it caused more damage than any other typhoon because of massive rainfall, especially in Taiwan's southwestern region. **Figure 5** shows the spatial distribution of rainfall in Taiwan for the six-day rainfall during Typhoon Morakot. This "monster "brought significant rainfalls causing severe debris flows, shallow and deep landslides, and debris dam-break in the mountainous areas of the central and southern Taiwan. Consequently, 675 people were dead; 34 people were hurt; the economic loss was up to 164 million NT dollars.

Figure 6 shows the time series of hourly rainfall data and cumulative rainfall during Typhoon Morakot obtained from Alishan station in central Taiwan. On the basis of this hourly rainfall

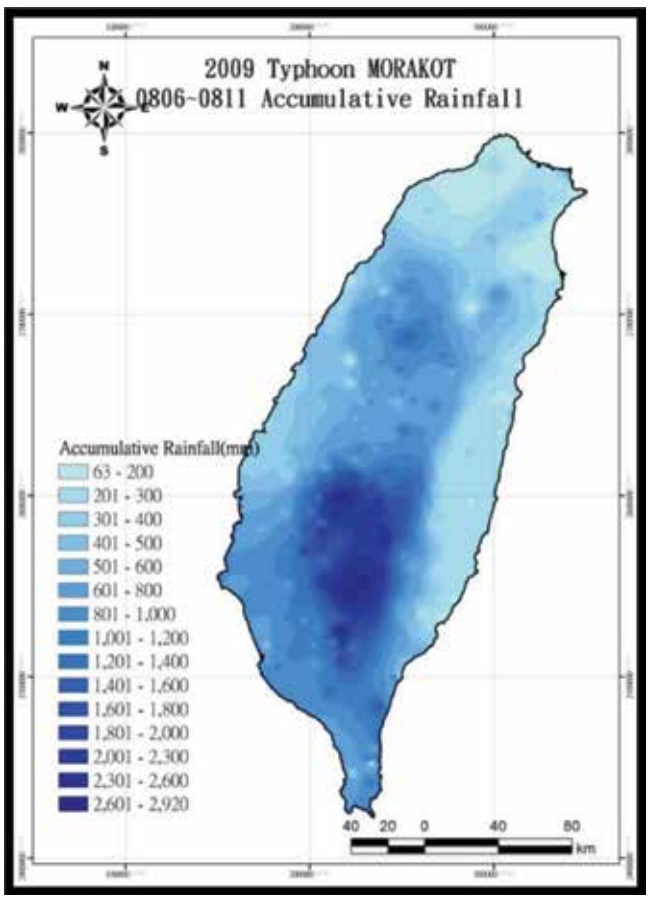

Figure 5. Spatial distribution of rainfall in Taiwan for Typhoon Morakot during six days.

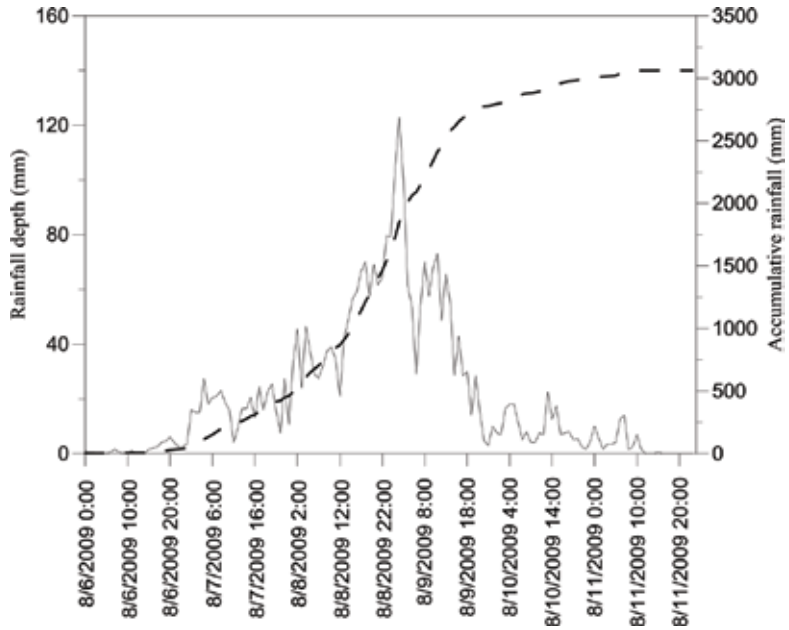

Figure 6. Time series of hourly rainfall amount and its accumulative rainfall from Aug. 6_{th} to the end of Aug. 8th in 2009. This rainfall data is obtained from the records of the Alishan station.

data, the maximum 1-hour, 6-hour, 24-hour, 48-hour and 72-hour rainfall near the headwaters of the Cishan River watershed were 123 mm, 549 mm, 1623 mm, 2361 mm and 2748 mm, respectively. Both the previous 1-hour (113 mm by Typhoon Herb) and 48-hour (1978 mm by Typhoon Herb) rainfall records were broken. The 24-hour and 48-hour rainfall records approximate the world record (1825 mm and 2476 mm, respectively) [12], as shown in **Figure 7**. Moreover, the return periods for 24-hour, 48-hour, and 72-hour rainfall at the Alishan station both exceeded

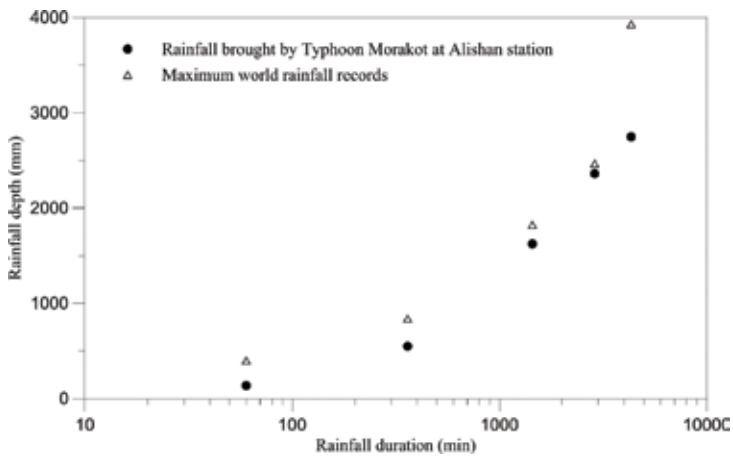

Figure 7. Diagram of rainfall depth-duration for Typhoon Morakot at the Alishan rainfall station near the Cishan River watershed in comparison with the maximum rainfall records in the world.

2000 years (WRA, 2010). Totally, Typhoon Morakot released about 3063 mm rainfall depth during 6 days. This total value is equivalent to about 90% of the annual rainfall in 2009 at Alishan station. In comparison with other typhoon storms, the magnitude of rainfall brought by Typhoon Morakot is quite huge as shown in **Figure 8**. These patterns indicate that this rainfall event can be characterized as high intensity, huge total accumulation and long duration in a large scale, and hence had generated severe hillslope erosion (e.g., landslides) in watersheds.

3.2. Landslides triggered in the Cishan River watershed

Taiwan has total landslides of 45,172 after the massive rainfall brought by Typhoon Morakot, ranging from 258 m^2 to 3,510,861 m^2 with an average of 12,488 m^2 (**Figure 9**). These landslides were identified and mapped from the fused Formosat-II images having resolutions of 2 m, with detailed field checking, and then were digitized into a geographic information system (GIS). Via the fused Formosat-II images (in 2008 and 2009), a pair of successive landslide inventories were mapped through the normalized difference vegetation index (NDVI). The NDVI data are helpful in determining the density of green planet presence via the wavelengths difference. Mathematically, the NDVI is expressed as follows [13]:

$$NDVI = \frac{NIR - IR}{NIR + IR} \tag{1}$$

where NIR is the near-infrared reflection and IR is the infrared reflection. These two reflections can be obtained by observing the different colors in wavelengths reflected by the plants. For landslide areas, the values of NDVI for a given pixel in the Formosat-II satellite images always range from −1 to 0.

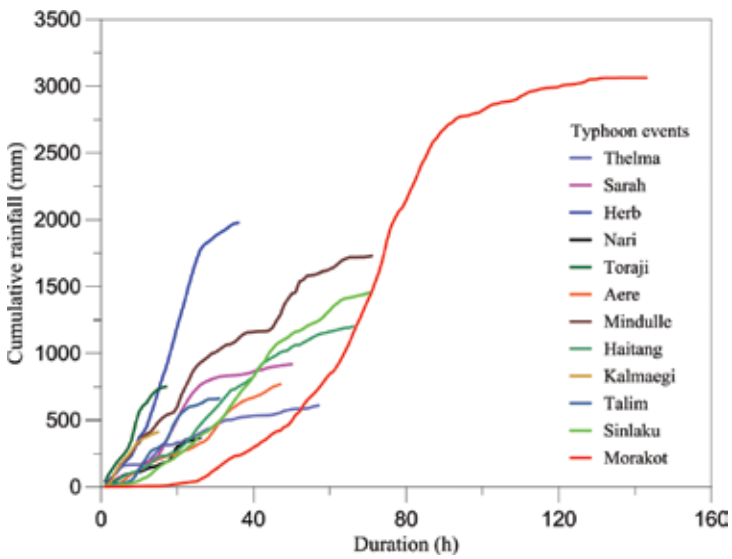

Figure 8. Cumulative rainfall in relation to its corresponding rainfall duration for different typhoons obtained from the records of Alishan rainfall stations.

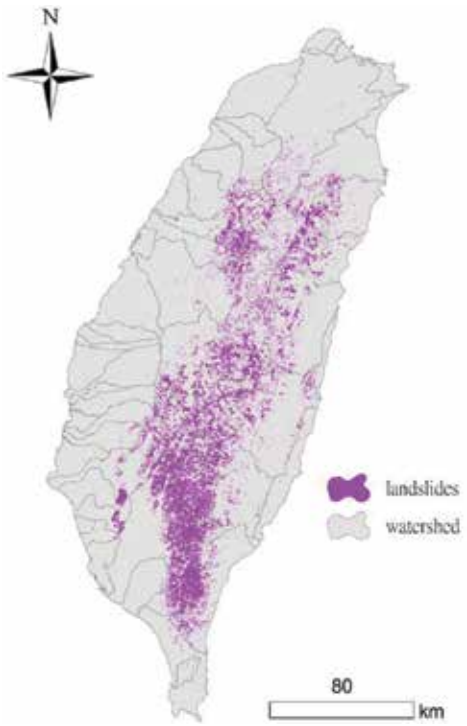

Figure 9. Location of landslides in Taiwan mapped after Typhoon Morakot. These 45,124 landslides range from 258 m^2 to 3,510,861 m^2, with an average of 12,488 m^2.

As shown in **Figure 9**, the landslide areas after Typhoon Morakot mainly concentrate on southern Taiwan that contains the Cishan River watershed (CRW). **Figure 10** shows the landslide area (see red colored regions in **Figure 8**) before (in 2008) and after (in 2009) Typhoon Morakot. In contrast, the total landslide area increased from 7.83 km^2 to 33.98 km^2 and the landslide density increased from 5.7×10^{-3} no./ha to 28.4×10^{-3} no./ha (total number of landslide/survey area) after the disturbance of Typhoon Morakot. On average, the mean landslide area is 0.012 km^2, ranging from a smallest area of 0.12 m^2 to a maximum value of ~2.49 km^2. These patterns indicate that Typhoon Morakot caused severe disturbances on the Cishan River watershed and could lead to significant changes in the geomorphic systems of this region, which we discuss later.

In addition, landslide rank against cumulative landslide area can exhibits the contribution of different landslide magnitude to erosion processes. In this investigation region, landslides were ranked in a series of numbers from the smallest area (No. 1) to the largest area (No. 2338), as shown in **Figure 11**. As a consequence, the largest 10 landslides (0.43% of total number) account for 27% of total landslide area, the largest 58 landslides (2.5% of total number) account for 50% of total landslide area, and the largest 649 landslides (27% of total number) account for 90% of total landslide area. This result indicated that large landslides can majorly dominate denudation processes in the CRW.

These landslide data were further analyzed by using a fractal model. The dependence of landslide frequency on landslide magnitude is an aspect of critical importance to hazard risk

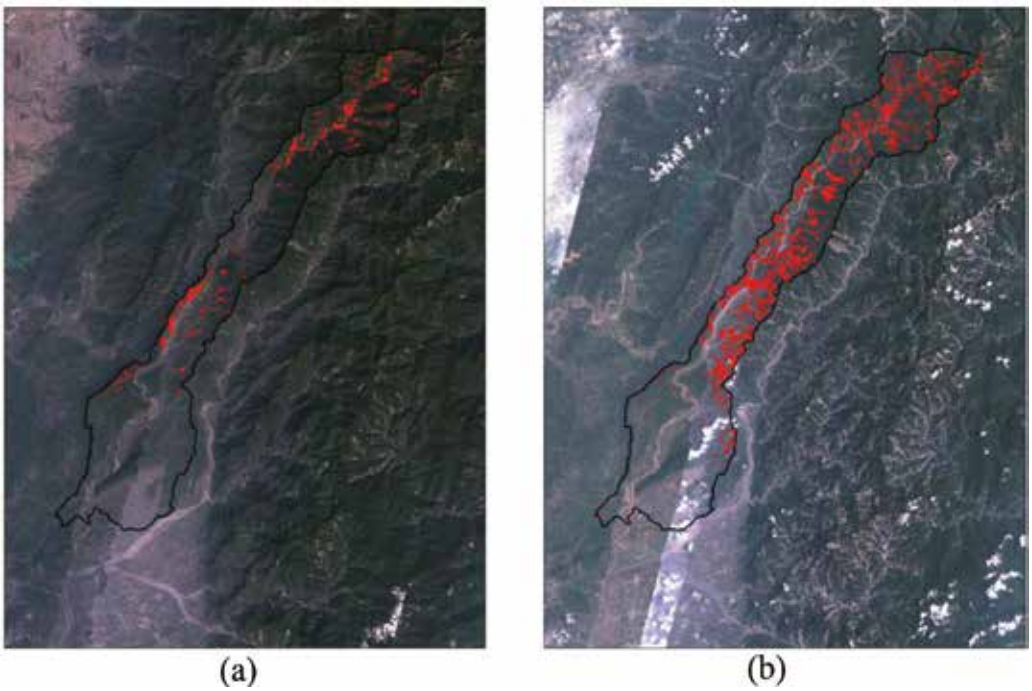

Figure 10. Landslide inventories mapped from a pair of Formosat-II satellite images in 2008 and 2009, respectively, for the Cishan River watershed. (a) Pretyphoon image in 2008. (b) Posttyphoon image in 2009.

assessment and management [14]. Based on the analysis of landslide inventories in worldwide regions, frequency distributions and PDFs (probability density functions) exist in landslide magnitude with heavy tail for medium and large landslides. The mathematical expression of this algebraic PDF right tail decay is generally explained as a linear fitting for power-law scaling [15–18, 45, 46]. Here we characterize the noncumulative frequency-area relations to clarify the landslide behavior in the CRW.

The present paper now considers the noncumulative relation as:

$$p(A_L) = CA_L^{-\beta} \tag{2}$$

where A_L is the magnitude of landslide area, the $p(A_L)$ is a PDF (probability density function) equivalent to $\frac{1}{N_{LT}}\frac{\Delta N_L}{\Delta A_L}$, and the $\triangle N_L$ is the number of landslides with area between A_L and $A_L + \triangle A_L$ and the N_{LT} is the total number of landslides. The constants C and β are obtained from fitting medium and large landslides in order to detect the right heavy tailed decay of PDF through a power-law. We increase our bin width $\triangle A_L$ with increasing area A_L, so that bin widths are approximately equal in logarithmic coordinates. In the CRW, the noncumulative relation of the total 2338 landslides caused by Typhoon Morakot in 2009 based on Eq. 1 is given in **Figure 12**. Above the cutoff at 645 m^2, the landslides displayed power law frequency-area scaling with exponent, $\beta = 1.69$, intercept, $C = 60$, and a determination coefficient (r^2) of 0.99. This result was derived from the scaling of the landslide area between 645 m^2 and 2.48 km^2.

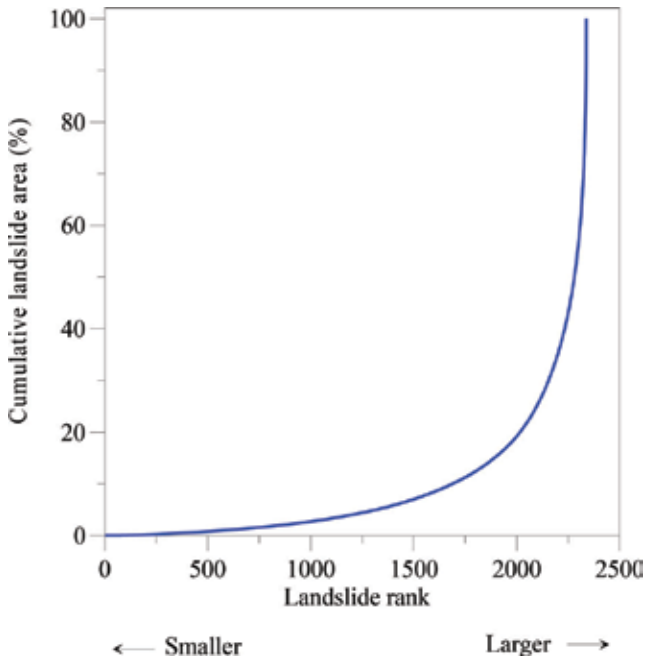

Figure 11. Cumulative percentage of landslide area against to the ranking numbers of 2338 landslides identified after typhoon Morakot in 2009 in the CRW. These landslides were ranked in a series of numbers from the minimum area (no. 1) to the maximum area (no. 2338). The cumulative area of the first 58 largest landslides accounts for 50% of the total landslide area while the first 649 largest landslides for 90% of the total landslide area.

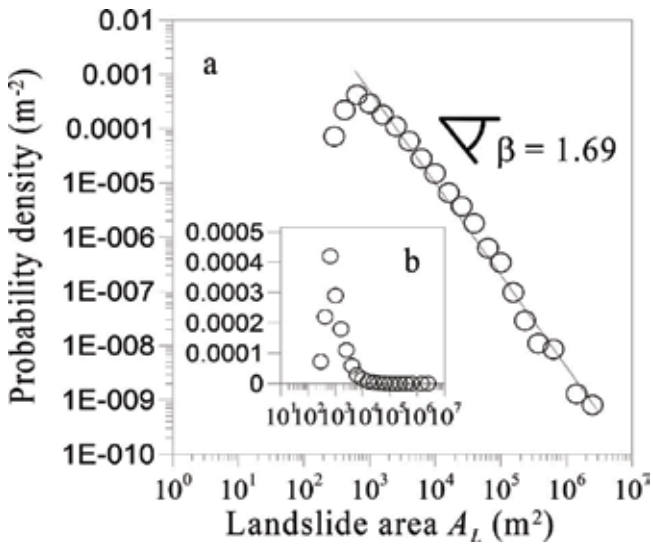

Figure 12. Noncumulative landslide frequency–area distributions in the CRW, based on landslide data after typhoon Morakot in 2009. The landslides of area larger than 645 m^2 display a fractal model with $\beta = 1.69$.

This phenomenon is described by self-organized criticality (SOC). Bak [19] indicates that if a system is well described by power-law scaling over a large portion of its event magnitude range, the system may be in a quasi-static state with SOC. In the CRW, landslides caused by Typhoon Morakot satisfies (2) with $\beta = 1.69$ and suggest that landslide triggering has SOC in this region. **Table 1** lists the values of β based on (2) for the frequency distribution of landslide area derived from the worldwide regions. In comparison, the value of β in the CRW is smaller than 2.5 in this study, among the lowest observed worldwide [27], showing our study area has higher societal risk caused by the higher occurrence probability of large landslides.

3.3. Landslide triggering response to geomorphic characteristics on hillslopes

Landslides tend to occur in groups. Occurrence of landslides on hillslopes is therefore influenced by the geomorphic characteristics of subaerial surface because some geomorphic condition can provide suitable environments for the development of landslide. Hence, the investigation of landslide abundance and its corresponding spatial distribution in relation to the factors in situ is necessary for landslide hazard assessment. Here we used 5 × 5 m digital elevation model (DEM) (provided by Water Resources Agency, WRA) to analyze different geomorphic settings such as elevation, slope, aspect, surface residual, surface curvature, and fractal dimension in the CRW. Also, the distribution of lithologic complexes was obtained from the geological map provided by the Center of Geological Survey, Taiwan. These above mentioned factors were examined with the location of landslide triggering in the CRW, as tabulated in **Table 2**.

The percentage of landslide area (C_a) for a watershed is defined as the total landslide area ALT divided by the watershed area A, i.e., $C_a = A_{LT}/A$. Ca expresses the overall extent of damage caused by landslides done to the land [18, 28] and this proportional damage indicator is used

Region	α	β
Japan [20]	0.89	1.89
Western Southern Alps, New Zealand (Hovius et al., 1997)	1.1	2.1
Challana Valley, Bolivia [21]	1.6	2.6
Alameda, USA [21]	2.3	3.3
Umbria, central Italy [22]	1.5	2.5
California, USA [22]	1.3	2.3
Lombardy, northern Italy [23]	0.85	1.85
Southern California, USA [24]	1.1	2.1
Fiordland, New Zealand [25]	1.07	2.07
Val di Fassa, Italy [26]	1.56	2.56
TWR and CYL watersheds, Taiwan [18]	0.65	1.65
CRW, Taiwan	0.69	1.69

Table 1. Exponent values of fractal model for landslide frequency-area distribution collected form the worldwide observations.

	Classification	$C_{a'}$ %	D_L	$R_{L'}$
Elevation	0–500	0.52	2.89	1.17
	500~1000	1.47	8.19	11.74
	>1000	2.67	14.89	6.92
Aspect	North	0.47	2.62	4.65
	Northeast	0.51	2.83	6.75
	East	0.62	3.43	6.64
	Southeast	0.70	3.91	5.95
	South	0.57	3.15	4.43
	Southwest	0.68	3.76	4.91
	West	0.63	3.50	4.26
	Northwest	0.49	2.76	3.56
Slope gradient	S < =5%	0.01	0.07	0.09
	5% < S < =15%	0.08	0.42	1.06
	15% < S < =30%	0.31	1.72	2.49
	30% < S < =40%	0.46	2.55	4.29
	40% < S < =55%	1.11	6.21	6.89
	55% < S < =100%	2.45	13.67	8.05
	S > 100%	0.23	1.30	7.07
Geologic settings	Loam	0.08	0.45	0.76
	Slate	0.13	0.75	25.45
	Interbedded slate and sandstone	0.08	0.43	3.05
	Interbedded sandstone and shale	4.07	22.67	6.00
	Hard sandstone	0.13	0.73	4.46
	Hard shale	0.17	0.92	3.35
	Gravel	0.00	0.02	0.09
Curvature	Convex	1.98	11.03	4.40
	Flat	0.08	0.42	1.57
	Concave	2.60	14.50	5.71
Surface roughness	0~0.3	1.50	7.99	4.71
	0.3~0.6	2.03	10.81	5.19
	0.6~0.9	0.80	4.28	4.46
	0.9~1.2	0.23	1.25	4.45
	1.2~1.5	0.03	0.15	3.17
	1.5~1.8	0.00	0.02	6.54
	2~2.2	0.00	0.03	1.61

	Classification	C_a, %	D_L	R_L,
Fractal dimension	2.2~2.4	2.47	12.96	6.43
	2.4~2.6	2.02	10.58	4.91
	2.6~2.8	0.08	0.42	0.66
	2.8~3	0.003	0.02	0.09

C_a is the percentage of landslide area in the region in relation to total watershed area. D_L is the landslide density equivalent to ratio of landslide number in the region to total watershed area. R_L is the landslide rate equivalent to the percentage of landslide area in the region in relation to the corresponding region area.

Table 2. Landslide distribution in response to geomorphic and geologic settings in the CRW.

in the evaluation of other hazard [29]. Landslide density D_L is the ratio of numbers of landslide to the watershed area. Landslide rate R_L is the percentage of landslide area in the region of each geomorphic characteristic to the extent of geomorphic characteristics. These landslide variables can help us to clarify the landslide triggering in response to diverse geomorphic and geologic settings.

As shown in **Table 2**, landslide distributed in the different geomorphic and geologic settings cropping out CRW after Typhoon Morakot. The largest elevation group in the CRW is the region lower than 500 m that extends 44% of total watershed area. This region only cropped out C_a of 0.52%, landslide density (D_L) of 2.89 No./km^2 and is covered 1.16% of total by landslides. The smallest unit is the region that its elevation is between 500 m and 1000 m, only accounting for 13.98% with landslide density of 8.19 of 2.89 No./km^2 and has landslide rate of 10.51%. In addition, the region of elevation higher than 1000 m has landslide density of 14.89 No./km^2 and landslide rate of 6.47%. Results show that landslides tend to occur at the region of elevation higher than 500 m on hillslopes.

On the basis of the Soil and Water Conservation Technical Guide issued from Taiwan government, the terrain gradient in the CRW can be categorized into seven classes as well as shown in **Table 2**. In this watershed, the hillslopes are most widely mantled by the sixth-class slope gradient (between 55% and 100%, i.e., between 28.8° and 45°; see **Table 1**), with 32.9% of the total watershed area (842 km^2) and has the greatest values for landslide density (13.67 No./km^2) and landslide rate (7.45%), respectively. In other words, the smallest unit is the gradient of hillslopes less than 5% (i.e., 2.86°) and therefore has the lowest values for landslide density of 0.07 No./km^2 and landslide rate of 0.09%. Aspects of hillslopes were also classified into eight groups (**Table 2**). It is clear that there are no evident differences in each hillslope aspect that accounts for about 8–15% of the total watershed area. The largest unit is west-facing slopes that extends 15.33% of the 843 km^2 CRW area, with the quite small values of landslide density (3.5 No./km^2) and landslide rate (4.68%). Of particularly, landslides in the CRW after Typhoon Morakot cropped out the similar values of C_a, D_L and R_L in eight aspect groups, ranging from 0.47 to 0.7%, from 2.62 No./km^2 to 3.91 No./km^2 and from 3.43 to 5.26%, respectively. These patterns suggest that there are no significant variations in landslide distribution in diverse hillslope aspects, indicating the aspect has low effect on landslide triggering.

The above mentioned geomorphic characteristics are usually used to be as landslide triggers, and to examine landside occurrence in response to geomorphic systems. However, those

geomorphic characteristics are simple and using those characteristics (i.e., elevation, slope and aspect) could not represent complex geomorphic systems in natural environments, e.g., convergent slopes and surface roughness. To consider the complexity of geomorphic conditions, we employed curvature, surface roughness and fractal dimension, comparing with the location of landslide occurrence to find out the 'hotspot' or 'prone area' in the CRW.

Curvature is the changing rate of slope along x and y direction and can be categorized into three groups of divergent, flat and convergent based on curvature values of greater than zero, equal to zero and smaller than zero, respectively [47], as shown in **Table 2**. In comparison, divergent and convergent slopes individually lie the most regions of the total watershed area (about 47 and 48%). On the divergent slope, landslide triggering after Typhoon Morakot accounted for 1.98% of the total watershed area with 11.03 landslides per km^2 and landslide rate of 4.21%. In other words, the convergent slopes have 2.6% percentage of landslide area comparing with the area of the CRW, landslide density of 14.5 No./km^2 and landslide rate of 5.4%. Results show that both of divergent and convergent slopes can provide suitable condition for the development of landslides. Divergent slopes can lead to landslide triggering due to the effect of gravity along slope. Convergent slopes can concentrate water flow leading to increase in groundwater level and pore water pressure, therefore generating landslides on hillslopes. However, **Table 2** still indicates that landslides slightly tend to occur on convergent slopes in comparison with divergent slopes in the CRW. In addition, the flat region is not appropriate to landslide triggering and hence strictly has 0.42 landslides per km^2.

Here we define the surface roughness is a residual topography that can be derived from the cell by cell subtraction of original 5 × 5 m DEM and the mean of this DEM. Mean DEM was created by averaging elevation values within a 3-cell moving window. The raster of residual topography was then calculated as the cell-by-cell difference between the original DEM and the mean DEM. In the Cishan River watershed, surface roughness (i.e., residual topography) was calculated as the above mentioned flow and further categorized into six groups by 0–0.3, 0.3–0.6, 0.6–0.9, 0.9–1.2, 1.2–1.5 and 1.5–1.8. Based on this classification, the largest unit of surface roughness is the region of the values from 0.3 to 0.6 that covers about 39.32% of the total CRW area, with 10.81 landslides per km^2 respect to this region. Note that there is no significant difference between landslide rates in each surface roughness settings, ranging from 3.07% to 6.14%. These patterns suggest that landslides tend to be triggered in group in the region of surface roughness between 0 to 0.6. Above this cutoff, the landslide density and landslide rate evidently decrease as well as shown in **Table 2**.

In other words, natural landscapes generally have fractal characteristics. Terrain can be considered self-similar in the two horizontal directions and self-affine in cross-section [30]. This leads to the discussion of the relationships of landslide triggering with respect to the self-similarity or fractals of topography be necessary. Fractal dimension in the CRW was calculated using the Landserf software on the basis of 5 × 5 m DEM, comparing with the location of landslide occurrence. Landserf implements the variogram method (e.g., [31]), which we use in this study. The variogram is calculated as:

$$D = \frac{1}{2n(h)} \sum_{i=1}^{n} \sum_{j=1}^{n} \left(z_i - z_j\right)^2 \tag{3}$$

where h is the lag between measured cells and n is the number of pairs considered. Landserf calculates D within a moving window around each cell across the raster. This calculation can represent how the surface roughness/complexity changes over the study area. D is computed at different window sizes for $n \geq 9$ and its value is between 2 (flat surface) and 3 (a space filling rough surface). In the CRW, the fractal dimension of land surface was digitalized in Landserf, then comparing with the landslide inventory after Typhoon Morakot (**Table 2**). Classification of fractal dimension in the CRW is defined as 2.0–2.2, 2.2–2.4, 2.4–2.6, 2.6–2.8 and 2.8–3. Results show that the most regions have the values of fractal dimension from 2.2 to 2.4 and from 2.4 to 2.6, accounting for 38.45% and 40.54%, respectively. Meanwhile, percentage of landslide area, landslide densities and landslide rates are quite larger in these regions (D values between 2.2 and 2.4 and between 2.4 and 2.6) than that in other regions. In particular, total landslide density is very high with 23 No./km^2 in the regions of D values ranging from 2.2 to 2.6, indicating that landslides tend to occur in this region.

In general, Geologic settings determine the strength of rocks that can further influence sediment production caused by weathering processes on hillslopes. Soft rock can usually lead to weak resistance to erosion. Based on geologic map provided by Central Geological Survey, MOEA, Taiwan, we can find that the largest geologic unit is interbedded sandstone and shale, cropping out about 72% of the total CRW area. We also examined landslide distribution in response to geologic settings. Results show that percentage of landslide area C_a, landslide density D_L, and landslide rate R_L are 4.07%, 22.67 No./km^2 and 5.66%, respectively, in the region of interbedded sandstone and shale and these values are much greater than that in other regions, as shown in **Table 2**. Other regions crop out geologic units of gravel, loamy sand, slate, interbedded slate and sandstone, hard sandstone, and hard shale, respectively. These geologic units are usually recognized as hard rocks and structural settings. Although some of them are composed of loose materials that are tended to landslide triggering (loamy sand and gravel), but just crops out only 10.83 and 4.52% of total watershed area in the CRW.

The geologic setting crops out interbedded sandstone and shale that has weak, low resistance to erosion and lies most regions of the CRW, favoring the generation of landslides on hillslopes.

The above landslide inventory shows that landslide triggering can be influenced by geomorphic and geologic settings. The hillslope with elevation of 500 m, slope between 28.8° and 45°, convex slopes, surface roughness index from 0 m to 0.6 m, fractal dimension from 2.2 to 2.6 and geologic unit composed of sandstone has high potential for the development of landslides.

3.4. Aftermath of typhoon Morakot in the CRW

Denudation processes play a very important role in the fluvial systems of a watershed. A large amount of sediment materials produced by landslides could be entrained downslope from hillslopes into river channels, influencing the evolution of river morphology. Typhoon Morakot led to severe hillslope erosion in the CRW (**Figure 8**), and its consequent generation of sediment materials could deposit on hillslopes and river channels, changing the geomorphic response of the CRW. Here we compared the river borne suspended sediment and river bathymetry of the Cishan River to show the aftermath effect of Typhoon Morakot on the CRW.

3.4.1. Changes in river-borne suspended sediment concentrations

River-borne suspended sediment is an important feature of the global denudation system and is often adopted as a measure of terrestrial erosion rates and the intensity of erosion processes in watersheds [32, 33]. Here we quantitative the impact of Typhoon Morakot on the sediment loads of Cishan River by using the measurement of suspended-sediment discharge of Shenlin-bridge river stage station from 1987 to 2005 and 2010 (no measurement from 2007~2009). The water discharge is daily recorded, and the sediment concentration is measured fortnightly using a USDH-48 suspended-sediment sampler from the Water Resources Agency of Taiwan. Evaluating the amount of sediment loads can use the formula of rating curve based on water discharges. Fitting the plots of suspended-sediment discharge on log-log scale using least square can obtain an equation as

$$C_s = aQ^b \tag{4}$$

where C_s is sediment concentration (ppm), a is the unit sediment concentration and b is the sediment mobilization capacity of water discharges. By fitting model curves based on (5) to both pretyphoon (from 1987 to 2005) and posttyphoon (in 2010) data, while keeping the exponent fixed to permit comparison between models, we obtained model coefficients a_{pre} and a_{post}. The ratio of a_{post} to a_{pre} denoted by $\triangle a$ that can be used to estimate the influence of Typhoon Morakot on the fluvial system of the CRW. If $\triangle a > 1$, it means unit sediment concentration increased after the typhoon events.

Figure 13 shows the river-borne suspended-sediment rating curves of the Cishan River on the basis of data recorded by the Shanlin Bridge gauge. The power-law relation of measurement data before Typhoon Morakot (from 1987 to 2005; see red line) fitted by least-square regression is expressed as

$$C_s = 16\,Q^{0.7} \tag{5}$$

and the relation of that after the typhoon events (in 2010; see black line) fitted by least-square regression is expressed as

$$C_s = 160\,Q^{0.7} \tag{6}$$

According to (5) and (6), change in unit sediment concentration for the Cishan River after Typhoon Morakot is equivalent to 10 (i.e., $\triangle a = 10$). Suspended-sediment concentrations in the Cishan River after the disturbance of Typhoon Morakot are as much as 10 times greater than decadal background value. This elevated posttyphoon erosion rate has resulted from the abundant landslide triggered by the typhoon events, and led to rich sediment supply from the hillslopes into river channels.

Here we calculated the annual river-borne suspended-sediment loads via the estimates of the rating curve for the Cishan River that combines the relationship of suspended-sediment concentration with respect water discharges, with the instrumental records of daily water discharges. In addition, we estimated the suspended-sediment loads driven by Typhoon

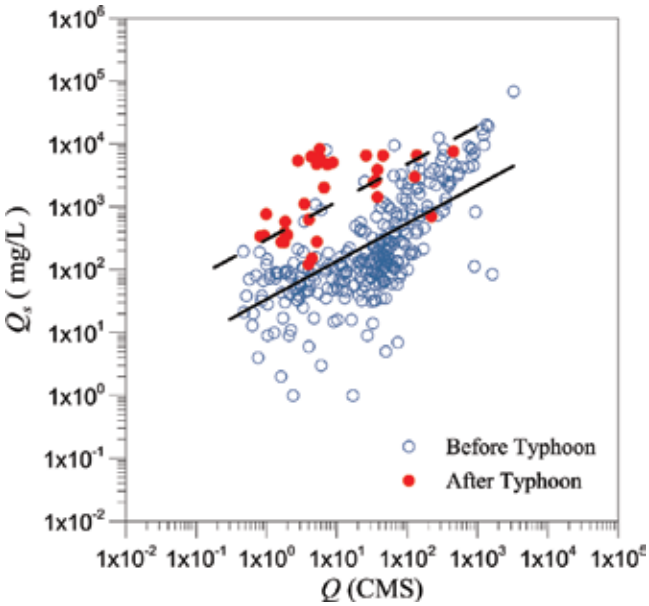

Figure 13. Suspended-sediment rating curves for the Cishan River. Red circles show measurements made before Typhoon Morakot; blue circles show measurements after the typhoon storms. Dashed lines are power-law relations fitted to pretyphoon data using log-transformed least-squares regression; solid lines are power-law relations fitted only to posttyphoon data.

Morakot for the Cishan River by the rating curve regression employing 4 successive daily water discharges at the beginning of 6 Aug. Note that all the records of daily water discharges were obtained from the Shanlin Bridge gauge.

Figure 14 shows the mean annual sediment load, Q_{sy}, the annual sediment load in 2009, Q_{s09} and the sediment load brought by Typhoon Morakot, Q_{sm} for the Cishan River. On average, the annual river-borne suspended-sediment loads were ~ 1.06 Mt./y for the Cishan River. The total mass flushed out from the Cishan River watershed in 2009 was about 0.71 Mt. and, 0.64 Mt. of which was mobilized by Typhoon Morakot. It shows that Typhoon Morakot determined erosion processes on hillslopes, removing the most sediment materials from the CRW and accounted for 91% of total river-borne suspended-sediment during the period of 4 days. Only about 10% of sediment materials (~0.06 Mt) was transported by the Cishan River during the other period in 2009. Moreover, four-day suspended-sediment loads generated by Typhoon Morakot reached 61% of the decadal mean annual value.

3.4.2. Changes in the riverbed elevation of the Cishan River

In general, in mountain belts, sediment produced by storm-triggered landslides usually rapidly transfers into the fluvial systems and could not taking a long time to storage on hillslopes. However, we have shown a large amount of sediment materials deposited on hillslopes at the end of 2010 after Typhoon Morakot in the above section. Landslides caused by Typhoon Morakot supplied magnificent sediment to the Cishan River and could lead to sedimentation in the river channels. Here we collected the elevation data for the 62 cross section of

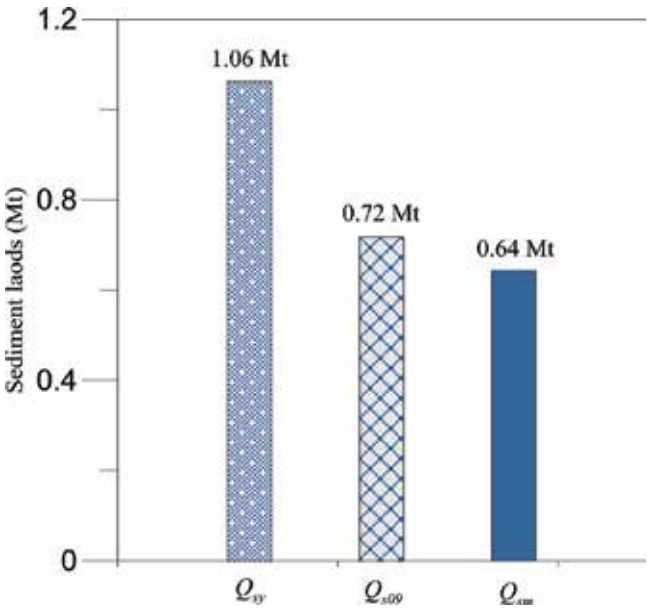

Figure 14. Mean annual sediment loads, Q_{sy}, annual sediment loads in 2009, Q_{s09} and sediment loads brought by Typhoon Morakot, Q_{sm} in the Cishan River derived from rating curve estimates.

the Cishan River, from Jiashian weir to Erren-Yuemei weir and the river reach is shown in **Figure 15**, which was reported by Water Resources Planning Institute [34].

The longitudinal profile is a continuous line by the lowest elevations at each stream cross sections. **Figure 16** shows the longitudinal profile of this 22.8 km river reach for the Cishan River, illustrated by the measurement data of each stream cross section during the periods of pretyphoon (in 2005) and posttyphoon (in 2010). Result indicates that the riverbed has a slight scour cumulative distance of below 1 km and above 18 km for the original cross section No. 22, respectively, but other reaches had significant sedimentation. To quantitative the effect of changes in the riverbed on the transport capacity for this river reach (**Figure 15**), the unit stream power [35] was used as

$$\omega = \rho g Q S / w \tag{7}$$

where ω is the unit stream power on river bed (W/m^2), ρ is water density (1000 kg/m3), Q is discharge of river channel (m^3/s), S is the gradient of river channel and w is channel width (m). In Taiwan, the channel width can be represented as [6]

$$w = Q^{0.5} \tag{8}$$

replacing the w (7) by Eq. (8), we can obtain as following equation:

$$\omega = \rho Q^{0.5} S \tag{9}$$

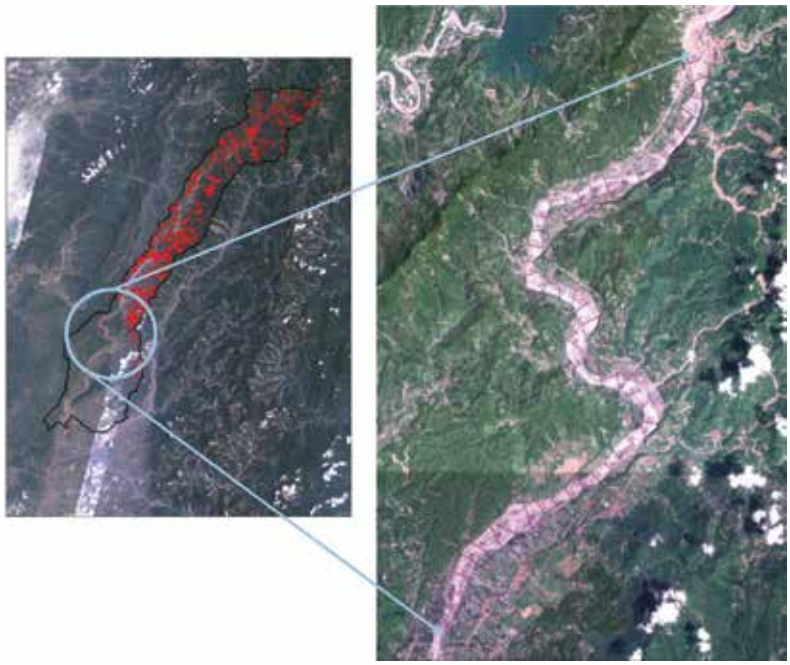

Figure 15. Formosat-II images of river reach with 62 cross section measurement for the Cishan River from Jiashiang weir to Erren-Yuemei weir.

Of particular interest, (9) infers that unit stream power could be only influenced by changes in the gradient of riverbed, because water density and water discharges could be treated as the same values in the same stream reach. Hence, based on (9), we can only examine the gradient of riverbed pretyphoon and posttyphoon to describe shifts in unit stream power for the river reach as shown in **Figure 16**. Calculating the gradient of longitudinal profile for the river reach form the measurement data in situ show that the pretyphoon riverbed gradient (in 2005) was 2.8% and the posttyphoon riverbed gradient (in 2010) was 1.3%, respectively. This indicates that unit stream power for the Cishan River had been significantly decreased (about 55%) after the disturbance of Typhoon Morakot and could lead to the lowering of transport capacity for the fluvial system, increasing sedimentation on the riverbed.

In other words, the longitudinal profile for the river reach is further separated into four parts with the cumulative distances of ~5 km, dissecting shifts in the unit stream power the river channels influenced by Typhoon Morakot. **Figure 17** shows the variations in the gradients of the riverbed calculated by the pretyphoon and posttyphoon measurement data in situ. Before the typhoon disturbance in 2005, the gradients of the riverbed were 0.00794, 0.00539, 0.00586 and 0.00705 for the upstream to the downstream, indicating that unit stream power in the river reach gradually decreased along the longitudinal river profile and had an increase in the riverbed gradient approximating the Erren-Yuemei weir. Sedimentation in the river

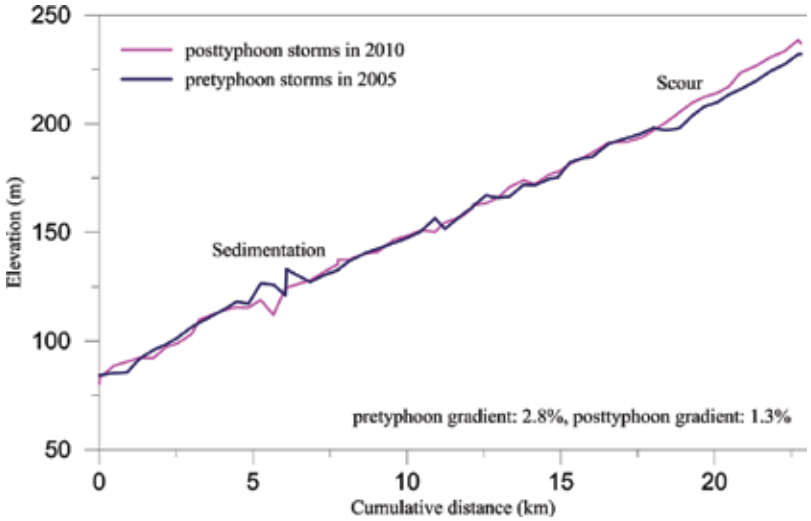

Figure 16. Longitudinal profiles of river reach for the Cishan River from Jiasiang weir to Erren-Yuemei weir obtained from the elevation data of pretyphoon and posttyphoon measurement.

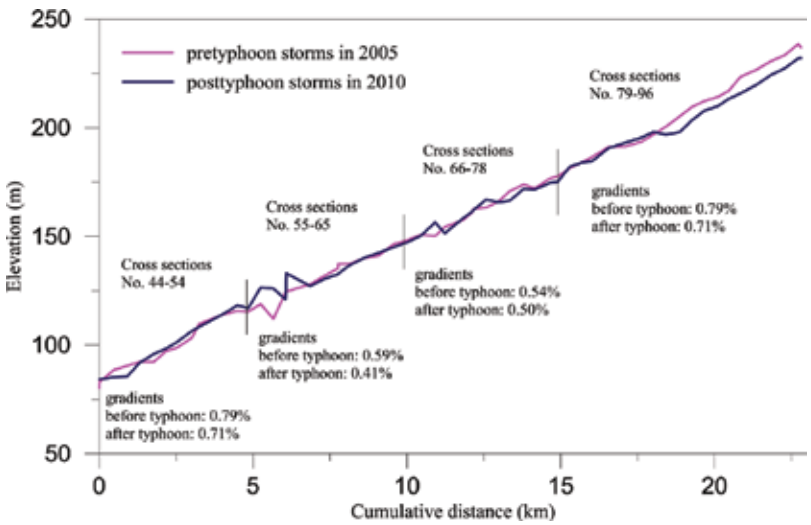

Figure 17. River gradients of four reaches along the Cishan River from Jiasiang weir to Erren-Yuemei weir before and after the disturbance of Typhoon Morakot.

channel was elevated by TypvMorakot, leading to reduction in its riverbed gradient and lowered about 10, 7, 29 and 7% of unit stream power for those four river reaches from the upstream to the downstream. These patterns suggest that significant sedimentation processes can be observed in this reach for the Cishan River, because the lowering of river transport capacity and abundant sediment supplied from the hillslopes in the CRW after Typhoon Morakot. Hence, the increased likelihood of flood inundation in the reach of the Cishan River (**Figure 14**) are expected due to its elevated riverbed.

3.4.3. Widening of the Cishan River

Sediment sources produced by Typhoon Morakot was richly supplied from hillslopes to the fluvial system, elevating the riverbed of the Cishan River. This elevated riverbed lowered the unit stream power of the river channel and could lead to water flow centrally erode the riverbanks. To investigate changes in the riverbanks for the Cishan River, we used a pair of Formosat-II images to digitalize the pretyphoon (in 2008) and posttyphoon (in 2009) edges of the riverbanks within GIS. Then, HEC-RAS was used to extract the river widths per 100 m along the river channel before and after the disturbance of Typhoon Morakot. **Figure 18** shows the box-whisker plot of the river widths estimated from pretyphoon and posttyphoon data for the Cishan River. The second and third quartiles of the pretyphoon river widths are ~110 and 190 m, respectively, with a maximum of 728 m, a minimum of 16 m, and an average of 144 m. However, after the typhoon disturbance, the Cishan River widths were evidently widened and had the second and third quartiles of 260 and 471 m. Its maximum and minimum river widths were shifted into 2090 and 17 m, with an average of 342 m. This is clear that river widths increased by more than a factor of 2 to those statistical estimate values before the hit of the typhoon. Results show that Typhoon Morakot caused severe riverbank erosion for the Cishan River, leading to its consequent river width widening.

Comparing these two river channel inventories (in 2008 and in 2009) can show changes in river widths caused by Typhoon Morakot. Subtraction between the pretyphoon and posttyphoon river widths in each river cross section indicates that only about 22 cross sections display contracting adjustment, i.e., the river widths in 2009 smaller than that in 2008, only accounting for

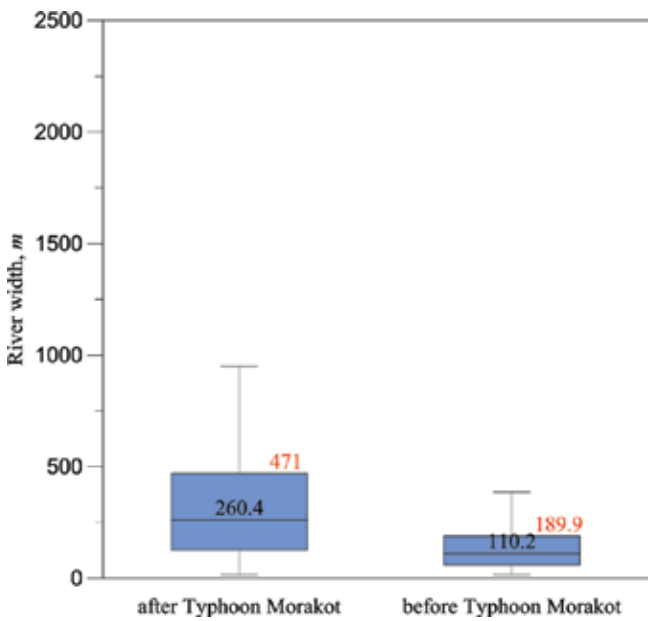

Figure 18. Box and whisker plot of river widths along the Cishan River estimated from pretyphoon and posttyphoon mapping based on a pair of Formosat-II images in 2008 and 2009, respectively.

1.6% of total 1357 cross sections. Most of the river widths show widening adjustment after the typhoon disturbance. Here we focused on the widening adjustment of the 1335 cross sections for the Cishan River in 2009. Also, we characterized the noncumulative frequency-widening relations to clarify whether the river widening has a SOC phenomenon. The noncumulative frequency distribution of river widening can be mathematically expressed as

$$p(R_w) = \alpha R_w^{-\beta} \tag{10}$$

where R_w is the magnitude of river widening, the $p(R_w)$ is a PDF (probability density function) equivalent to $\frac{1}{N_w}\frac{\Delta N_w}{\Delta R_w}$, and the $\triangle N_w$ is the number of cross sections with widening between R_w and $R_w + \triangle R_w$ and the R_{wT} is the total number of river cross section widening. The constants α and β are obtained from fitting medium and large river widening in order to detect the right heavy tailed decay of PDF through a power-law. We increase our bin width $\triangle R_w$ with increasing area R_w, so that bin widths are approximately equal in logarithmic coordinates. **Figure 19** shows that river widening having R_w larger than 64 m could be well interpreted by a power-law statistic with $\alpha = 25.6$ and $\beta = 1.93$ with $r^2 = 0.98$.

Of particular interest, the β value for river widening is greater than that for landslides driven by the same external trigger, i.e., Typhoon Morakot, suggesting that the occurrence likelihood of large magnitude of river widening is smaller than that of large landslides in the CRW for the perspective of environmental risks. Also, typhoon-induced river widening could have self-organized criticality. However, the β values in (10) are very limited on the basis of worldwide observations and are not like the β values in (2) for landslides that can be obtained

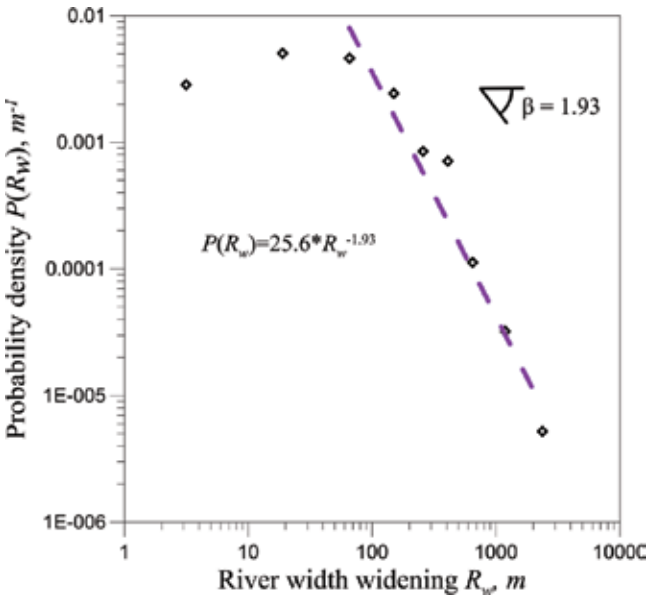

Figure 19. Noncumulative frequency distribution of river width widening after Typhoon Morakot for the Cishan River. Above the cutoff of 64 m, the river width widening satisfies a power-law relation with exponent β = 1.93.

from the many regions of the globe. Hence, more data of river channel inventories and its corresponding field checking should be necessary to examine whether the β values in (10) still holds on true in other environments, or these values have a variation.

4. Discussion

In this chapter, we characterize landslides triggered by Typhoon Morakot in 2009, and its corresponding frequency-area distribution. Results show that the exponent value of a noncumulative relation for these landslides approximates the lowest limitation of worldwide observation. This infers that the hillslopes of the CRW has high potentials on landslide triggering. Meanwhile, ambient sediment materials produced by landslides could deposit on hillslopes and river channels and cause the adjustments of hillslope and fluvial systems, which can be observed from raised river-borne suspended-sediment concentration in the Cishan River (i.e., rich-supply hillslopes) and its decreased stream power (severe sedimentation in river channels). These patterns indicate that landslides not only pose threats to people's life and properties, but also have significant influence on the downstream. Hence, long-term and short-term strategies for landslide countermeasures are both necessary. The long-term strategies are the comprehensive management and regulation of basins and watersheds. The short-term strategies are the development of real-time warning systems for landslide triggering on hillslopes. In Taiwan, the present real-time warning system developed for landslide hazards are described as follow.

4.1. Landslide warning system adopted by the Taiwan's government

Before hit by this typhoon storms, the Central Geological survey, MOEA (2009) in Taiwan has used logistic equation to estimate landslide ratios via the potential values obtained from the combination of 100-year return period hourly rainfall depth and cumulative daily rainfall to map the landslide susceptibility. On the basis of this susceptibility, Taiwan's hillslopes were categorized in three regions of high risk, medium risk and low risk. Comparing with the location and initiation time in situ of landslides or rock avalanching (total of 909; provided by Soil and Water Conservation Bureau and Central Geologic Survey) show that these geomorphic erosion processes crop out the regions of high risk ~43% of totals. 90% of total can be observed when we consider both of high risk and medium risk regions. However, although the construction of landslide susceptibility can provide some useful information on mapping landslide-prone areas, the effect of real-time rainfall during typhoon storms should be necessary for landslide warning, still. Considering only landslide-prone area could also lead to the over-issued orders of hazard mitigation from landslide warning and also the wasting of governmental administrative resources.

Rainfall brought by typhoon storms plays a majorly important role in triggering landslides on hillslopes. Typically, some topographic and geologic regimes could provide suitable conditions for landslide triggering but landslides are still needed to be initiated by external triggers such as rain infiltration and its consequent saturation. The evolution of soil pore pressure can

be mainly influenced by these triggers, leading to the change of normal and shear stresses for a soil profile, further reducing slope failure [36, 37]. Many researchers have investigated landslide and debris flow triggering in response to different rainfall parameters [18, 38–40, 42, 43], showing that different rainfall characteristics can affect the initiation of debris flows and landslides from place to place. The precise relationship between landslides and rainfall parameters remains unclear, leading to the need of studies on the characteristics of rainfall-triggered landslides on hillsides in different regions [18].

To analyze the relationships of landslide triggering with respect to rainfall characteristics, Jan [41] collected 15 landslide inventories for different periods, comparing with its corresponding different rainfall parameters that include 3-hour average rainfall intensity I_3, 6-hour average rainfall intensity I_6, 12-hour average rainfall intensity I_{12} and 24-hour average rainfall intensity I_{24}, obtained from the records of near rainfall stations. Results indicate that the strongest correlation is between landslide occurrence and 3-hour average rainfall intensity based on logistic regression analysis, with determined coefficient r^2 equivalent to 0.679. In other words, **Figure 20** shows the relationships between different average rainfall intensities (i.e., I_3, I_6, I_{12} and I_{24}) and accumulative rainfall amount calculated from hourly rainfall data recorded by the Shinfa gauge. Red dots represent landslides occurred in that rainfall event and triangles represent no landslides occurred in that rainfall event (see **Figure 20**). These patterns suggest that I_3 can be recognized as a suitable indicator to the warning of rainfall-induced, shallow landslide [41].

In Taiwan, the rainfall-threshold warning system is well constructed for debris flow mitigation. Referring the rainfall parameter considered in the warning system for debris flow

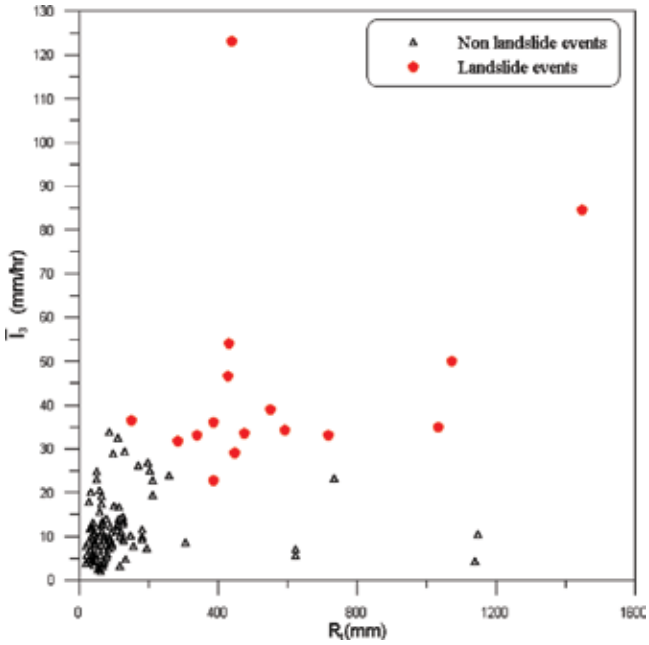

Figure 20. Effective accumulative rainfall (R_t) against 3-hour average rainfall intensity ($\bar{I}_3$) illustrated from hourly rainfall data recorded by Shinfa gauge.

mitigation and the above mentioned works, Jan [41] has proposed a rainfall-threshold index for landslide mitigation as follow:

$$LRTI = \bar{I}_3 \times R_t \tag{11}$$

where *LRTI* is the landslide rainfall triggering index, R_t is the effective accumulative rainfall, and $\bar{I}_3$ is the 3-hour average rainfall intensity. To establish rainfall threshold for evaluating landslide triggering, the Weibull distribution was used to estimate the values of *LRTI* for the cumulative frequencies at 70% and 90%, respectively, for total rainfall events. During typhoon storms, if its corresponding *LRTI* is greater than the value for the cumulative frequency at 70% (denoted by $LRTI_{70}$), the landslide warning system would issue 'yellow' warning; if the *LRTI* value is greater than the value for the cumulative frequency at 90% (denoted by $LRTI_{90}$), the landslide warning system would issue 'red' warning, as reported by Jan [41]. On the basis of those two LRTI values (at 70 and 90% of cumulative frequency), the operation of landslide warning issuance is suggested following the criterion as

- Level 2 warning would be released when the values of real rainfall data gauging is higher than $LRTI_{70}$.
- Level 1 warning would be released when the values of real rainfall data gauging during a 3-hour period is simultaneously higher than $LRTI_{70}$.
- Level 1 warning would be reduced to Level 2 when the values of real rainfall data gauging during a 3-hour period is simultaneously lower than $LRTI_{70}$.
- Level 2 warning would be left when the values of real rainfall data gauging during a 3-hour period is simultaneously lower than $LRTI_{70}$.

This rainfall-induced, shallow landslide warning system is used to provide information on the decision making of landslide hazard mitigation for Soil and Water Conservation Bureau of Taiwan.

5. Conclusions

Severe typhoon storms and the consequent landslide hazards on hillslopes have frequently posed threats to economic implementation whose impacts on the wealth and property may exhaust the available resources to deal with the aftermath of those disasters. In Taiwan, the countermeasures of debris flow have been well developed in recent 20 years, gradually. However, the development of shallow landslide mitigation measures and warning systems are still limited and should be emergent in the future. Moreover, it must need to strengthen public awareness of landslide hazards, educating people on how to respond to landslide hazards on hillsides, especially during rainy seasons. Meanwhile, more research on landslide mechanics, warning system, and its corresponding rationale prediction and assessment methods are necessary.

Occurrence of landslides on hillslopes is not only a real challenge of natural hazard mitigation, but also river channel management. As we above mentioned, ambient Typhoon Morakot had led to significant sedimentation in the Cishan River and the dredging of river channels therefore becomes an important issue after the typhoon disturbance on landscapes. Landslide triggering can simultaneously influence the evolution of hillslope and fluvial systems, leading to its regulation should be integrated and consistent. Hence, Compound-disaster perspective and its domino effect on each disaster are necessary to be considered in the development of landslide countermeasures. In addition, for disaster evaluation in the case of emergency, satellite images, aerial photography and field survey immediate after typhoon storms are necessary to construct high resolution digital topography models that can be used in the aftermath analysis and modeling. Also, more fruitful research on the understanding of landslide mechanics, from which we can develop appropriate design codes in building and installing sediment-control structures, are pressingly needed in Taiwan.

Acknowledgements

This work was supported by the Ministry of Science and Technology in Taiwan under the Grant No. MOST 104-2221-E-006 -053 -MY3 and MOST 106-2625-M-006-018 -. The writers sincerely appreciate the help of Y.C Wang in digitalizing the widths of the Cishan River.

Author details

Ssu-Yao Yang[1,2]*, Chyan-Deng Jan[1] and Ji-Shang Wang[3]

*Address all correspondence to: henry740913@gmail.com

1 Department of Hydraulic and Ocean Engineering, National Cheng Kung University, Tainan, Taiwan

2 USDA-ARS National Soil Erosion Research Lab, Purdue University, West Lafayette, IN, USA

3 Ecological Soil and Water Conservation Research Center, National Cheng Kung University, Tainan, Taiwan

References

[1] Keefer DK. The importance of earthquake-induced landslides to long-term slope erosion and slope-failure hazards in seismically active regions. Geomorphology. 1994;**10**:265-284

[2] Guzzetti F, Ardizzone F, Cardinali M, Rossi M, Valigi D. Landslide volumes and landslide mobilization rates in Umbria, Central Italy. Earth and Planetary Science Letters. 2009;**279**:222-229

[3] Collins BD, Znidarcic D. Stability analyses of rainfall induced landslides. Journal of Geotechnical and Geoenvironmental Engineering. 2004;**130**(4):362-372

[4] Sivrikaya O, Kilic AM, Yalcin MG, Aykamis AS, Sonmez M. The 2001 Adana landslide and its destructive effects, Turkey. Environmental Geology. 2008;**54**:1489-1500

[5] Jan CD, Chen CL. Debris flow caused by typhoon herb in Taiwan. In: Jakob M, Hunger O, editors. Debris-Flow Hazards and Related Phenomena. Berlin: Springer; 2005. pp. 539-563

[6] Dadson SJ, Hovius N, Chen HG, Dade WB, Hsieh ML, Willett SD, Hu JC, Horng MJ, Chen MC, Stark CP, Lague D, Lin JC. Links between erosion, runoff variability and seismicity in the Taiwan orogen. Nature. 2003;**426**:648-651

[7] Kuo CY, Tai YC, Chen CC, Chang KJ, Siau AY, Dong JJ, Han RH, Shimamoto T, Lee CT. The landslide stage of the Hsiaolin catastrophe: Simulation and validation. Journal of Geophysical Research. 2011;**116**:F04007. DOI: 10.1029/2010JF001921

[8] Tsou CY, Feng ZY, Chigira M. Catastrophic landslide induced by typhoon Morakot, Shiaolin, Taiwan. Geomorphology. 2011;**127**:166-178

[9] Central Geological Survey. Query system of environmental geological hazard; 2010. Available at http://envgeo.moeacgs.gov.tw/ (in Chinese)

[10] Dong JJ, Li YS, Kuo CY, Sung RT, Li MH, Lee CT, Chen CC, Lee WR. The formation and breach of a short-lived landslide dam at Hsiaolin Village, Taiwan-part I: Post-event reconstruction of dam geometry. Engineering Geology. 2011. DOI: 10.1016/j.enggeo.2011.04.001

[11] Lee SP, Chen YC, Shieh CL, Kuo YS. Using real-time abnormal hydrology observations to identify a river blockage event resulted from a natural dam. Landslides. 2014;**11**:1007-1017. DOI: 10.1007/s10346-013-0441-1

[12] TGRU. Taiwan geomorphological research unit, Department of Geography, National Taiwan University, Taipei. In: Natural Hazards of Taiwan. Taiwan (in Chinese): Taiwan and Council of Agriculture, Taipei; 2001

[13] Deering DW. Rangeland reflectance characteristics measured by aircraft and spacecraft sensors. In: Ph. D. Dissertation, Texas A & M University. College Station, TX; 1978. p. 338

[14] Dai FC, Lee CF. Frequency-volume relation and prediction of rainfall-induced landslides. Engineering Geology. 2001;**59**:253-266

[15] Hovius N, Stark CP, Allen PA. Sediment flux from a mountain belt derived by landslide mapping. Geology. 1997;**25**(3):231-234

[16] Stark CP, Hovius N. The characterization of landslide size-frequency distributions. Geophysical Research Letters. 2001;**28**(6):1091-1094

[17] Ten Brink US, Geist EL, Andrews D. Size distribution of submarine landslides and its implications to tsunami hazard in Puerto Rico. Geophysical Research Letters. 2006; **33**:L11307. DOI: 10.1029/2006GL026125

[18] Jan CD, Yang SY, Su YW, Huang WS. Investigation about rainfall-induced shallow landslides in CYL and TWR watersheds, Taiwan. Environment and Earth Science. 2016;**75**:898. DOI: 10.1007/s12665-015-5215-8

[19] Bak P. How Nature Works: The Science of Self-Organized Criticality. New York: Springer; 1996

[20] Fujii Y. Frequency distribution of landslides caused by heavy rainfall. Journal of the Seismological Society of Japan. 1969;**22**:244-247

[21] Malamud BD, Turcotte DL. Self-organized criticality applied to natural hazards. Natural Hazards. 1999;**20**:93-116

[22] Guzzetti F, Malamud BD, Turcotte DL, Reichenbach P. Power-law correlations of landslide areas in Central Italy. Earth and Planetary Science Letters. 2002;**195**:169-183

[23] Crosta GB, Negro PD, Frattini P. Soil slips and debris flows on terraced slopes. Natural Hazards and Earth System Sciences. 2003;**3**:31-42

[24] Lave J, Burbank D. Denudation processes and rates in the transverse ranges, southern California: Erosional response of a transitional landscape to external and anthropogenic forcing. Journal of Geophysical Research. 2004;**109**:F01006. DOI: 10.1029/2003JF000023

[25] Clarke BA, Burbank DW. Bedrock fracturing, threshold hillslopes, and limits to the magnitude of bedrock landslides. Earth and Planetary Science Letters. 2010;**297**:577-586

[26] Frattini P, Crosta GB. The role of material properties and landscape morphology on landslide size distribution. Earth and Planetary Science Letters. 2013;**361**:310-319

[27] Hergarten S. Landslides, sandpiles, and self-organized criticality. Natural Hazards and Earth System Sciences. 2003;**3**:505-514

[28] Hufschimidt G, Crozier MJ. Evolution of natural risk: Analysing changing landslide hazard in Wellington, Aotearoa/New Zealand. Natural Hazards. 2008;**45**:255-276

[29] Kreibich H, Thieken AH, Petrow T, Mueller M, Merz B. Flood loss reduction of private households due to building precautionary measures-lessons learned from the Elbe flood in August 2002. Natural Hazards and Earth System Sciences. 2005;**25**:117-126

[30] Turcotte DL. Fractals and Chaos in Geology and Geophysics. Cambridge, UK: Cambridge University Press; 1992. p. 221

[31] Mark DM, Aronson PB. Scale-dependent fractal dimensions of topographic surfaces: An empirical investigation with applications in geomorphology and computer mapping. Mathematical Geology. 1984;**16**(7):671-683

[32] Latrubesse EM, Restrepo JD. Sediment yield along the Andes: Continental budget, regional variations, and comparisons with other basins from orogenic mountain belts. Geomorphology. 2014;**216**:225-233

[33] Walling DE, Fang D. Recent trends in the suspended sediment loads of the world's rivers. Global and Planetary Change. 2003;**39**:111-126

[34] Water Resources Planning Institute. Report on river planning of Chi-San River. In: Water Resources Agency. 2011

[35] Bagnold RA. An approach to the sediment transport problem from general physics. U.S. In: Geological Survey Professional Paper 422-J. 1966

[36] Berti M, Simoni A. Field evidence of pore pressure diffusion in clayey soils prone to landsliding. Journal of Geophysical Research. 2010;**115**:F03031. DOI: 10.1029/2009JF001463

[37] Iverson RM. Sensitivity of stability analyses to groundwater data. In: Bell, editor. Landslides. Balkema, Rotterdam; 1991. pp. 451-457

[38] Caine N. The rainfall intensity–duration control of shallow landslides and debris flows. Geograf Annal. 1980;**62A**:23-27

[39] Tatard L, Grasso JR, Helmstetter A, Garambois S. Characterization and comparison of landslide triggering in different tectonic and climatic settings. Journal of Geophysical Research. 2010;**115**:F04040. DOI: 10.1029/2009JF001624

[40] Wieczorek GF. Effect of rainfall intensity and duration on debris flows in Central Santa Cruz Mountains, California. In: Costa W, editor. Debris Flows/Avalanches: Processes, Recognition and Mitigation. Reviews in Engineering Geology 7. Geological Society of America. 1987. pp. 23-104

[41] Jan CD. A study on the warning system for rainfall-induced sediment disasters. Research Report (SWCB-106-118), Submitted to the Soil and Water Soil Conservation Bureau, Taiwan (in Chinese); 2017

[42] Central Geological Survey. Research on application of the investigation results for the upstream watershed of flood-prone area. In: Central Geological Survey. Chinese: MOEA; 2009

[43] Dadson SJ, Hovius N, Chen H, Dade WB, Lin JC, Hsu ML, Lin CW, Horng MJ, Chen TC, Milliman J, Stark CP. Earthquake-triggered increase in sediment delivery from an active mountain belt. Geology. 2004;**32**:733-736

[44] Feng ZY. The seismic signatures of the surge wave from the 2009Xiaolin landslide-dam breach in Taiwan. Hydrological Processes. 2012;**26**:1342-1351

[45] Chen CY, Yu FC, Lin SC, Cheung KW. Discussion of Landslide Self-Organized Criticality and the Initiation of Debris Flow, Earth Surf. Process. Landforms; 2007;**32**:197-209

[46] Stark CP, Guzzetti F. Landslide rupture and the probability distribution of mobilized debris volumes. Journal of Geophysical Research. 114, F00A02. 2009. DOI: 10.1029/2008JF001008

[47] Wilson JP, Gallant JC. Digital terrain analysis. In: Wilson JP, Gallant JC, editors. Terrain Analysis: Principles and Applications. New York: John Wiley; 2000:1-27

Chapter 3

Analyzing Wildfire Suppression Difficulty in Relation to Protection Demand

Matthew P Thompson, Zhiwei Liu, Yu Wei and
Michael D Caggiano

Additional information is available at the end of the chapter

http://dx.doi.org/10.5772/intechopen.76937

Abstract

In recent years, the field of wildfire risk management has seen dramatic advances. One notable improvement is in the realm of pre-fire suppression response planning, in particular the expansion from the assessment of risks posed by fire to the assessment of opportunities to effectively manage fire. Such proactive assessment and planning is critical to ensure that suppression response strategies and tactics are more likely to be safe and efficient. In this paper we will review the state-of-the-art in wildfire suppression planning, and illustrate application of advanced planning tools on a fire-prone landscape in Colorado, USA. Specifically we will use geospatial tools to quantify a composite index of suppression difficulty, and map this layer in relation to two key protection priorities that often drive suppression response decisions: built structures, and high value watersheds. We will discuss how our assessment results can inform planning and prioritization efforts, and offer suggestions for future research.

Keywords: decision support, GIS, hazard, modeling, planning, risk assessment, risk management

1. Introduction

Wildfire is an important natural process, and when it functions within acceptable parameters it can promote landscape heterogeneity, enhance forest resilience, and exhibit self-regulating characteristics [1, 2]. At the same time, wildfire can result in negative consequences, including public and firefighter fatalities, increased rates of respiratory disease, destruction of homes and timber, and impairment of critical infrastructure [3–5]. A particularly acute issue is the presence and expansion of human development in fire-prone areas [6, 7]. Increased attention to the fire

problem coupled with improved technological capacity have spurred development of innovative mapping and assessment techniques to inform prioritization and mitigation efforts [8–10].

These efforts reflect broader trends of increasing sophistication of risk assessment and risk management within the global fire science and decision support communities [11–16]. One notable advancement relates to analysis of risk transmission (i.e., the analysis of ignition patterns, potential fire flow pathways, and simulated fire perimeters) in order to determine areas on the landscape that have a higher propensity to be a source of damaging fires [17–21]. Such analyses can inform demarcation of firesheds to support community wildfire planning, evaluation of comparative transmission rates across land designations and ownerships, and strategic identification of fuel treatment, ignition prevention, and suppression preparedness needs.

A related advancement is in the realm of pre-suppression response planning, particularly the assessment of opportunities to effectively manage fire. Proactive assessment and planning can reduce time pressures and uncertainties, thereby helping ensure that suppression response strategies and tactics are more likely to be safe and efficient [22, 23]. Information from risk assessment can play a critical role in planning efforts and development of suppression objectives, for instance identifying areas where aggressive suppression would be warranted due to a high likelihood of fire transmission to developed areas, or where less aggressive suppression might be appropriate to achieve resource objectives [24, 25]. The operational relevance of pre-suppression planning is enhanced though consideration of factors that influence suppression effectiveness, notably the identification of areas of high suppression difficulty as well as their converse, areas of high likelihood for effective fire control [26–29]. Developing maps with such information can help fire managers forecast likely suppression resource needs, develop strategic courses of action and plans for mobilization of suppression resources, and inform tactical deployment decisions of where to send suppression resources.

The research presented in this paper builds on the aforementioned body of work in the field of pre-suppression planning, with a focus on two key analytical products and planning tools: (1) the suppression difficulty index (SDI) [29]; and (2) a network of potential wildfire operational delineations (PODs) [24]. SDI, a raster layer, is a dimensionless metric that combines variables related to fire behavior (flame length, heat per unit area) with variables related to suppression operations (road and fuelbreak density, firefighter accessibility, fireline production, and cycle time for aerial resources). All else being equal, SDI increases with more extreme fire behavior. Similarly, SDI decreases as road density and firefighter accessibility increase, for example. For our purposes here, we use a modified version of SDI called the terrestrial SDI (tSDI) that excludes air support [27]. In the 2017 fire season in the USA, tSDI products were delivered to fire managers for real-time decision support on more than a dozen large fires.

PODs are polygons whose boundaries are relevant to fire control operations, such as roads, trails, ridgetops, drainages, and fuel transitions. In effect, PODs can be thought of as fire management units, within which risks and other fire-relevant information can be summarized. The process of POD delineation can range from full automation in a GIS environment to being hand-drawn by local managers using expert judgment assisted by maps of tSDI and potential control locations [26, 27]. The POD concept has been used to support strategic response planning [24], large fire response optimization [25], and fuel treatment optimization [30]. As with tSDI, POD

products were utilized during the 2017 fire season in the USA, specifically on the Tonto National Forest in Arizona to support large fire planning and management decisions.

In summary, generating maps of tSDI and PODs can provide useful information for suppression response planning and decision making. tSDI can be used to identify locations on the landscape where potential flame lengths and heat intensities may make it unsafe for direct attack tactics, scouting, or ground transportation. This might be particularly important where rapid initial response using direct attack tactics is the predominant response to ignitions that could threaten the wildland-urban interface (WUI). Similarly, summarizing tSDI along administrative boundaries could facilitate identification of areas where suppression efforts may be more or less likely to inhibit fire transmission onto adjacent ownerships. tSDI can also facilitate identification of potential control locations and their aggregation into POD polygons. POD boundaries can help answer questions of how, where, and when to engage the fire along these predetermined potential control locations. In the context of risk transmission, the objective is to replace land ownership boundaries as artificial locations for suppression effort by identifying existing built and natural barriers that could slow fire spread or provide convenience for dispatching engines and personnel.

Here we aim to demonstrate not only the value of these geospatial planning tools as standalone products, but also how stronger integration could lead to enhanced decision support. Specifically, we summarize tSDI values within each POD. This research direction is partly inspired by recent work in wildfire risk assessment that similarly integrates raster- and polygon-based modeling approaches [31]. Further, we quantify and map tSDI and POD layers in relation to two key protection priorities that often drive suppression response decisions: built structures and high value watersheds. Relative to a raster analysis, POD polygons provide a more logical and useful analysis unit to summarize protection demands, especially when incorporating information on suppression difficulty. We perform our case study analysis on a fire-prone landscape encompassing the Arapaho and Roosevelt National Forests in the Front Range of Colorado, USA. We discuss how our assessment results can inform planning and prioritization efforts, and offer suggestions for future research.

2. Case study location

We selected a case study landscape encompassing the Arapaho and Roosevelt National Forests, which is in north-central Colorado, USA. **Figure 1** provides a map of the continental USA with the state of Colorado and the National Forests identified. **Figure 2** further presents a topographic basemap and county boundary as reference for the study site. The study area includes the Front Range, which is located to the west of a heavily populated urban corridor stretching from Denver north to Fort Collins. The study area is 622,222 hectares in total, which includes 292,889 hectares from the Arapaho National Forest and 329,333 hectares from the Roosevelt National Forest [32]. Elevation of the study area ranges from mesas and high prairies at 1500 meters to mountain peaks exceeding 4250 m, with steep river canyons and dramatic changes in vegetation along the elevation gradient.

Figure 1. Location of the National Forests within Colorado, USA.

Addington et al. [33] summarize important characteristics of the Front Range that influence forest conditions and fire management concerns. A dry climate (average annual precipitation ~25–50 cm) combined with shallow soils that have relatively low moisture-holding capacity leads to low site quality and slow accumulation of fuels relative to other more productive pine forests in the western USA. The highly dissected topography creates variability in productivity and fuel loadings, which tended to promote a mixed-severity fire regime. However, a legacy of fire exclusion in the Front Range has led to changes in forest composition and density, which has in turn shifted the low-mid elevation ponderosa pine and dry mixed-conifer forests from a relatively frequent, low- and mixed-severity regime to a higher-severity regime. Hence increased concern in the region over the potential for large damaging wildfires that are resistant to control. In particular, wildfire damages to structures in the wildland-urban interface (WUI) and municipal watersheds are key concerns [7, 10, 21, 31, 34, 35]. Notably, the 2012 High Park Fire in the study area resulted in 35,323 hectares burned, at least 259 homes destroyed, one casualty, and increased water treatment costs [5, 36]. Other high loss fire events from the region include the 2002 Hayman Fire (132 homes destroyed; 6 fatalities; human-caused), the 2010 Fourmile Canyon Fire (168 homes destroyed; human-caused), the 2012 Lower North Fork Fire (16 homes destroyed; 3 fatalities; human-caused), the 2012 Waldo Canyon Fire (346 homes destroyed; human-caused), and the 2013 Black Forest Fire (464 homes destroyed, 2 fatalities; human-caused) [21].

Here we opt to focus on National Forest lands to simplify our illustration. This is not meant to diminish the importance of other federal, state, and local land and fire management agencies operating within the case study landscape (e.g., Rocky Mountain National Park). Rather, it

http://dx.doi.org/10.5772/intechopen.76937

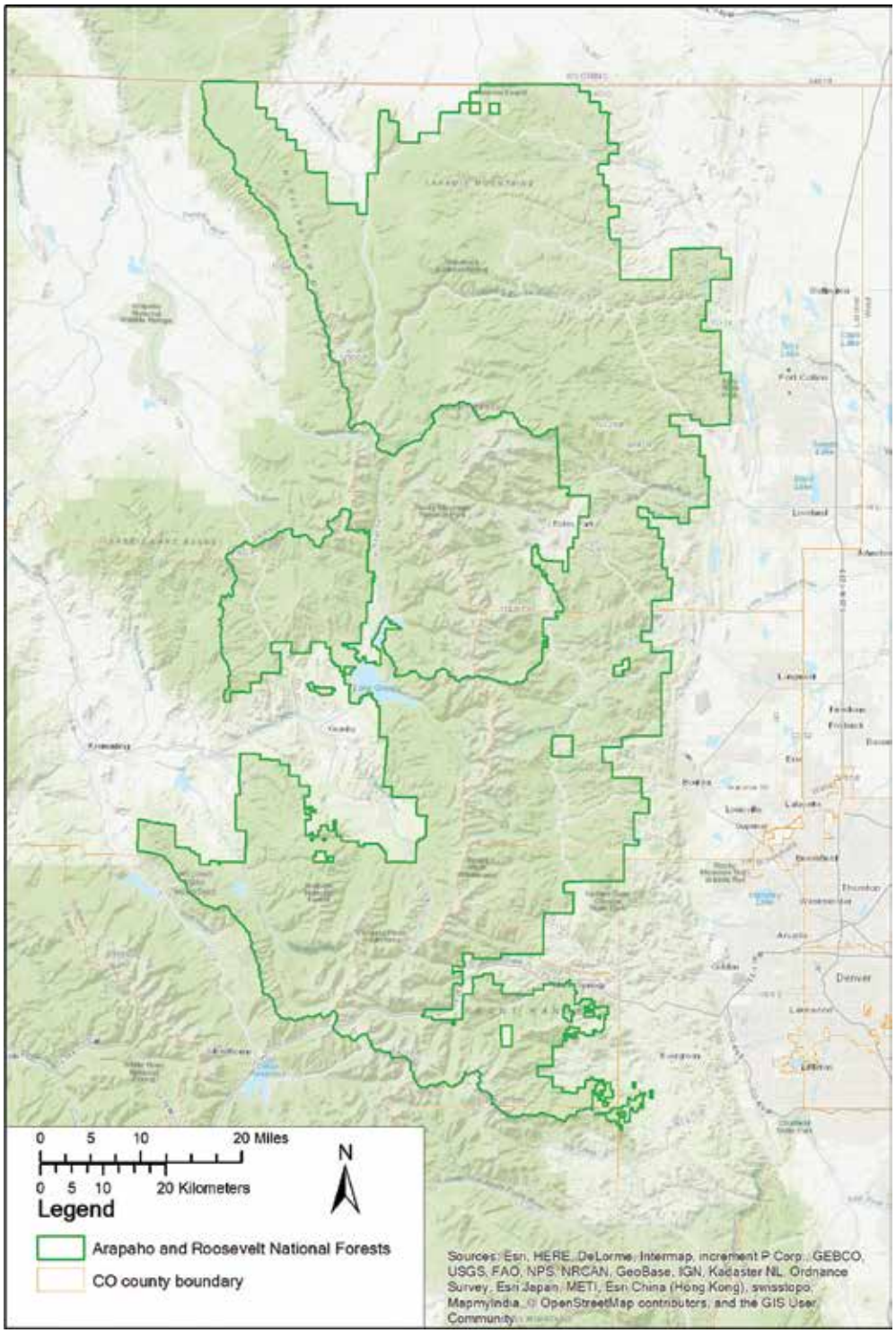

Figure 2. Study site including the Arapaho and Roosevelt National Forests.

allows us to focus particular attention on the problem of one-way risk transmission across ownership boundaries and its relevance to suppression difficulty and protection priority. Further, as of this writing, the Forests and local partners are actively involved in landscape-scale prioritization and planning efforts incorporating tSDI and POD products.

3. Materials and methods

3.1. Analysis framework

Table 1 presents a generalized framework for the types of variables included our analysis. The tSDI variables are calculated for every raster cell on the landscape, whereas other variables are summarized at the polygon-level for each POD. We describe the primary analytical steps in the following sub-sections.

3.2. Generate POD network

We generated PODs within our study area using GIS data and analysis techniques described in [25]. The boundaries between adjacent PODs are either major roads, streams, or ridge tops. Our assumption is that fire management activities such as enhancing natural fire breaks, constructing fireline, or conducting burn out operations could be performed along these geographic features. The geospatial layers for stream and ridge (catchment boundary) locations are acquired from the U.S. EPA and U.S. Geological Survey's NHDPlusV2 dataset, and the road transportation layers are acquired locally from the US Forest Service. Rather than identifying PODs for every hectare on the landscape, we limited our consideration to areas within and proximal to National Forest boundaries, and attempted to maintain a fairly contiguous analysis landscape.

The desired size distribution of PODs will vary with the scale of the planning application [22]. The process we use intentionally creates small PODs, relative to PODs created elsewhere for

Variable	Definition
Raster-level summaries	
tSDI	Terrestrial suppression difficulty index
SDI_AR	Ratio-scale index of relative tSDI and area ratios for predefined analysis units
POD-level summaries	
mSDI	Mean tSDI of all raster cells in POD
F2F	Forests to Faucets Surface Drinking Water Importance Score
dWUI	Areal density of structures in the WUI
PP_F2F	Protection priority for F2F
PP_dWUI	Protection priority for dWUI

Table 1. Primary variables in analysis.

the purposes of developing broad-scale strategic wildfire response zones [24]. This allows for identification of specific locations on the landscape that are high priority for protection, and facilitates targeted scheduling of activities like hazardous fuel reductions projects. The small-scale POD network could also facilitate optimal aggregation into larger PODs that are relatively homogenous with respect to suppression difficulty and protection demand.

3.3. Calculate tSDI

We used an automated Python script to calculate the tSDI across the case study landscape. The script requires raster inputs including fuel model, flame length, heat per unit area, roads, trails, digital elevation model, slope, aspect. tSDI is calculated for each raster cell based on the equations originally developed by [29] and later modified by [27]. SDI is a sum of six sub-indices: the energy behavior sub-index (I_{ce}, Eq. 1, a function of flame length (FL) and heat per unit area (HUA)), the accessibility sub-index (I_a), the mobility sub-index (I_m), the penetrability sub-index (I_p), aerial resources sub-index (I_{ar}) and fireline opening sub-index (I_c) (Eq. 2). The first five sub-indices each has a value that ranges from 1 to 10. The last sub-index has a value between 1 and 20. A_i is the area of each fuel model and A_t is the size of total study area managed within each cell or pixel. In our case, tSDI values were calculated at a 30 × 30 m resolution, which is identical to the resolution of the fuel models, so in practice the area adjustment ratio in Eq. 1 is always equal to one. Further, since we did not consider aerial resources, the value of I_{ar} is set to 0, and we quantify tSDI accordingly (Eq. 3). Based on these scaling coefficients, the final SDI values can range from 0 to 1.67 with all sub-indices included, and the final tSDI values can range from 0 to 2.5 with the aerial sub-index excluded.

$$I_{ce} = \left[\sum \left(\frac{2 \times FL_i \times HUA_i}{FL_i + HUA_i}\right) \times (A_i/A_t)\right] \tag{1}$$

$$SDI = \left[\frac{\sum (I_{ce})}{\sum \left(I_a + I_m + I_p + I_{ar} + I_c\right)}\right] \tag{2}$$

$$tSDI = \left[\frac{\sum (I_{ce})}{\sum \left(I_a + I_m + I_p + I_c\right)}\right] \tag{3}$$

Two critical inputs for calculating tSDI are fuel models and modeled fire behavior metrics. Our primary source for data on fuel models was LANDFIRE 2014 [37, 38]. We then updated these data to account for treatments and other disturbances that occurred on the landscape in the intervening years up to 2016. We used two sets of treatment mosaics to reflect the changing of fuel treatments within the study area: treated areas identified through the Front Range Round Table 2016 Interagency Fuel Treatment Database, and the USDA Forest Service's Natural Resource Manager Forest Activity Tracking System. We then distinguished the effects of different fuel treatment types (e.g., mastication, surface fuel treatment, prescribed fire, thin from below) and used rulesets to update the fuel models after corresponding treatment. To model fire behavior we used the FlamMap fire modeling system [39], using 90th percentile

weather conditions for fuel moisture conditions and wind speed/direction, drawn from the Redfeather Remote Automated Weather Station.

Finally, we mapped tSDI at four spatial scales of decreasing size, hereafter analysis units (**Table 2**). The rationale for scaling down tSDI values to within National Forest boundaries is to focus on suppression difficulty in relation to risk transmission and prospects for preventing fire from spreading onto adjacent lands. To compare tSDI values across predefined analysis units it was necessary to adjust by the respective area of these units. We defined ratio-scale indices (SDI_AR, **Table 1**) that relate ratios of total tSDI to ratios of total area across analysis units. Eq. 4 presents an example calculation for the F and P analysis units, where A_F and A_P are the area of each analysis unit. These ratios are always calculated using the larger analysis unit as the denominator. Where the index is equal to 1, it suggests that the difference in suppression difficulty across analysis units is directly proportional to the difference in area. Where the index is greater than 1, it suggests that suppression difficulty is disproportionately higher in the smaller analysis unit, and vice versa. Using these four analysis units, we arrive at six possible pairwise comparisons (F_P, B5_P, B2_P, B5_F, B2_F, and B2_B5).

$$SDI\_AR_{F-P} = \frac{(\sum tSDI_F / \sum tSDI_P)}{(A_F / A_P)} \tag{4}$$

3.4. Quantify protection demand and protection priority

To quantify protection demand we use variables related to the WUI and to municipal watersheds (**Table 1**). For the WUI layer, we used high resolution built structure data derived from [10]. We summarized total count of structures by POD, and then divided by total POD area to derive an areal density measure for each POD (dWUI, **Table 1**). For the watersheds layer, we used data obtained from the Forest Services's Forests to Faucets (F2F, **Table 1**) project [40]. Specifically we used a layer that assigns surface drinking water relative importance scores (0–100) to each 12-digit hydrologic unit code catchment. More information on this layer and its use in risk assessments can be found in [40, 41]. The data layer we use assigns each catchment a score on a range, and we use the midpoint of that range to assign each POD a unique surface drinking water importance score (e.g., 75 from 70 to 80). In cases where a POD overlapped multiple catchments, we used the importance score from the catchment that comprised the majority of POD area (across the case study landscape, on average the majority catchment selected accounted for >99% of total POD area).

Analysis Unit	Definition
P	Area within entire POD network
F	Area within National Forest boundaries
B5	Area within 5-km buffer internal to National Forest boundaries
B2	Area within 2-km buffer internal to National Forest boundaries

Table 2. Analysis units for analyzing tSDI ratios, sorted in order of decreasing size.

To quantify protection priority, we merged tSDI results with protection demand layers. We created individual priority indices for F2F and dWUI, which are calculated simply as the product of each POD's mSDI and its protection demand level. Eq. 5 presents an example of protection priority calculated for F2F.

$$PP\_F2F = mSDI * F2F \tag{5}$$

To identify "high" priority PODs, we sorted PODs on the basis of protection priority and selected only those with protection priority levels in the top 10th percentile for F2F and dWUI. We further identified which PODs, if any, were included in the top 10th percentile for both F2F and dWUI. These PODs we identify as "very high" priority.

4. Results

4.1. POD network

Figure 3 displays the POD network in relation to boundaries of the National Forests as well as the Forest to Faucets catchments. In total we identified 8772 PODs for further analysis, which ranged in size from <1 to 2532 hectares. The mean POD size was 125 hectares, and the median POD size was 63 hectares. For operational purposes users would likely make post-hoc adjustments to the POD network created through automation, for example eliminating very small PODs by incorporating them into adjacent PODs.

There are a few noteworthy observations. First, POD boundaries rarely align with Forest boundaries, but often align with catchment boundaries. Second, PODs are much smaller than catchments, such that each catchment may contain multiple PODs. This reflects our analytical process that uses smaller catchment boundaries as well as the presence of roads on the landscape. The full extent of this POD network corresponds to analysis unit P (**Table 2**), and is used for summarizing results in the remainder of this paper.

4.2. tSDI results

Figure 4 presents tSDI values mapped to the full extent of the POD network as depicted in **Figure 3**. Some patterns are immediately evident. High elevation areas along the Continental Divide have zero or near-zero tSDI values due to lack of burnable vegetation. The scar from the High Park Fire in the northeast portion of the landscape similarly has very low tSDI values. This appears as a break between an otherwise largely uninterrupted corridor of high tSDI values running along the eastern edge of the analysis area. Isolated patches of high tSDI values elsewhere appear at least partially driven by steep slopes, sometimes in remote or wilderness areas with low road density (see **Figure 2**).

The most notable aspect of **Figure 4** is the concentration of high tSDI values located on the eastern side of the analysis area. This simultaneously highlights the importance and challenge of fire management in these areas, where aggressive suppression would likely be warranted in

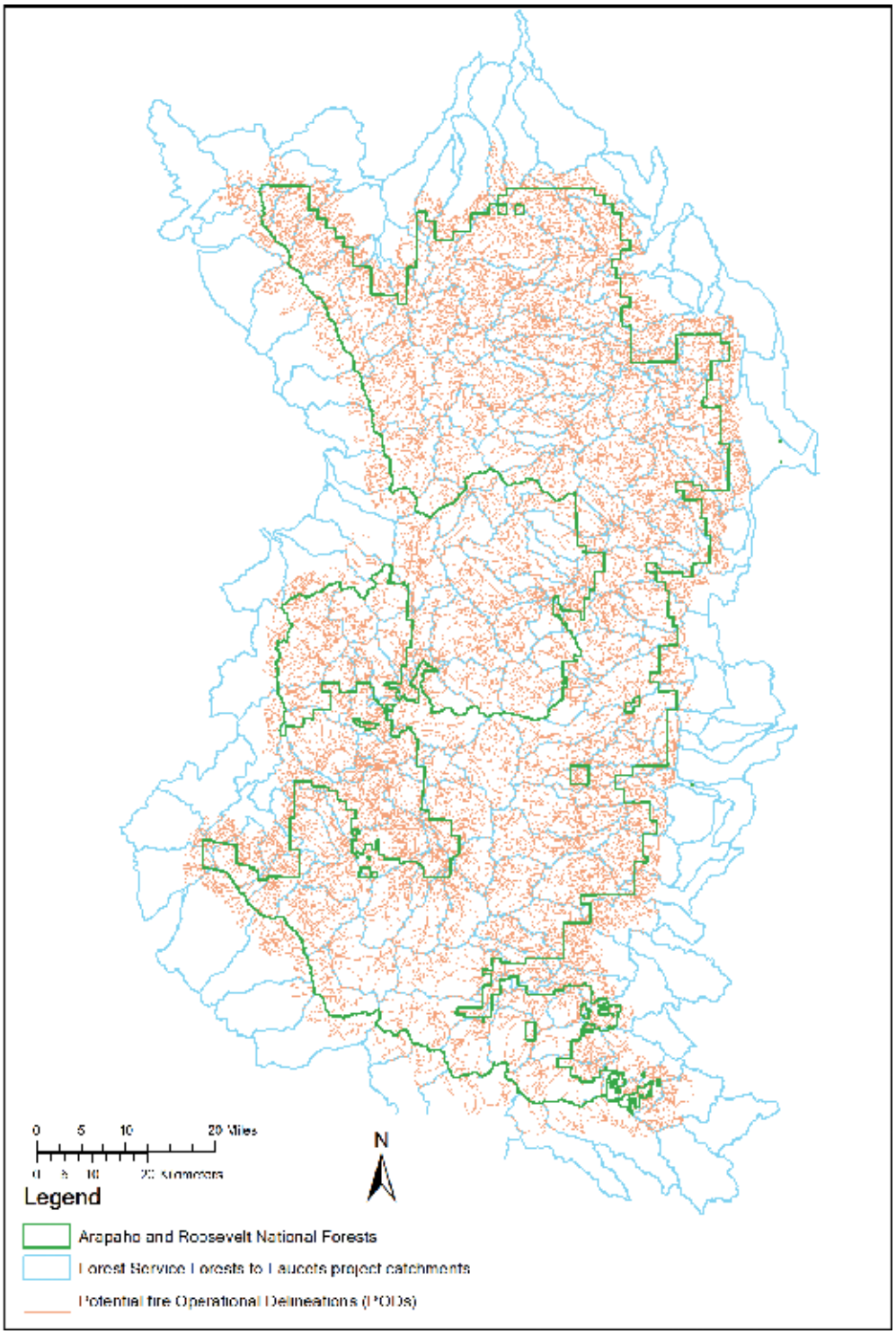

Figure 3. Derived POD network, overlaid with National Forest boundaries and Forests to Faucets catchment boundaries.

http://dx.doi.org/10.5772/intechopen.76937

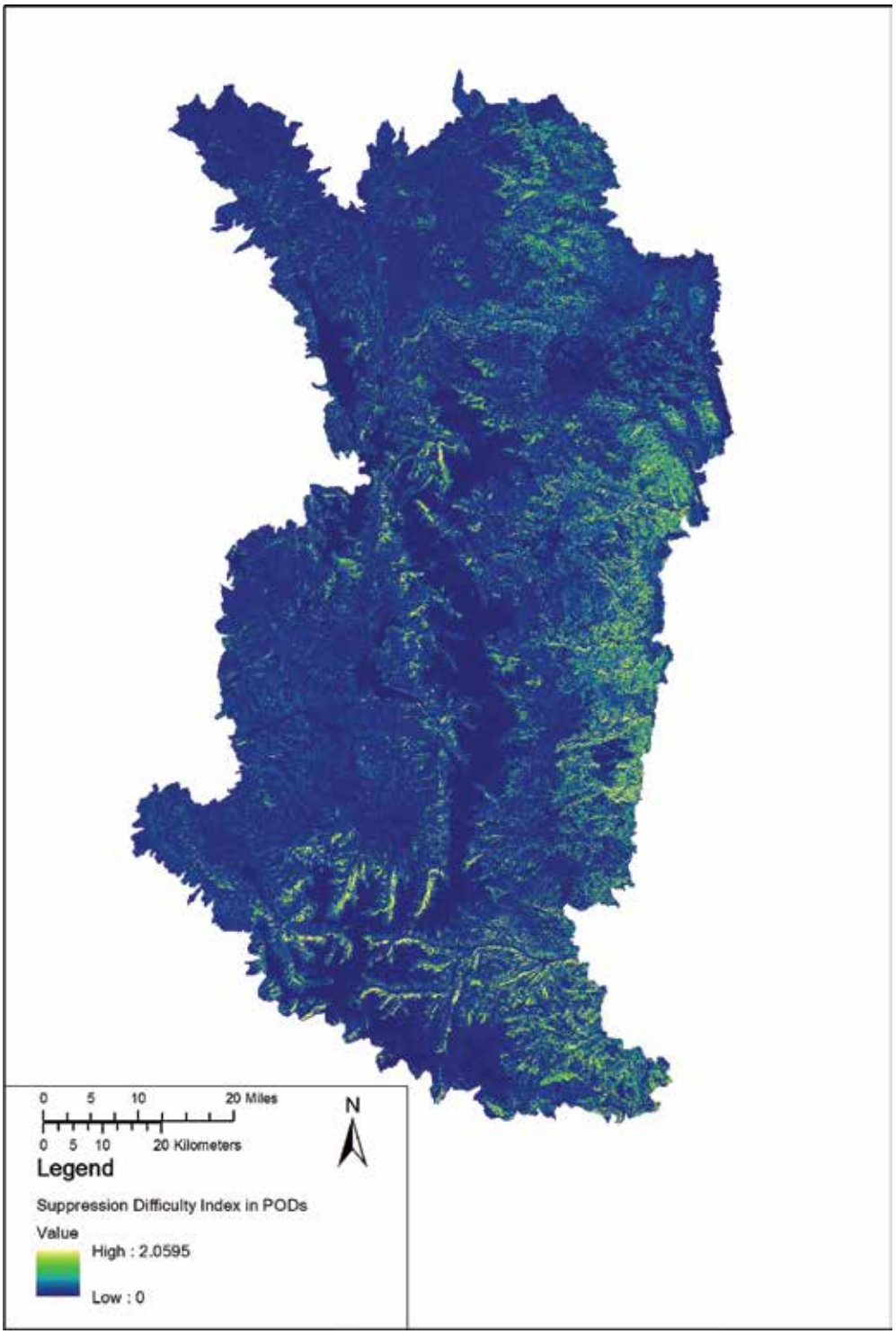

Figure 4. tSDI values mapped to the extent of the POD network (**Figure 3**).

order to avoid the spread of fire onto adjacent lands where fires could threaten the WUI and other infrastructure. The vast majority of cells on the landscape have low tSDI values: 46% are <0.1, 76% are <0.2, and 89% are <0.5. By contrast, only 4% have values >1.

Table 3 presents results for SDI_AR indices across all six analysis unit pairwise comparisons. All indices relating to the analysis unit P are >1, which reflects the spatial distribution of low tSDI values outside of National Forest boundaries (**Figure 4**). Buffers B5 and B2 are effectively proportional, but all have indices >1 with respect to units F and P. Findings suggest therefore that suppression would be more challenging proximal to Forest boundaries, such that the probability of failing to prevent risk transmission could be substantial. Notably, these ratios would be even higher if we limited our buffers to the eastern and southern edges of the POD network.

4.3. Protection demand and protection priority

Figure 5 displays POD-level summarization of F2F and dWUI protection demand. For F2F, importance scores ranged from 25 to 95, with a mean of 64.33 and a median of 65. For dWUI,

Analysis units	tSDI ratio	Area ratio	SDI-AR
F_P	0.66	0.64	1.04
B5_P	0.44	0.40	1.11
B2_P	0.22	0.20	1.12
B5_F	0.67	0.63	1.07
B2_F	0.33	0.31	1.07
B2_B5	0.50	0.50	1.00

Table 3. Ratio-scale indices comparing area-adjusted tSDI values within and across various analysis units.

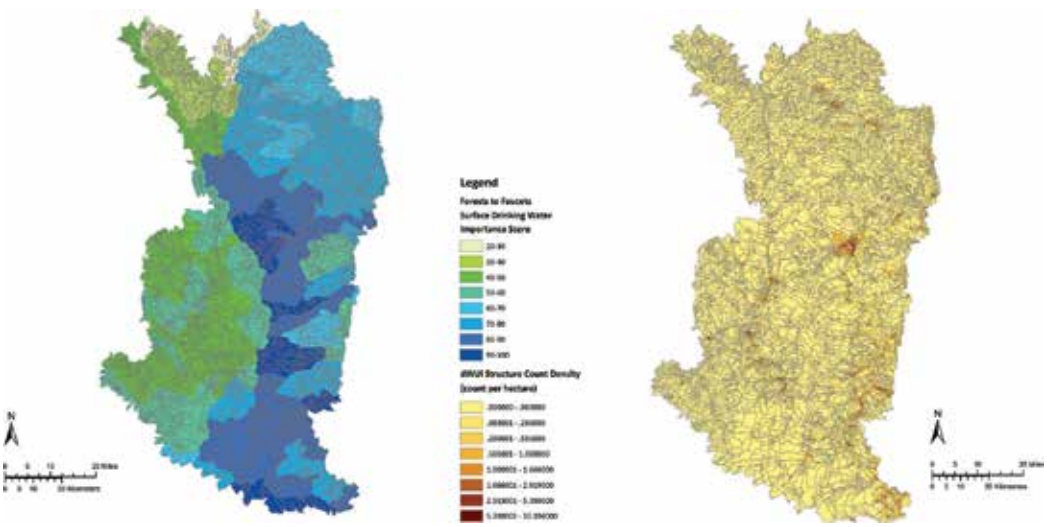

Figure 5. POD-level protection demand for F2F and dWUI.

structure density values ranged from 0 to 9.87, with a mean of 0.12 and a median of 0. A total of 5447 PODs contained zero structures, with a total of 62,359 structures contained within the remaining 3325 PODs. For F2F, the importance values differ sharply on the western and eastern sides of the Continental Divide, with the highest values generally located in the southeastern portion of the POD network. For dWUI, the highest values similarly occur in the eastern portions of the POD network, although generally further to the east than the highest F2F values.

Figure 6 displays a three-dimensional scatterplot of mSDI, F2F, and dWUI, along with two-dimensional slices for pairwise comparisons (dWUI vs. mSDI; dWUI vs. F2F; F2F vs. mSDI). The preponderance of low mSDI values is evident in the 3D scatterplot, with a corresponding lack of points clustered in the high-mSDI, high-F2F, and high-dWUI space. In terms of pairwise comparisons, higher dWUI values tend to be align with lower mSDI values, which could in part reflect higher road densities and shallower slopes commonly associated with higher density human development. There is slight positive association with dWUI and F2F, particularly noticeable for the surface water importance scores of 85, which suggests opportunity to readily identify some PODs as very high protection demand. Referring back to **Figure 5**, some of these PODs are located near the community of Estes Park in the central-eastern

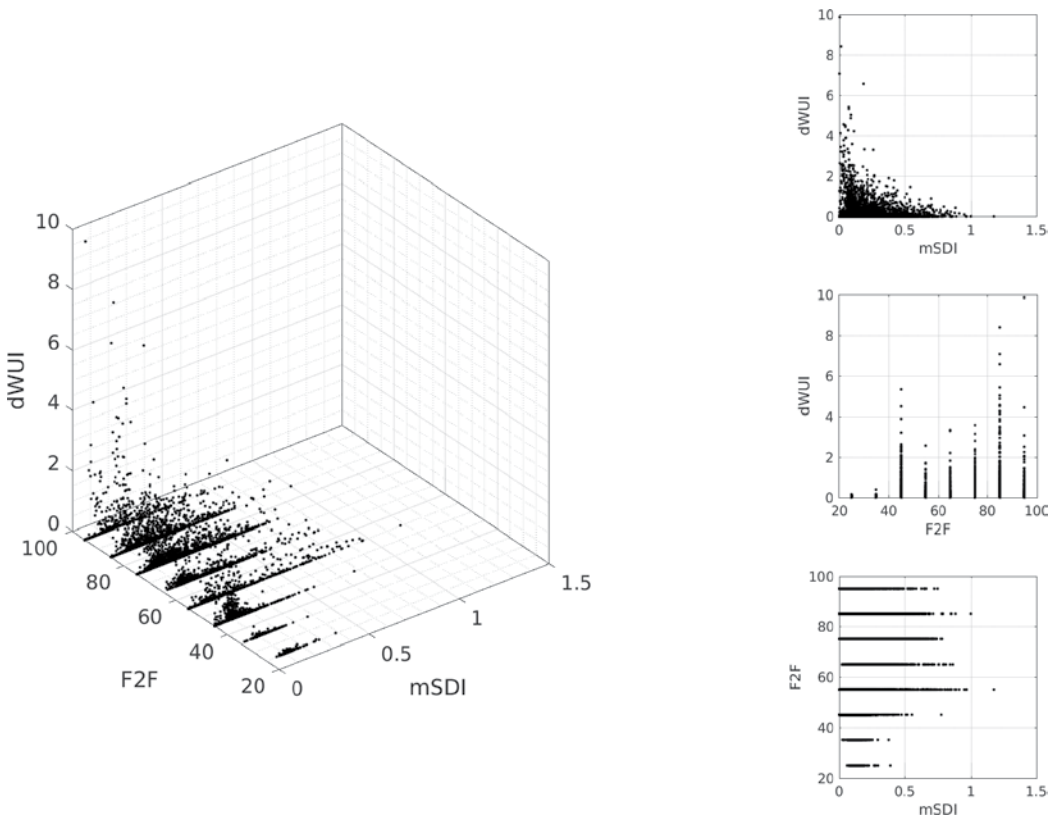

Figure 6. Three-dimensional scatterplot of mSDI, dWUI, and F2F, along with two-dimensional slices for pairwise comparisons.

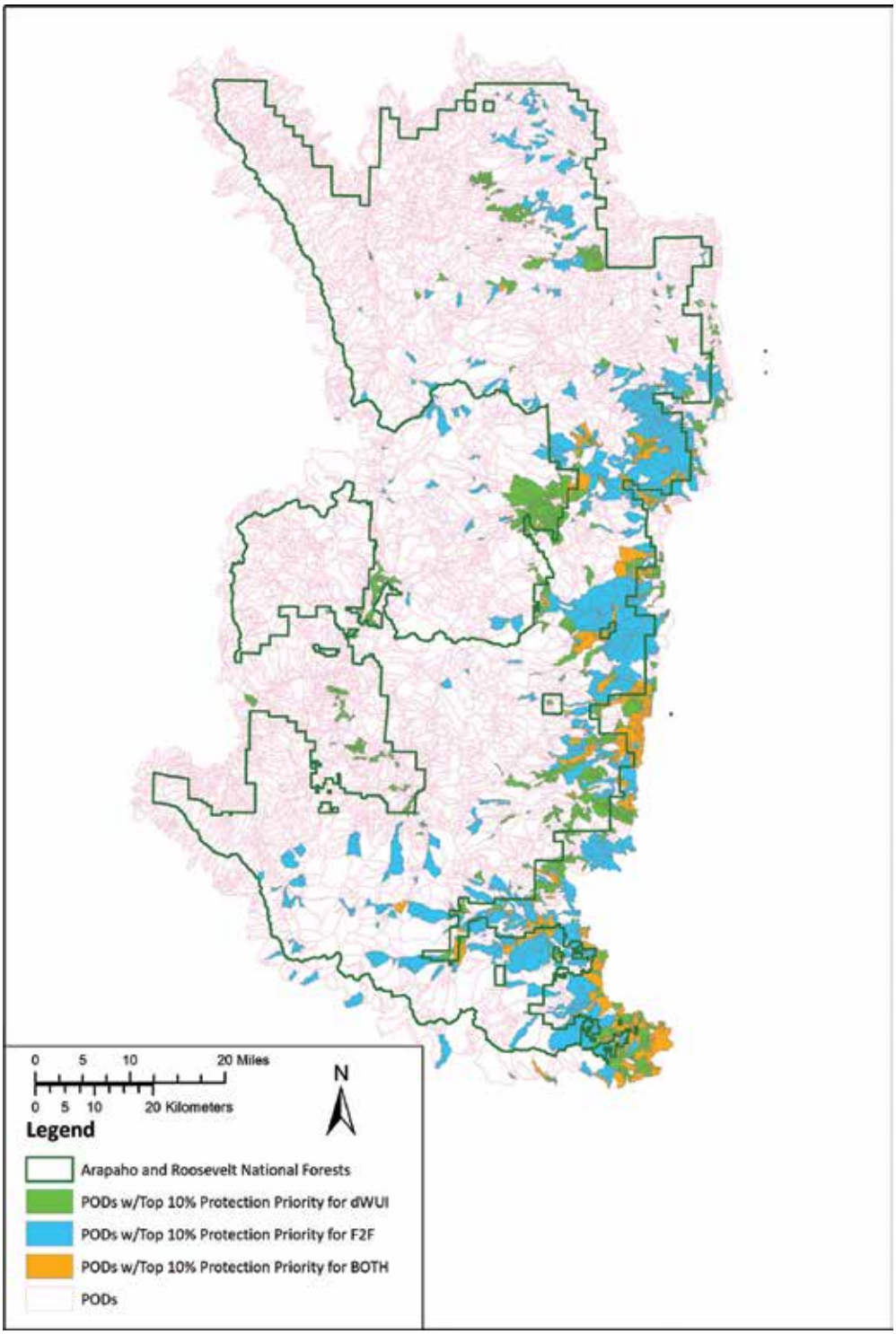

Figure 7. POD-level protection priority for F2F, dWUI, and both.

portion of the map. Lastly, F2F and mSDI values tend to show little relationship, apart from lower mSDI values tending to align with lower F2F values.

Figure 7 displays the PODs identified as "high" and "very high" protection priority. In total 1524 PODs are identified, 646 each that correspond to the top 10th percentile for either PP_F2F or PP_dWUI (**Table 1**, Eq. 5), and 232 of which correspond to PODs in the top 10th percentile for both. To reiterate, the latter category is what we deem to be "very high" protection priority. Not surprisingly given results in **Figures 4** and **5**, the greatest levels of protection priority run along the eastern flank of the POD network, many of which are within National Forest boundaries. The joint concentration of high suppression difficulty and high protection demand highlight this area as for preventative risk management activities.

5. Discussion

Two primary innovations we introduce here are the summarization of tSDI within various analytical units to determine differences in area-adjusted suppression difficulty, and the summarization of tSDI within PODs to determine protection priorities. Notably, we attempted to expand the concept of risk transmission to include opportunities to safely and effectively restrict fire spread across ownership boundaries. The incorporation of suppression difficulty and control opportunities has, to date, been largely absent from the literature on wildfire risk transmission. What we presented here ideally informs decisions related to the need for suppression where protection demand is high, as well as decisions related to the need for suppression where the potential for risk transmission is high.

There are a number of foreseeable near- and long-term extensions to this work. Perhaps most immediate, the analysis could be extended across multiple ownerships to create a common operating picture for co-management of risk. Models of fire spread and containment could be updated to account for suppression difficulty, and could be used to game out various scenarios and alternative response strategies [42]. Similarly, models designed to optimize initial attack response could be updated to account for variable suppression resource needs as a function of tSDI [43]. Calculating tSDI values under different weather scenarios could be informative for gaming out how suppression opportunities change with conditions, and could further serve as the basis for prioritization of fuel treatment investments designed to enhance suppression effectiveness [44]. Analysis of tSDI values along POD boundaries could identify potential weakness in the POD network, which could also help inform prioritization of fuel treatments.

Incorporating structure and watershed susceptibility to fire through more rigorous fire effects analysis, as well as incorporating fire likelihood, would likely allow for targeted identification of protection priority [41]. It is not necessarily the case that higher F2F importance weights imply higher potential for post-fire erosion, for example, or that higher mSDI values imply higher intensity fire leading to greater damage. Opting for more refined risk assessment of course comes with greater investment of time and resources, a tradeoff which must be evaluated in light of the marginal value that is added for decision processes [13]. This point encapsulates a common aspect of designing and delivering decision support, which is that modeling frameworks do not necessarily need to be complicated to demonstrate potential

utility, and further that not every application requires a complicated solution. Lastly, the tSDI layers, along with the basic concept of suppression difficulty, could be broadened to include factors such as safety zones, egress routes, and the impacts of other disturbances on fire behavior and resistance to control [45, 46].

6. Conclusion

The work presented in this chapter represents incremental improvement in wildfire decision support by integrating information on suppression difficulty with information on demand for protection of important fire-susceptible assets. By summarizing tSDI within PODs, and further by summarizing area-adjusted tSDI values in different analysis units, we are able to pinpoint areas of high concern in relation to suppression opportunity and risk transmission. We identified a case study landscape where a high density of human development in areas with increased fire hazard presents significant forest and fire management challenges. More importantly, we were able to work with local managers to assimilate this information into ongoing assessment and planning processes. As of this writing, the layers we developed on tSDI, dWUI, and F2F are being incorporated into a geodatabase that will be delivered to the Arapaho and Roosevelt National Forests to facilitate landscape prioritization and support real-time fire incident response.

In summary, we developed techniques to study the opportunity and viability of conducting fire suppression to manage fire risks at high priority locations, and to facilitate targeted identification of those high priority areas. Results can help fire managers understand how and where fire management activities could be planned and implemented to mitigate fire threats. In this chapter, we demonstrated not only proof-of-concept, but also results that delivered actionable information to local fire managers. We aim to continue to improve techniques and relevance of decision support through additional science-management partnerships, and hope this chapter inspires other fire scientists to do the same.

Acknowledgements

Christopher D O'Connor shared a Python script to calculate tSDI and provided rulesets to update fuel models. Alex Masarie helped with data visualization. This research was partially funded by the Colorado Agriculture Experimental Station project COL0050 and by the 14-JV-11221636-029 project between the USDA Forest Service Rocky Mountain Research Station and Colorado State University. The National Fire Decision Support Center also supported this effort.

Conflict of interest

The authors declare no conflict of interest.

Author details

Matthew P Thompson[1]*, Zhiwei Liu[2], Yu Wei[2] and Michael D Caggiano[2]

*Address all correspondence to: mpthompson02@fs.fed.us

1 United States Department of Agriculture Forest Service, Fort Collins, CO, USA

2 Colorado State University, Fort Collins, CO, USA

References

[1] Boisramé G, Thompson S, Collins B, Stephens S. Managed wildfire effects on forest resilience and water in the Sierra Nevada. Ecosystems. 2017;**20**(4):717-732

[2] Parks SA, Holsinger LM, Miller C, Nelson CR. Wildland fire as a self-regulating mechanism: The role of previous burns and weather in limiting fire progression. Ecological Applications. 2015;**25**(6):1478-1492

[3] Gómez-González S, Ojeda F, Fernandes PM. Portugal and Chile: Longing for sustainable forestry while rising from the ashes. Environmental Science & Policy. 2018;**81**:104-107

[4] Liu JC, Pereira G, Uhl SA, Bravo MA, Bell ML. A systematic review of the physical health impacts from non-occupational exposure to wildfire smoke. Environmental Research. 2015;**136**:120-132

[5] Writer JH, Hohner A, Oropeza J, Schmidt A, Cawley KM, Rosario-Ortiz FL. Water treatment implications after the high Park wildfire, Colorado. Journal of American Water Works Association. 2014;**106**(4):E189-E199

[6] Gill AM, Stephens SL. Scientific and social challenges for the management of fire-prone wildland–urban interfaces. Environmental Research Letters. 2009;**4**(3):034014

[7] Liu Z, Wimberly MC, Lamsal A, Sohl TL, Hawbaker TJ. Climate change and wildfire risk in an expanding wildland–urban interface: A case study from the Colorado Front Range Corridor. Landscape Ecology. 2015;**30**(10):1943-1957

[8] Bar-Massada A, Stewart SI, Hammer RB, Mockrin MH, Radeloff VC. Using structure locations as a basis for mapping the wildland urban interface. Journal of Environmental Management. 2013;**128**:540-547

[9] Scott JH, Thompson MP, Gilbertson-Day JW. Exploring how alternative mapping approaches influence fireshed assessment and human community exposure to wildfire. GeoJournal. 2017;**82**(1):201-215

[10] Caggiano MD, Tinkham WT, Hoffman C, Cheng AS, Hawbaker TJ. High resolution mapping of development in the wildland-urban interface using object based image extraction. Heliyon. 2016;**2**(10):e00174

[11] Pacheco AP, Claro J, Fernandes PM, de Neufville R, Oliveira TM, Borges JG, Rodrigues JC. Cohesive fire management within an uncertain environment: A review of risk handling and decision support systems. Forest Ecology and Management. 2015;**347**:1-17

[12] Calkin DE, Cohen JD, Finney MA, Thompson MP. How risk management can prevent future wildfire disasters in the wildland-urban interface. Proceedings of the National Academy of Sciences. 2014;**111**(2):746-751

[13] Thompson MP, Haas JR, Gilbertson-Day JW, Scott JH, Langowski P, Bowne E, Calkin DE. Development and application of a geospatial wildfire exposure and risk calculation tool. Environmental Modelling & Software. 2015;**63**:61-72

[14] Papakosta P, Xanthopoulos G, Straub D. Probabilistic prediction of wildfire economic losses to housing in Cyprus using Bayesian network analysis. International Journal of Wildland Fire. 2017;**26**(1):10-23

[15] Chuvieco E, Aguado I, Jurdao S, Pettinari ML, Yebra M, Salas J, Hantson S, de la Riva J, Ibarra P, Rodrigues M, Echeverría M. Integrating geospatial information into fire risk assessment. International Journal of Wildland Fire. 2014;**23**(5):606-619

[16] Castillo ME, Molina JR, Silva FR, García-Chevesich P, Garfias R. A system to evaluate fire impacts from simulated fire behavior in Mediterranean areas of Central Chile. Science of the Total Environment. 2017;**579**:1410-1418

[17] Alcasena FJ, Salis M, Ager AA, Castell R, Vega-García C. Assessing wildland fire risk transmission to communities in northern Spain. Forests. 2017;**8**(2):30

[18] Price O, Borah R, Bradstock R, Penman T. An empirical wildfire risk analysis: The probability of a fire spreading to the urban interface in Sydney, Australia. International Journal of Wildland Fire. 2015;**24**(5):597-606

[19] Scott JH, Thompson MP, Gilbertson-Day JW. Examining alternative fuel management strategies and the relative contribution of National Forest System land to wildfire risk to adjacent homes—A pilot assessment on the Sierra National Forest, California, USA. Forest Ecology and Management. 2016;**362**:29-37

[20] Ager AA, Day MA, Finney MA, Vance-Borland K, Vaillant NM. Analyzing the transmission of wildfire exposure on a fire-prone landscape in Oregon, USA. Forest Ecology and Management. 2014;**334**:377-390

[21] Haas JR, Calkin DE, Thompson MP. Wildfire risk transmission in the Colorado Front Range, USA. Risk Analysis. 2015;**35**(2):226-240

[22] Dunn CJ, Thompson MP, Calkin DE. A framework for developing safe and effective large-fire response in a new fire management paradigm. Forest Ecology and Management. 2017; **404**:184-196

[23] Thompson MP, MacGregor DG, Calkin DE. Risk management: Core principles and practices, and their relevance to Wildland Fire. USDA Forest Service, Rocky Mountain

Research Station. In: General Technical Report: RMRS-GTR-350; Fort Collins, CO, USA; 2016

[24] Thompson MP, Bowden P, Brough A, Scott JH, Gilbertson-Day J, Taylor A, Anderson J, Haas JR. Application of wildfire risk assessment results to wildfire response planning in the southern Sierra Nevada, California, USA. Forests. 2016;**7**(3):64

[25] Wei Y, Thompson M, Haas JR, Dillon GK, O'Connor CD. Spatial optimization of operationally relevant large fire confine and point protection strategies: Model development and test cases. Canadian Journal of Forest Research. 2018;**48**(999):1-14

[26] O'Connor CD, Calkin DE, Thompson MP. An empirical machine learning method for predicting potential fire control locations for pre-fire planning and operational fire management. International Journal of Wildland Fire. 2017;**26**(7):587-597

[27] O'Connor CD, Thompson MP, Rodríguez y Silva F. Getting ahead of the wildfire problem: Quantifying and mapping management challenges and opportunities. Geosciences. 2016; **6**(3):35

[28] Rodríguez y Silva F, González-Cabán A. Contribution of suppression difficulty and lessons learned in forecasting fire suppression operations productivity: A methodological approach. Journal of Forest Economics. 2016;**25**:149-159

[29] Rodríguez y Silva F, Martínez JRM, González-Cabán A. A methodology for determining operational priorities for prevention and suppression of wildland fires. International Journal of Wildland Fire. 2014;**23**(4):544-554

[30] Thompson MP, Riley KL, Loeffler D, Haas JR. Modeling fuel treatment leverage: Encounter rates, risk reduction, and suppression cost impacts. Forests. 2017;**8**(12):469

[31] Thompson MP, Gilbertson-Day JW, Scott JH. Integrating pixel-and polygon-based approaches to wildfire risk assessment: Application to a high-value watershed on the Pike and San Isabel National Forests, Colorado, USA. Environmental Modeling and Assessment. 2016;**21**(1):1-15

[32] USFS. NFS Acreage by State, Congressional District and County. 2007. Available from: https://www.fs.fed.us/land/staff/lar/2007/TABLE_6.htm

[33] Addington RN, Aplet GH, Battaglia MA, Briggs JS, Brown PM, Cheng AS, Dickinson Y, et al. Principles and practices for the restoration of ponderosa pine and dry mixed-conifer forests of the Colorado front range. Vol. 121, No: RMRS-GTR-373. Fort Collins, CO: US Department of Agriculture, Forest Service, Rocky Mountain Research Station; 2018. p. 373

[34] Warziniack T, Thompson M. Wildfire risk and optimal investments in watershed protection. Western Economics Forum. 2013;**12**(2):19-28

[35] Jones KW, Cannon JB, Saavedra FA, Kampf SK, Addington RN, Cheng AS, MacDonald LH, Wilson C, Wolk B. Return on investment from fuel treatments to reduce severe wildfire and erosion in a watershed investment program in Colorado. Journal of Environmental Management. 2017;**198**:66-77

[36] High Park Burned Area Emergency Response (BAER) Report. 2012. Available from: https://www.nrcs.usda.gov/Internet/FSE_DOCUMENTS/nrcs144p2_061214.pdf

[37] Ryan KC, Opperman TS. LANDFIRE—A national vegetation/fuels data base for use in fuels treatment, restoration, and suppression planning. Forest Ecology and Management. 2013;**294**:208-216

[38] LANDFIRE. 2014. Available from: https://www.landfire.gov/lf_140.php

[39] Finney MA. An overview of FlamMap fire modeling capabilities. In: Fuels Management—How to Measure Success: Conference Proceedings; Fort Collins, CO: USDA Forest Service, Rocky Mountain Research Station; March, 2006. pp. 28-30

[40] USDA Forest Service. Forests to Faucets. Available online: http://www.fs.fed.us/ecosystem-services/FS_Efforts/forests2faucets.shtml

[41] Thompson MP, Scott J, Langowski PG, Gilbertson-Day JW, Haas JR, Bowne EM. Assessing watershed-wildfire risks on national forest system lands in the rocky mountain region of the United States. Water. 2013;**5**(3):945-971

[42] Riley KL, Thompson MP, Scott JH, Gilbertson-Day JW. A model-based framework to evaluate alternative wildfire suppression strategies. Resources. 2018;**7**(1):4

[43] Wei Y, Bevers M, Belval E, Bird B. A chance-constrained programming model to allocate wildfire initial attack resources for a fire season. Forest Science. 2015;**61**(2):278-288

[44] Wei Y. Optimize landscape fuel treatment locations to create control opportunities for future fires. Canadian Journal of Forest Research. 2012;**42**(6):1002-1014

[45] Dennison PE, Fryer GK, Cova TJ. Identification of firefighter safety zones using lidar. Environmental Modelling & Software. 2014;**59**:91-97

[46] Page WG, Alexander ME, Jenkins MJ. Wildfire's resistance to control in mountain pine beetle-attacked lodgepole pine forests. The Forestry Chronicle. 2013;**89**(6):783-794

Chapter 4

Assessment of the Riparian Vegetation Changes Downstream of Selected Dams in Vhembe District, Limpopo Province on Based on Historical Aerial Photography

John M. Mokgoebo, Tibangayuka A. Kabanda and Jabulani R. Gumbo

Additional information is available at the end of the chapter

http://dx.doi.org/10.5772/intechopen.78329

Abstract

Dams have been associated with various impacts on downstream river ecosystems, including a decrease in stream flow, species biodiversity, water quality, altered hydrology and colonisation of the area by invasive alien plant species. The impacts normally interfere with the ecosystem functioning of riparian and aquatic environments, thereby leading to decreased biodiversity. This study aims to assess the impacts of dams on downstream river ecosystems, using data from aerial photographs and orthophotos, supplemented by field work. Five dams in Limpopo Province, South Africa, were selected (Albasini, Damani, Mambedi, Nandoni and Vondo), and photographs from different years were used. The area devoid of trees of certain species both downstream and upstream of the dams was calculated using grids of predetermined square sizes on each available photograph. Aerial photographs and orthophoto data were supplemented by field work. The nearest-individual method was used in the field to determine tree density of particular tree species. The environments downstream of the dams show a loss of obligate riparian vegetation and an increase of obligate terrestrial vegetation (*Acacia Karroo, Acacia Ataxacantha* and *Bauhinia galpinii*). Treeless area increased in all cases, especially in the case of Mambedi and Vondo dams, indicating lower resilience and higher fragility there.

Keywords: downstream, upstream, aerial orthophoto, riparian vegetation, damming of rivers

1. Introduction

Dams across the world have been associated with many negative environmental, social and economic impacts. In particular, dams tend to affect downstream water flow, leading to vegetation species loss. Many dammed rivers around the world have been characterised by decline in species biodiversity, increase in invasive alien plants and pollution. Mumba and Thompson [1] argue that flow disturbance provides stimulus for the establishment of opportunistic plants, particularly alien invasive species. In Limpopo, the most northerly province of South Africa, the impacts of dams have also been accelerated by the alternating wet and dry climatic conditions that greatly affect the flow regimes of rivers. This is because dams create barriers to natural water flow and interfere with ecological processes of riparian zones that influence vegetation composition, richness and diversity [2]. Dams have been associated with water pollution generated from industries and agricultural sectors, such as the release of litter, hot water, pesticides and fertilisers into streams and rivers [3].

The decrease in downstream flow is strongly associated with negative impacts on downstream riparian ecosystems. The decrease in water quality and quantity downstream alters the vegetation composition, natural irrigation of floodplains and microclimates. These downstream impacts are associated with a decrease in biological diversity, changes in successional stages, altered biogeochemical cycles and alteration of downstream natural ecosystems. Toxins that accumulate in dams can be released during flush periods and is often accompanied by irreparable damage to the downstream environment. The presence of dam results in landscape modification and changes in hydrology, channel morphology and physiochemical properties result in the dramatic decrease in biodiversity in riparian and aquatic ecosystems (upstream & downstream) [4]. About half of South Africa's rainfall is stored in dams [5]. There are about 550 government dams that carry about approximately 37 million m^3 of water. There are about 25 registered dams in Limpopo Province [6].

The dams of Limpopo, with much of the Province characterised by wet-dry climatic cycles have remarkable and sometimes irreversible impacts on downstream ecosystems. These dams usually change vegetation composition, reduce species diversity, alter flow characteristics and encourage alien species invasion that alter the ecosystem functioning of rivers downstream. Need therefore arises that the impact of these dams on their downstream river ecosystems be studied using historical aerial photograph data to determine whether the upstream existence of dams impacts on downstream vegetation density. The main purpose of the study was to use historical aerial photography to assess the impact of selected Luvuvhu/Mutale dams of the Limpopo Province on their downstream river ecosystems. The specific objectives were to study the nature of vegetation changes along downstream river courses, and to compare upstream and downstream vegetation species richness.

2. Materials and methods

The study area is riverine vegetation that is located upstream and downstream of the following dams: Albasini, Nandoni, Damani, Mambedi and Vondo dam that are located in Vhembe

http://dx.doi.org/10.5772/intechopen.78329

district, Limpopo province of South Africa. The major rivers Luvuvhu and Mutshindudi originate from Soutpansberg Mountains and the vegetation types range from co-regions 2.01 Sour Lowveld Bushveld, Soutpansberg Arid Mountain Bushveld and patches of Afromontane Forest to the eco-regions to 2.15 Northeastern Mountain Grassland and Afromontane Forest [8].

2.1. The study area

2.1.1. Albasini dam

The dam is situated at 23°06′25″S and 30°07′30″E. It was built on the Luvuvhu River in 1952 and was raised by means of spillway gates in 1970/1971. The dam was built to supply water to the Levubu Irrigation Scheme to irrigate tropical fruits such as bananas, litchis, mangos, avocados and macadamia nuts (**Figure 1**). Its maximum water carrying capacity is 25.6×10^6 m^3 [6]. It lies 22 km south-east of Makhado (formerly Louis Trichardt) and approximately 45 km west (upstream) of the Nandoni dam, which also lies on the Luvuvhu River. It has a surface area of 350 ha. The rainfall station in the vicinity of the dam is Goedehoop.

2.1.2. Damani dam

The Damani dam is on the Mbwedi River and was established in 1991 (**Figures 1** and **2**). The dam is situated at 22°50′07″S and 30°31′22″E and was built to supply water to the former Damani Coffee Estate which required $4.08\times10^6 m^3$ per annum. It supplies irrigation water to the surrounding commercial farms owned by local community members. Its maximum water carrying capacity is 12.4×10^6 m^3 and it has a surface area of 130 ha [6].

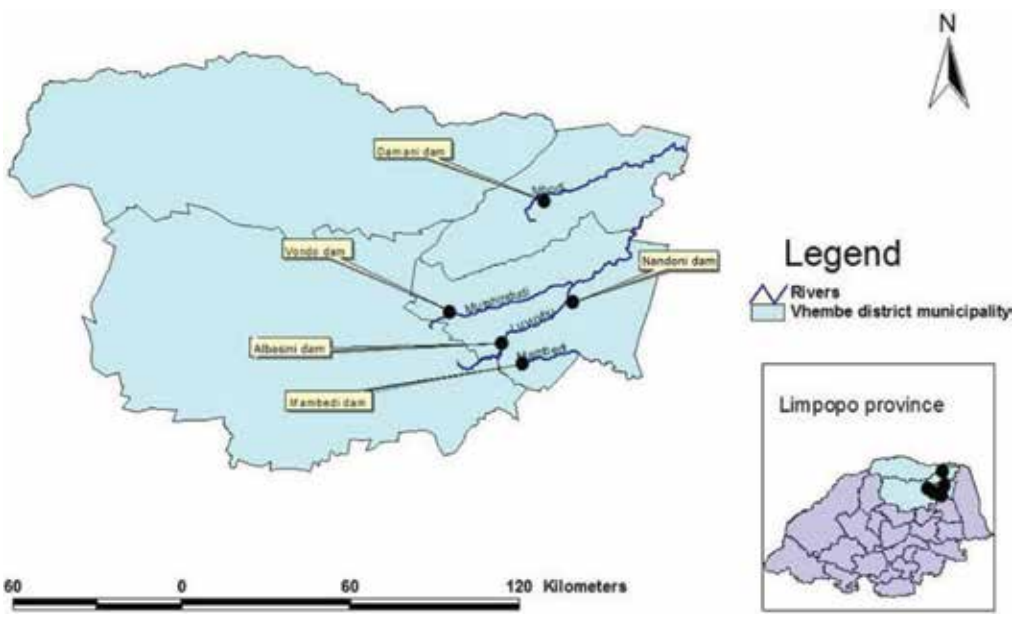

Figure 1. The locations of selected dams in the study area.

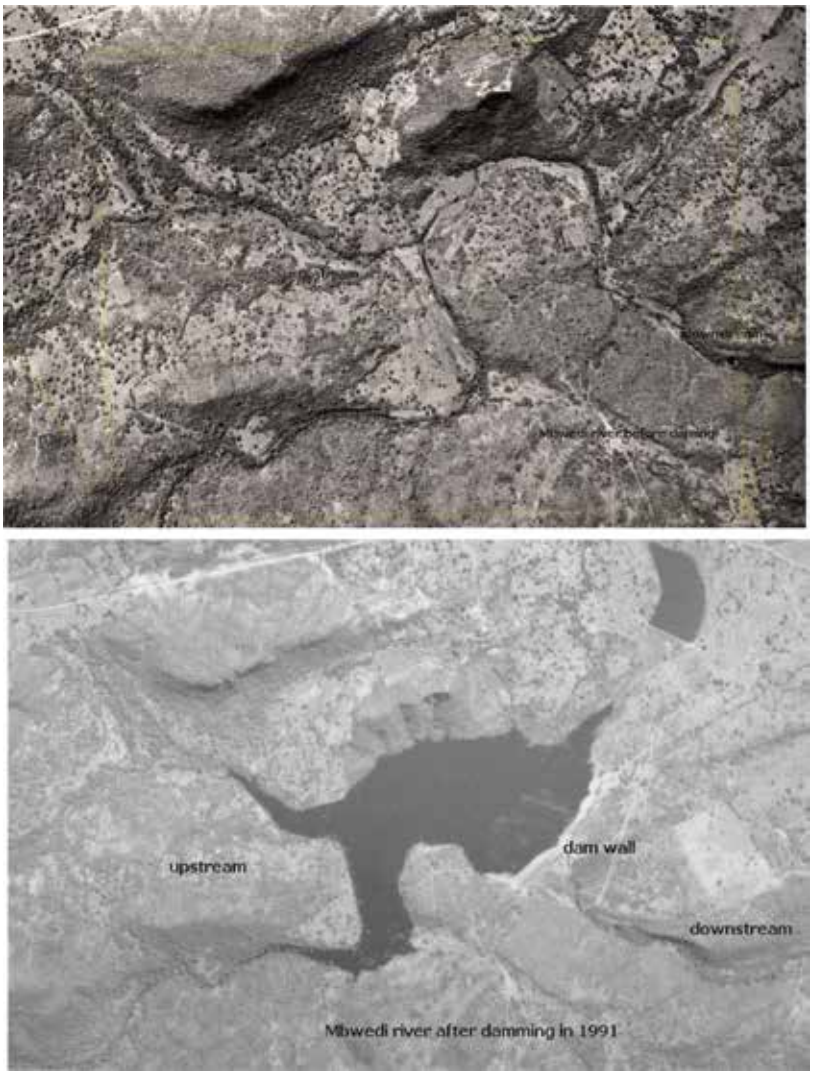

Figure 2. The riverine vegetation along Mbwedi River before the damming (top) and after construction of the Damani dam (bottom).

2.1.3. Mambedi dam

The dam was built on the Mambedi River to supply water to the Sapekoe Tea Company. The dam suffered a partial collapse in the year 2000 after its wall failed to contain an increase in flow during the heavy downpour caused by cyclone Eline. The dam had a carrying capacity of 7×10^6 m^3 prior to its collapse. This left the dam completely non-functional. The dam is situated at 23°07′27″S and 30°13′13″E [6].

http://dx.doi.org/10.5772/intechopen.78329

2.1.4. Nandoni dam

The Nandoni dam lies on the Luvuvhu River and was constructed in 2005. The dam is situated at 22°56′ 45″S and 30°20′07″ E. It was completed in 2009 and its water carrying capacity is $163\times10^6 m^3$ [6]. The dam has a surface area of 1570 ha. The Nandoni dam lies 40 km east (downstream) of the Albasini dam. It was built to supply water to the Nandoni water works and provide water for small scale irrigation [6].

2.1.5. Vondo dam

The Vondo dam was established in 1982 on the Mutshindudi River near Thohoyandou and Sibasa. The dam is situated at 22°56′45″S and 30°20′07″E. It has a capacity of 30.54×10^6 m^3 and a surface area of 219 ha. It was built to supply water to the Tate-Vondo Tea Estate [6].

2.2. The characteristics of the vegetation in the selected study area

A check sheet for vegetation data was used. This was used to record data on vegetation type, morphology and density. Data for these variables were collected both upstream and downstream of the dams. Before the actual collection of data a pilot survey was done to record the type of vegetation found along the major river courses of the Luvuvhu and Mutale river catchment. This was done to study the ecological setting of the study area and to identify points where data were to be sampled. Vegetation was categorised into trees, shrubs and herbs. All three life forms where identified in the field and measurements were done to determine pattern of vegetation change and density both downstream and upstream of the dams. Pattern of change was identified by studying vegetation composition along riparian zones both upstream and downstream of the dams to compare vegetation composition associated with water-deficient (downstream) and water-rich (upstream) environments. This was done to establish whether there was an increase in terrestrial vegetation along dry and wet riparian zones and to assess changes in morphological characteristics of the vegetation (whether short, dispersed or clustered).

Tree density was considered as the concentration of *Acacia* tree species within a given area, expressed in square meters. The nearest individual method of Kent and Coker [7]) and the simple plotless sampling was carried out to measure tree density. Since the study area was characterised by tall, dense and sometimes scattered trees, plotless sampling as a form of random sampling was used. Dense, sparse and tall tree species of the area limited the use of quadrants and other probabilistic sampling methods. With plotless sampling, sampled points were randomly selected using random walk procedures. These sampled points are called random walk points. The random walk points were chosen using random numbers selected from a random number table. The first selected random number represented the direction of the location of the random walk point. A standard prismatic compass was used to measure the direction of the randomly selected spots, ranging from 0 to 360°. The second random number represented the distance that was travelled to locate a sampled point, in the direction that was previously chosen. Tree density measurements were taken at 16 random walk points around each dam – 8 upstream and 8 downstream of the dam.

All the random walk points were used as starting points to measure tree density using the nearest individual method. For each selected spot a total of five distance measurements were taken and all measurements were averaged to determine the mean distance of each tree species from the random walk point. Acacia tree species were used for the purpose of this measurement. A 30 m tape was used to measure distances from selected random walk points to the nearest individual tree species. Five distance measurements between similar individual species, per random walk point, were taken and averaged to determine the mean distance of individual tree species from the random walk points. All distances were then averaged and squared to determine the mean area of Acacia tree species using a formula (1) adapted from Kent and Coker [7] as follows:

$$A = N^2 \tag{1}$$

where A is the mean area of tree species and N is the mean distance to the nearest individual species.

After the calculation of mean area, tree density was also calculated using a formula (2) adapted from Kent and Coker [7] as follows:

$$TD = \sqrt{\frac{A}{2}} \tag{2}$$

where TD is the tree density.

2.3. The use of aerial photographs and orthophotos for treeless cover area

Tree cover was defined as the extent of tree canopy cover in relation to the ground surface. The identification of trees on aerial photographs (**Table 1**) was based on size, shape, tone or shades of grey, pattern and texture.

To reduce bias and error in object identification a stereoscopic view was generated for adjacent aerial photographs to verify the shape, sizes, texture, pattern and tone of trees as suggested by Jensen [8]. Vertical aerial photographs (1:16,666) and orthophoto maps (1:10,000) of Luvuvhu/Mutale area were used to calculate the size of treeless area in all studied dams. These scales were chosen because they are able to show many landscape features and minimise misinterpretation of features. Booth et al. [9] argue that the accuracy of land or vegetation characterisation from remote sensing data is a function of spatial resolution. They recommend the use of the lowest-resolution photographs (1:60,000 to 1:40,000). This is why in this study of dams in the Luvuvhu and Mutale river catchment, the resolutions of 1:10,000 and 1:16,666 were used to study vegetation density changes both upstream and downstream of the dams. Orthophotos (=) (1:10,000) were also used because they were considered more accurate and could supplement measurements and object identification from vertical aerial photographs. Cameron et al. [10] argue that orthophotos are in fact rectified photographs showing objects in their true planimetric positions. The size of treeless area was considered to be the total surface area devoid of trees in a given area. The size of treeless area in each photograph was

http://dx.doi.org/10.5772/intechopen.78329

Aerial photographs for job number 908 of 1987			
Strip number	Photo number	Area	Scale
10	163 & 164	Damani	1: 16 666
11	364 & 365	Vondo	1: 16 666
12	274 & 275	Nandoni	1: 16 666
Aerial photographs for job number 932 of 1989			
2	2068 & 2070	Albasini	1: 16 666
Aerial photographs for job number 982 of 1995			
7	392 & 393	Damani	1: 16 666
9	108 & 109	Nandoni	1: 16 666
9	113 & 114	Vondo	1: 16 666
11	184, 185, 186, 187, 188 & 189	Mambedi & Albasini	1: 16 666
1: 10 000 orthophotos			
Title			Area
2330 AA 7 STERKSTROOM			Albasini
2330 AA 12 WOLVEROODE			Albasini
2330 AA 13 RIVERSANDS			Albasini
2330 AA 14 DRIEFONTEIN			Albasini
2230 DC 6 TSHIRONGA			Damani (Mvuwe)
2230 CD 10 MUHUYU			Damani (Mvuwe)
2230 DC 11 VONDWE			Damani (Mvuwe)
2230 CD 15 NGWENANI			Damani (Mvuwe)
2230 AA 14 MVUWE			Mambedi
2230 AA 15 BEAUFORT			Mambedi
2230 DC 21 MPHEGO			Nandoni
2230 DC 22 MPONDI			Nandoni
2230 DC 23 MAKUMEKE			Nandoni
2330 BA 1 DIDIDI			Nandoni
2330 AA 15 BEAUFORT			Nandoni
2230 CD 17 VHUSHAVHELO			Vondo
2230 CD 18 VONDO			Vondo
2230 CD 22 KHONGORONI			Vondo
2230 CD 23 MAPATE			Vondo

Table 1. Aerial photographs and orthophotos for Luvuvhu and Mutale dam areas (surveys and mapping: Department of Land Affairs).

calculated within an area of 4.5 km^2 both upstream and downstream of dams making a total surface area of 9 km^2 for each dam. This size of an area was chosen because it was possible to determine any tree cover variations between downstream and upstream sections of the dams.

On the aerial photographs of a scale of 1:16,666, a grid of 0.2 cm squares, with 4125 squares, was used to calculate the total surface area devoid of tree species both downstream and upstream of the dams. The size of the grid was 15 cm × 11 cm, equivalent to 2.5 km × 1.8 km on the ground, which is the total surface area of 4.5 km^2. All squares with no tree species were added together to obtain the total surface area devoid of tree species. The total number of squares with no tree species was then converted to square kilometres to determine the size of the area on the ground that was devoid of trees. The total surface area (3) devoid of trees was calculated as follows:

$$\begin{aligned} A &= S^2 \\ &= \frac{0.2 \times 16,666}{100,000} \times \frac{0.2 \times 16,666}{100,000} \\ &= 0.033\ \text{km} \times 0.033\ \text{km} \\ &= 0.001089\ \text{km}^2 \times 4125\ (\textit{number of sample squares}) \\ &= 4.5\ \text{km}^2 \end{aligned} \tag{3}$$

where ***A*** is the total surface area of one sample square, ***S*** is the one side of a square.

From the given formula, the total number of squares that contained no tree species was multiplied by 0.001089 km^2 to determine the total surface area devoid of tree species in km^2.

For the available 1:10,000 orthophoto maps, a grid of 0.25 cm square size was used with a total square of 7200. The size of the grid was 25 cm × 18 cm, which is an equivalent of 2.5 km × 1.8 km on the ground. Each square represented a total surface area of 0.000625 km^2. Therefore, the total surface area covered by the grid can be simplified as 0.000625 km^2 × 7200 to represent 4.5 km^2. The total surface area (4) devoid of trees was also calculated as follows:

$$\begin{aligned} A &= S^2 \\ &= \frac{0.25 \times 10,000}{100,000} \times \frac{0.25 \times 10,000}{100,000} \\ &= 0.025\ \text{km} \times 0.025\ \text{km} \\ &= 0.000625\ \text{km}^2 \times 7200\ (\textit{number of sample squares}) \\ &= 4.5\ \text{km}^2 \end{aligned} \tag{4}$$

2.4. Data analysis

The remotely sensed data was analysed qualitatively by describing the vegetation cover on aerial photographs and orthophotos. Tree cover from the remotely sensed images was described based on Dansereau's method [11] of vegetation description of physiognomy and structure as highlighted by Kent and Coker [7]. The method of Dansereau [11] describes cover based on the following criteria:

Barren (b): An area characterised open land with no trees and grass, or sparse trees of poor quality.

Continuous (c): An area characterised by uniform, unbroken dense vegetation cover.

Discontinuous (i): An area characterised by dense, but intermittent, cover. The interruption occurs as a result of in environmental gradients (slope, altitude, topography) and disturbed or degraded surfaces.

Tufts and groups (p): Bushes growing in clusters or groups, and is separated from one another by noticeable environmental gradients or degraded surfaces.

3. Results and discussion

3.1. Aerial photograph and orthophoto analysis of tree cover data

From the aerial photograph data, vegetation cover data has been presented in tabular and graphical form, showing areas upstream and downstream in the vicinity of dams that are

http://dx.doi.org/10.5772/intechopen.78329

Dam	Number of squares upstream	Number of squares downstream	Total area in km² upstream	Total area in km² downstream	Total area in km²	Photo year
Albasini	756	944	0.82	1.02	1.84	1989
	749	986	0.82	1.07	1.89	1995
Damani	287	295	0.31	0.32	0.63	1987
	391	420	0.42	0.46	0.88	1995
Mambedi	1934	2280	2.10	2.48	4.58	1995
	2663	2393	2.90	2.60	5.50	2001
Nandoni	1023	1078	1.11	1.17	2.28	1987
	1066	1121	1.16	1.22	2.38	1995
Vondo	1755	1869	1.91	2.03	3.94	1987
	2120	2345	2.30	2.55	4.85	1995

Table 2. Surface areas devoid of trees upstream and downstream of studied dams (from aerial photographs).

devoid of trees. **Table 2** summarises the calculated surface areas devoid of trees for different aerial photographs.

Table 3 shows the size of area devoid of trees derived from orthophotos both upstream and downstream of the studied dams. **Table 3** shows the total surface area devoid of trees for all studied periods on aerial photographs and orthophotos.

Table 4 shows the total surface areas devoid of tree cover that were measured using aerial photographs. The total surface areas have been expressed in square kilometres.

Table 1 shows that for the Albasini dam area on the Luvuvhu River, the surface area devoid of trees immediately upstream of the dam remained about the same = at 0.82 km² between 1989 and 1995 (**Tables 1** and **3**). The area downstream of the dam devoid of trees during the same period increased from 1.02 to 1.07 km². This is an increase in treeless area by 0.05 km² in a period of 6 years (**Tables 1** and **3**). This density increase in the treeless area is expected because of the shortage in water that would have occurred probable due to the upstream presence of the dam. The total surface area devoid of trees for the whole study area (9 km²) in 1989 was 1.84 and 1.89 km² in 1995. However, the size of treeless area upstream of the dam from 1995 to 1997 (latest studied period) increased from 0.82 to 0.84 km². This is growth of treeless area by 0.02 km². The size of the treeless area downstream of the dam from 1995 to 1997 increased from 1.07 to 1.13 km²

Dam	Number of squares upstream	Number of squares downstream	Total area in km² upstream	Total area in km² downstream	Total area in km²	Orthophoto year
Albasini	1357	1812	0.84	1.13	1.97	1997
Damani	658	873	0.42	0.55	0.96	2004
Mambedi	3397	4201	2.12	2.50	4.62	1997
Nandoni	1923	2301	1.20	1.44	2.64	2004
Vondo	3867	4125	2.42	2.58	5.00	2004

Table 3. Surface areas devoid of trees upstream and downstream of the studied dams (from orthophoto calculation).

Area	Period studied	Size of area devoid of trees in km² (upstream)	Size of area devoid of trees in km² (downstream)	Total surface area in km²
Albasini	1989-1995 (6 years)	0.00	0.05	0.05
	1995-1997 (2 years)	0.02	0.06	0.08
Total area	1989-1997 (8 years)	0.02	0.11	0.13
Damani	1987-1995 (8 years)	0.10	0.14	0.24
	1995-2004 (9 years)	0.00	0.09	0.09
Total area	1987-2004 (17 years)	0.10	0.23	0.33
Mambedi	1995-1997 (2 years)	0.02	0.02	0.04
	1997-2001(4 years)	0.78	0.10	0.88
Total area	1995-2001 (6 years)	0.80	0.12	0.92
Nandoni	1987-1995 (8 years)	0.05	0.05	0.10
	1995-2004 (9 years)	0.04	0.22	0.26
Total area	1987-2004 (17 years)	0.09	0.27	0.36
Vondo	1987-1995 (8 years)	0.39	0.52	0.91
	1995-2004 (9 years)	0.12	0.03	0.15
Total area	1987-2004 (17 years)	0.51	0.55	1.06

Table 4. Total surface area devoid of tree species of the selected dams in the Luvuvhu and Mutale river catchment.

(**Tables 1** and **2**). This is a growth by 0.06 km² (**Tables 2** and **3**). Therefore, the impact of shortage of water downstream of the dam was clearly reflected in the 1997 photographs. The total surface area devoid of trees for the study area from 1995 to 1997 was 0.08 km². Therefore, the total surface area devoid of trees for the dam study area between 1989 and 1997 grew from 1.84 to 1.97 km² (**Tables 1** and **2**) in a period of 6 years. This is an increase by 0.13 km² in 6 years (**Table 3**). From **Table 3** the total surface area devoid of trees downstream of the dam between 1989 and 1997 was bigger (0.11 km²) than upstream (0.02 km²). The increase in treeless area downstream of the dam can be explained with specific reference to alternating shortage of water downstream of the dam area. Shortage of water downstream of the dam during low-rainfall period gradually leads to a decline in riparian species richness and lower species diversity of colonising vegetation. This is because riparian species are selective when establishing themselves and they are sensitive to flooding frequency and duration [12–15]. Therefore, the diversity and function of riparian communities are impacted by river regulation [16]. Gordon and Meentemeyer [17] stated that reduced wetted perimeter of a river allows vegetation to increase by 50% along formerly inundated area. However, the colonising species are terrestrial, like *Acacia Karroo* along downstream reaches of Luvuvhu River at the Albasini dam.

For the Damani dam on the Mbwedi River, the total surface area devoid of trees upstream of the dam changed between 1987 and 1995 from 0.32 to 0.42 km² (**Tables 1** and **3**). This is an increase in area by 0.10 km² (**Table 3**). The area downstream of the dam devoid of trees between the same periods increased from 0.32 to 0.46 km². This is an increase in area by 0.14 km² in a period of 8 years. The total surface area devoid of trees for the whole dam study area (9 km²) in 1987 was 0.64 and 0.88 km² in 1995 (**Tables 1** and **3**). This is a total surface area devoid of trees of 0.24 km² in a period of 8 years (**Table 3**). However, the treeless area upstream of the dam from 1995 to 2004 (latest studied period) remained constant at 0.42 km² (**Tables 2** and **3**),

http://dx.doi.org/10.5772/intechopen.78329

while the treeless area downstream of the dam grew from 0.46 to 0.55 km^2 from 1995 to 2004. This is an increase in area by 0.09 km^2 (**Table 3**). Therefore, the total surface area devoid of trees grew from 0.64 to 0.97 km^2 between 1987 and 2004 within a studied dam area of 9 km^2. The total surface area devoid of trees between 1987 and 2004 grew by 0.33 km^2 within a dam area of 9 km^2. This means that the scale and magnitude of impact by upstream presence of the dam is bigger than at the Albasini dam area. This shows that downstream riparian vegetation does not receive sufficient water to support biomass production through photosynthesis. As with the Albasini dam area, the Damani dam area has also shown an increase in treeless area, with downstream reaches having bigger treeless areas.

For the Mambedi dam on the Mambedi River, the total surface area devoid of trees upstream of the dam changed between 1995 and 1997 from 2.10 to 2.12 km^2 (**Tables 1** and **2**). This is an increase in area by 0.02 km^2 (**Table 3**). The area devoid of trees immediately downstream of the dam during the same period increased from 2.48 to 2.50 km^2. This is also an increase in an area by 0.02 km^2 (**Table 3**). The total surface area devoid of trees for the whole dam study area in 1995 was 4.5 and 4.62 km^2 in 1997 (**Tables 1** and **2**). This is a total surface area of 0.04 km^2 (**Table 3**). However, the size of the treeless area upstream of the dam in the 2001 aerial photograph was 2.90 km^2 (**Table 2**). This is an increase in area from 2.12 km^2 (1997) to 2.90 km^2 (2001). This is an increase in area by 0.78 km^2 in a period of 4 years. The size of the treeless area immediately downstream of the dam increased from 2.50 km^2 (1997) to 2.60 km^2. This is an increase in area devoid of trees by 0.10 km^2 in a 4-year period. This means that the total treeless surface area for the whole dam within the studied area increased from 4.62 km^2 (1997) to 5.50 km^2 (2001), an increase of 0.88 km^2 over 4 years. However, the total surface area devoid of vegetation for the whole dam study area (9 km^2) devoid of trees grew from 4.58 km^2 (1995) to 5.50 km^2 (2001) (6-year period). This is an area of 0.92 km^2 (**Table 3**). This means that downstream riparian communities suffer water shortage during low rainfall months, and this is further worsened by the presence of the dam. This also explains why there is an increase in treeless area downstream of the dam. The size of treeless area upstream of the dam is further worsened by the fact that after the collapse of the dam wall in the year 2000, a large formerly inundated area was left dry, but was later replaced by terrestrial grass species and very few tree species. This is why the size of the treeless area in the 2001 photograph was bigger than the treeless area shown in the 1995 and 1997 aerial photographs respectively. **Plate 1** shows the area that was exposed after the failure of the Mambedi dam.

From **Plate 1** it can be seen in the background, where less water accumulates, that the area is characterised by fine thatching grass (*Hyparrhenia filipendula*) with a few unevenly scattered *Acacia ataxacantha* trees. Vegetation is still in its primary stage of succession and the stagnant water body that can be seen in the background has shown deterioration in water quality. From the photograph, it is evident that the failure of the dam reduced the aquatic environment and riparian and aquatic biota suffered from the failed water management project. The aquatic and riparian zones were colonised by terrestrial grass and woody plants. Orr [17] has stated that plant composition differs among recent and older sites as newer sites are dominated by a combination of grasses and early successional forbs. The same is true with the Mambedi dam. Again, the presence of low grass density on the banks will make the river banks more unstable and result in calving. Once this occurs, erosion of banks will increase and sedimentation will

Plate 1. The defunct Mambedi dam after the 2000 floods (December 2008).

also increase. Simon and Collison [18] have noted that if vegetation development progresses to trees banks are expected to be more stable than if banks are dominated by grass communities. This is why Russell et al. [19] have argued that without riparian vegetation, erosion and sedimentation will increase in dams. Channels that are characterised by low grass densities are more likely to lead to channel straightening [20, 21] .

For the Nandoni dam on the Luvuvhu river, the total surface area devoid of trees upstream of the dam increased between 1987 and 1995 from 1.11 to 1.16 km^2 (**Table 1**) This is an increase in area of 0.05 km^2 (**Table 3**). The area downstream of the dam devoid of vegetation during the same period increased from 1.17 to 1.22 km^2. This is also an increase of 0.05 km^2. The total surface area devoid of trees for the whole dam study area (9 km^2) was 2.28 km^2 in 1987 and 2.38 km^2 in 1995. This is a change in treeless area by 0.10 km^2, this change occurring equally upstream and downstream of the dam. This increase in treeless area both upstream and downstream of the dam might have occurred during the dry seasons accompanied by low flows due to the upstream presence of the dam. This might explain why an increase in treeless area was noted in the 1995 aerial photograph. The larger treeless area downstream of the dam between 1995 and 2004 appears to be a function of the upstream presence of the dam.

Just like with other studied dams (Albasini, Damani, Mambedi and Nandoni) there has been an increase in the size of the treeless area, especially downstream of the Vondo dam. For the Vondo dam on the Mutshindudi river, the total surface area devoid of trees upstream of the dam changed between 1987 and 1995 from 1.91 to 2.30 km^2 (**Table 1**). This is an increase in area of 0.39 km^2 in a period of 8 years (**Table 3**). The area immediately downstream of the dam devoid of trees between the same periods increased from 2.03 to 2.55 km^2; a higher increase in area of 0.52 km^2. The total surface area devoid of trees for the Vondo dam in 1987 was 3.94 and 4.85 km^2 in 1995 (**Table 1**). This means that from 1987 to 1995 the total surface area devoid of tree species grew by 0.91 km^2 within an area of 9 km^2.

http://dx.doi.org/10.5772/intechopen.78329

It can therefore be concluded that there is also insufficient water available for downstream vegetation during dry periods. This led to the disappearance of trees along downstream reaches of all studied dams, including Vondo dam. The area upstream of the dam increased from 2.30 km^2 (1995) to 2.42 km^2 in 2004 (**Table 2**). This is an increase of 0.12 km^2. However, the area downstream of the dam only increased from 2.55 to 2.58 km^2. This is increase of 0.03 km^2. This means that the total surface area between 1995 and 2004 increased from 4.85 to 5.00 km^2 (**Tables 1** and **2**). This is a total surface area of 0.15 km^2 (**Table 3**). Therefore, the total surface area devoid of trees in a 17 year period (1987–2004) increased from 3.94 to 5.00 km^2. This is the total surface area of 1.06 km^2 (**Table 3**).

Progressive increase in treeless area shows that the growing conditions might have been altered by reduced river discharge and alternating wet-dry periods. This means that the growing conditions that existed before or during the construction of the Vondo dam, differed from those existed after the construction. Therefore, colonisation and primary plant succession took place under different conditions that existed before the construction of the dam. Doyle et al. [22] also argued that succession of plant communities in the formerly inundated area will occur under very different conditions than those existed at the time of dam construction. This is why the succession conditions downstream of the studied dam areas favoured the proliferation of terrestrial species like *Acacia ataxacantha and Acacia Karroo*. An interesting observation by Vale et al. [23] was that reduction in moisture of the soil leads to reduction in water-related species such as *H. gralipes, I. laurina, A. edulis* and *I. vere.* This explains the presence of terrestrial tree species such *Acacia Karoo* in formally inundated downstream environments. Caskey [24] also noted that diversion-induced flow alteration in the Rocky Mountains of the Colorado led to the reduction in the frequency of hydrophytic wetland species and the proliferation of non-hydrophytic upland species. **Figure 3** shows the total surface areas of studied dams devoid of trees calculated from aerial photographs and orthophotos of different years as depicted in **Table 3**.

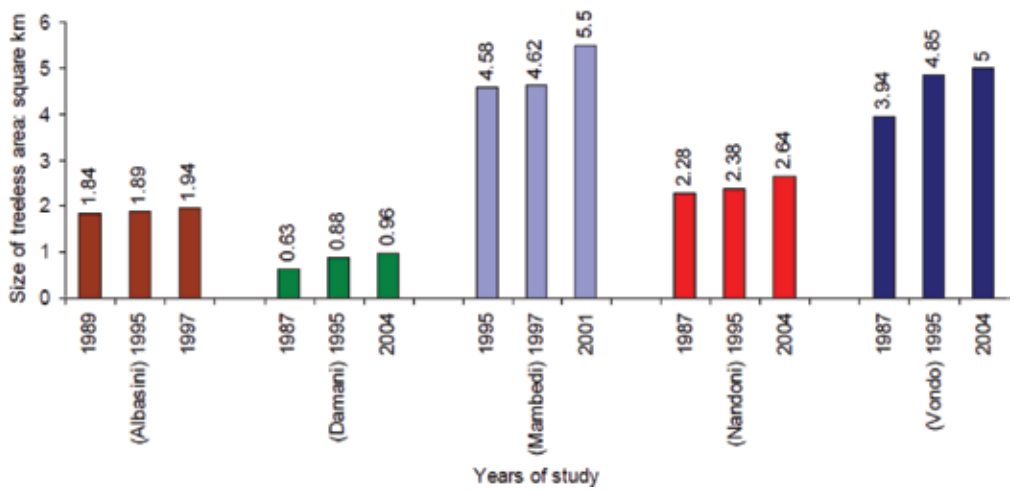

Figure 3. Total surface areas upstream and downstream of dams devoid of trees.

3.2. Tree cover data from aerial photographs and orthophotos

The degree of tree cover for all studied dams has been described based on the method of Dansereau [11] on vegetation description as highlighted by Kent and Coker [7]. **Table 5** shows the latest state of tree cover as studied from the latest aerial photographs of the study areas using Dansereau's method.

Tree density is a function of rainfall or moisture availability. Therefore, a cut in water downstream of the Luvuvhu/ Mutale dams, due to the upstream presence of the dams, has led to a decline in tree density (**Table 5**). Jones et al. [25] have also noted that tree stands decreased along the Colorado and Gila River systems of USA due to the existence of dams.

Study area	1st photograph	2nd photograph	3rd photograph
Albasini	1989	1995	1997
	Discontinuous (i) both upstream and downstream	Discontinuous (i) both upstream and downstream	Discontinuous (i) both upstream and downstream (signs of patchiness evident downstream)
Damani	1987	1995	2004
	Continuous (i) downstream (Before the existence of the dam in 1991) Continuous (c) upstream (before the existence of the dam in 1991)	Discontinuous (i) downstream with signs of patchiness Continuous (c) upstream. Dam present.	Discontinuous (i) downstream and close to barren Continuous (c) upstream
Mambedi	1995	1997	2001
	Discontinuous (i) downstream with signs of patchiness (barren) Discontinuous (i) upstream	Discontinuous (i) downstream with signs of patchiness (barren) Discontinuous (i) upstream	Discontinuous (i) downstream with signs of patchiness (barren) (after wall failure) Discontinuous (i) downstream with signs of patchiness (barren) (after wall failure)
Nandoni	1987	1995	2004
	Continuous (c) over the entire area before dam was constructed	Continuous (c) over the entire area but shows signs of discontinuity because of the existence of the small Mutoti dam and human settlements	Discontinuous (i) over the entire area because of the existence of the small agricultural lands and human settlements
Vondo	1987	1995	2004
	Tufts and groups (p) downstream and upstream of the dam because of tea plantation fields	Tufts and groups (p) downstream and upstream of the dam because of tea plantation fields	Tufts and groups (p) downstream and upstream of the dam because of tea plantation fields

Table 5. Latest state of tree cover for the five selected Luvuvhu/Mutale dams.

http://dx.doi.org/10.5772/intechopen.78329

3.3. Field data from the selected dams in the Luvuvhu and Mutale river catchment

3.3.1. Tree density

Tree density data was collected from the five dams studied through field survey. The mean distances for tree species from the Luvuvhu/Mutale dams were measured and the results are shown in **Table 6** and **Figure 3**. Tree densities upstream and downstream of the dams studied.

From **Figure 4** Vondo shows slightly higher upstream density and much lower downstream density. Vondo shows lower downstream density than all studied dam areas. Downstream of Vondo dam area, is less dense (10.11 m^2) than in all studied dam areas while Albasini dam area is denser.

However, the Vondo dam area is characterised by commercial agriculture and human settlement along the Mutshindudi River. Therefore, the extent of the impact of the dam downstream is complicated by the existence of settlements and intense commercial farming (tea plantations). The field data and photo data do not correspond in all cases but this happen to agree in this particular case because of the human settlements and tea plantations. For example, Kellog and Zhu [26] noted that during the construction of the Three Gorges Dam (China) clearing of vegetation for agriculture the average width of the upstream waterway increased from 0.6 to 1.6 km. This shows how dams negatively impact on their immediate environments. The same is true with the area in the vicinity of the Vondo dam. Therefore, the lower tree density downstream of the Vondo dam corresponds with the size of the treeless area (1.06 km^2) calculated from remotely sensed images. Results in **Table 6** and **Figure 3** also show that upstream tree

Dam	Mean distance (*m*) to nearest *n* individual species upstream	Mean distance (*m*) to nearest *n* individual species downstream	Tree density upstream in m^2	Tree density downstream in m^2	Tree species name
Albasini	8.29	8.32	5.86	5.88	Sweet thorn (*Acacia karroo*)
Damani	5.98	9.65	4.22	6.82	Flame thorn (*Acacia ataxacantha*)
Mambedi	10.04	12.06	7.09	8.52	Flame thorn (*Acacia ataxacantha*)
Nandoni	6.5	9.3	4.59	6.57	Flame thorn (*Acacia ataxacantha*)
Vondo	7.7	14.3	5.44	10.11	Flame thorn (*Acacia ataxacantha*)

Table 6. Tree density upstream and downstream of the dams studied (December 2009).

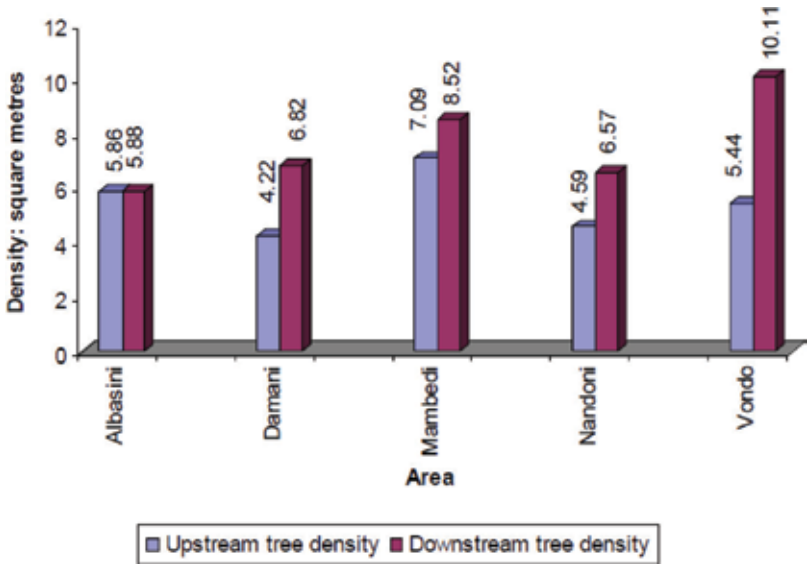

Figure 4. Tree densities downstream and upstream of the dams.

density is highest at Damani dam (4.22m^2) on the Mbwedi River and lowest at Mambedi dam (7.09m^2) on the Mambedi River. Downstream tree density is highest on the Albasini dam and lowest in all other dams. Downstream tree density is highest on the Albasini dam (5.88 m^2) and lowest on the Vondo dam (10.11m^2). Tree density upstream of Nandoni dam is higher (4.59 m^2) than downstream of the dam (6.57m^2). Thus, the growth in treeless area downstream of all studied dams occurs as a result of low flows which are available for riparian irrigation. This is caused by the upstream presence of the dams. This, according to Lees et al. [27] and Sutherland et al. [28], occurs because construction of dams leads to fragmentation and degradation of riparian zones which also leads to loss of ephemeral habitats.

The magnitude of degradation is a function of resilience and fragility of the area which is controlled by soil type, size of the dam, age of dam, size of degraded area during the construction of the dam, species diversity, succession stages, climatic variability, energy pools and routes and soil instability [29]. Albasini dam area has a smallest difference between the downstream (5.88 m^2) and upstream (5.86 m^2) tree density. This is a function of the age of the dam: vegetation, predominantly terrestrial, having had sufficient time to regenerate after the construction of the dam in 1952. Vale et al. [30] have noted that dam impact stabilises a few years after impoundment but becomes intense immediately after dam construction. This explains the smallest difference between downstream and upstream areas. However, Vondo dam area has lower tree density because it is located in a more humid area characterised by high rainfall and sensitive soils. Soils of the area are therefore dystrophic (nutrient-poor). This explains why the area became sensitive to water shortage downstream of the dam. Vegetation that thrived well under humid conditions suffered when river discharge was reduced downstream of the

http://dx.doi.org/10.5772/intechopen.78329

Vondo dam on the Mutshindudi river. This is because conditions became too dry for riparian communities resulting in loss of diversity. Graf [31] similarly argued that regulated reaches are less likely to support extensive ecosystem components requiring a dry period of summer, and the species diversity will be lower.

4. Conclusion

In all the five dams studied, downstream treeless area has increased progressively over the years. In all cases, aerial and orthophotos showed increasing discontinuity in downstream tree cover. Treeless area is bigger downstream than upstream in all cases (except the Mambedi dam, which failed in the year 2000). There is lower species richness downstream than upstream (again, except in the case of the failed Mambedi dam). In all the downstream riparian zones, the predominant vegetation is obligate terrestrial species. Downstream vegetation is less dense than previously and less dense than upstream, although in the case of the oldest dam (Albasini), the difference is small, as the terrestrial vegetation downstream has had more time to recover. These effects are ascribed to the probable presence of the dams causing reduced downstream flows during dry seasons.

From the above summary of the findings of all five dams studied, it can be concluded that any modification of river flow through damming alters flow characteristics and impacts negatively on nutrient cycling of lotic environments. This is accompanied by low downstream species diversity. All dams are characterised by low surface or runoff downstream. Changes in river flow due to damming have led to the replacement of riparian vegetation with terrestrial vegetation or alien plant species in other dams. All downstream sections of the studied dams are characterised by terrestrial vegetation in formerly inundated riparian zones. Total annual rainfall does not guarantee the regeneration of disturbed areas since regeneration depends on many combined factors such as size of dams, size of degraded area during dam construction, natural species diversity, successional stages, climatic variability, energy pools and routes and soil instability. The resilience and fragility of disturbed areas depend on the combination of some of these factors.

Acknowledgements

We are grateful to the Department of Research and Innovation, University of Venda for the provision of research funds (I369) that enabled us to complete the research.

Conflict of interest

The authors declare no conflict of interest.

Author details

John M. Mokgoebo[1]*, Tibangayuka A. Kabanda[2] and Jabulani R. Gumbo[3]

*Address all correspondence to: matjutla.mokgoebo@univen.ac.za

1 Department of Geography and Geo-Information Sciences, University of Venda, Thohoyandou, South Africa

2 Department of Geography and Environmental Science, North-West University, Mmabatho, South Africa

3 Department of Hydrology and Water Resources, University of Venda, Thohoyandou, South Africa

References

[1] Mumba M, Thompson JR. Hydrological and ecological impacts of dams on the Kafue flats floodplain system, southern Zambia. Physics and Chemistry of the Earth, Parts A/B/C. 2005;**30**(6-7):442-447

[2] Gope ET, Sass-Klaassen UG, Irvine K, Beevers L, Hes E. Effects of flow alteration on apple-ring Acacia (*Faidherbia albida*) stands, middle Zambezi floodplains, Zimbabwe. Ecohydrology. 2015;**8**(5):922-934

[3] de Souza Beghelli FG, Frascareli D, Pompêo ML, Moschini-Carlos V. Trophic state evolution over 15 years in a tropical reservoir with low nitrogen concentrations and cyanobacteria predominance. Water, Air, & Soil Pollution. 2016;**227**(3):95. DOI: 10.1007/s11270-016-2795-1

[4] Li J, Dong S, Peng M, Li X, Liu S. Vegetation distribution pattern in the dam areas along middle-low reach of Lancang-Mekong River in Yunnan Province, China. Frontiers of Earth Science. 2012 Sep 1;**6**(3):283-290

[5] Department of Water Affairs and Forestry (DWAF). Internal Strategic Perspective: Luvuvhu/Letaba Water Management Area. Pretoria: DWAF; 2004

[6] Department of Water Affairs and Forestry (DWAF). Internal Strategic Perspective: Crocodile (West) and Marico Water Management Area. Pretoria: Government Printer; 2004

[7] Angliss M, Ashton P, Cook C, Deacon A, Foord S, Fouche P, Henning D, Kleynhans N, Rodgers S, Roux D, Strydom W. State of Rivers Report: Letaba and Luvuvhu Systems. WRC report no: TT 165. Pretoria; 2001

[8] Kent M, Coker P. Vegetation Description and Analysis. A Practical Approach. New York: John Wiley & Sons; 1992

[9] Jensen JR. Remote Sensing of the Environment: An Earth Resource Perspective. New York: Pearson Education Inc; 2007

[10] Booth DT, Cox SE, Simonds G. Riparian monitoring using 2-cm GSD aerial photography. Ecological Indicators. 2007 Jul 1;**7**(3):636-648

[11] Cameron AD, Miller DR, Ramsay F, Nikolaou I, Clarke GC. Temporal measurement of the loss of native pinewood in Scotland through the analysis of orthorectified aerial photographs. Journal of Environmental Management. 2000 Jan;**58**(1, 1):33-43

[12] Dansereau P. Description and recording of vegetation upon a structural basis. Ecology. 1951 Apr 1;**32**(2):172-229

[13] Alldredge B, Moore G. Assessment of riparian vegetation sensitivity to river hydrology downstream of a major Texas dam. River Research and Applications. 2014;**30**(2):230-244

[14] Kupfer JA, Meitzen KM, Pipkin AR. Hydrogeomorphic controls of early post-logging successional pathways in a southern floodplain forest. Forest Ecology and Management. 2010;**259**(10):1880-1889

[15] Chabwela H, Chomba C, Chimbali D, Malama M. Rangeland condition and herbage utilization by herbivores of the Kafue flats north Bank: A historical perspective before the construction of the Itezhi-Tezhi dam, Zambia. Open Journal of Ecology. 2018;**8**(02):126

[16] Sankey JB, Ralston BE, Grams PE, Schmidt JC, Cagney LE. Riparian vegetation, Colorado River, and climate: Five decades of spatiotemporal dynamics in the Grand Canyon with river regulation. Journal of Geophysical Research: Biogeosciences. 2015 Aug 1;**120**(8):1532-1547

[17] Gordon E, Meentemeyer RK. Effects of dam operation and land use on stream channel morphology and riparian vegetation. Geomorphology. 2006;**82**(3-4):412-429

[18] Orr CH. Patterns of removal and ecological response: A study of small dams in Wisconsin [unpublished MS thesis]. Madison: University of Wisconsin; 2002

[19] Simon A, Collison AJ. Quantifying the mechanical and hydrologic effects of riparian vegetation on streambank stability. Earth Surface Processes and Landforms. 2002;**27**(5):527-546

[20] Congalton RG, Birch K, Jones R, Schriever J. Evaluating remotely sensed techniques for mapping riparian vegetation. Computers and Electronics in Agriculture. 2002;**37**(1-3):113-126

[21] Maluleke D. Flood risk on human settlements and economic activities along Luvuvhu River basin [Honours dissertation]. Department of Earth Sciences, University of Venda; 2003

[22] Doyle MW, Stanley EH, Orr CH, Selle AR, Sethi SA, Harbor JM. Stream ecosystem response to small dam removal: Lessons from the heartland. Geomorphology. 2005;**71**(1-2):227-244

[23] Vale VS, Schiavini I, Araújo GM, Gusson AE, Lopes SF, Oliveiral AP, Prado-Júnior JA, Arantes CS, Dia-Neto OC. Effects of reduced water flow in a riparian forest community: A conservation approach. Journal of Tropical Forest Science. 2015 Jan 1;**27**:13-24

[24] Caskey ST. Downstream effects of diversion dams on riparian vegetation communities in the Routt National Forest, Colorado [doctoral dissertation]. Colorado State University; 2013

[25] Jones KB, Edmonds CE, Slonecker ET, Wickham JD, Neale AC, Wade TG, Riitters KH, Kepner WG. Detecting changes in riparian habitat conditions based on patterns of greenness change: A case study from the upper San Pedro River basin, USA. Ecological Indicators. 2008;**8**(1):89-99

[26] Kellogg CH, Zhou X. Impact of the construction of a large dam on riparian vegetation cover at different elevation zones as observed from remotely sensed data. International Journal of Applied Earth Observation and Geoinformation. 2014;**32**:19-34

[27] Lees AC, Peres CA, Fearnside PM, Schneider M, Zuanon JA. Hydropower and the future of Amazonian biodiversity. Biodiversity and Conservation. 2016;**25**(3):451-466

[28] Sutherland WJ, Alves JA, Amano T, Chang CH, Davidson NC, Max Finlayson C, Gill JA, Gill RE, González PM, Gunnarsson TG, Kleijn D. A horizon scanning assessment of current and potential future threats to migratory shorebirds. Ibis. 2012;**154**(4):663-679

[29] Tivy J. Biogeography: A Study of Plants in the Ecosphere. New York: Longman; 1993

[30] Vale VS, Schiavini I, Prado-Junior JA, Oliveira AP, Gusson AE. Rapid changes in tree composition and biodiversity: Consequences of dams on dry seasonal forests. Revista Chilena de Historia Natural. 2015;**88**(1):13. DOI: 10.1186/s40693-015-0043-5

[31] Graf WL. Downstream hydrologic and geomorphic effects of large dams on American rivers. Geomorphology. 2006;**79**(3-4):336-360

Chapter 5

Experiences from the Fukushima Disaster

Hans J. Scheel

Additional information is available at the end of the chapter

http://dx.doi.org/10.5772/intechopen.77726

Abstract

The nuclear accident of the Fukushima Daiichi reactors on March 11, 2011, could have been prevented if the owner and the responsible Japanese ministries had considered the worst-case scenario when planning the reactors near the coast, including at least double redundancy of the emergency system. After the exceptionally strong earthquake, the reactors correctly switched off. The problem started due to the tsunami that destroyed the emergency generators, which should have driven the cooling pumps after the reactor-power had switched off. The Zr-alloy mantles of the fuel rods reacted at the high temperature with water to form ZrO_2 and hydrogen. The following explosions, destruction of the reactor buildings and meltdown caused large radioactive clouds and the evacuation of 150,000 people. This chapter shows how by immediate efforts most of this cloud could have been sucked off. The radioactive soil from large contaminated areas was later collected in plastic sacks. Continuous cooling led to huge amounts of contaminated water that was collected in large tanks. In future, the reactor has to be dismantled resulting in contaminated debris. In this chapter, the possible solutions of radioactive cloud, soil, water and rubble problems and the final deposit of used fuel rods are discussed. The experiences could become useful in case of a future nuclear accident.

Keywords: Fukushima accident, tsunami risk, radioactive cloud, contaminated soil and water, reactor dismantling, nuclear risk, energy future

1. Introduction

With increasing world population, with increasing industrialization of less-developed countries and with increasing electric mobility, the demand of nuclear energy will increase. When renewable energy from the wind and the sun increases worldwide, from the present 0.8%, then nuclear energy will be needed as base energy to compensate the lack of electric energy when the wind is not blowing and the sun not shining. Furthermore, with the limited world

resources of coal and oil, and with the required reduction of CO_2 emission with regard to the climate problem, the role of nuclear energy will increase in most industrialized countries. Accordingly, nuclear reactors are being built or are planned to be built in most countries except Germany and Switzerland where, by emotional decisions taken after the Fukushima accident, nuclear energy is planned to be terminated. These two countries could then be faced with lack of reliable electric power supply and with the increasing cost of electricity from 30 to 50%, a risk for industries and for the expected electric mobility. Their choice will be the import of nuclear energy from neighbor countries (with increasing risks of radioactive clouds in case of future accidents) or the installation of gas-power plants with dependence on gas supply and with emission of CO_2. Energy policies should be discussed in view of sustainable management of limited energy sources [1] until in the far future nuclear fusion energy may hopefully be developed [2].

Most of the present 450 plus nuclear reactors are of type II Pressurized Light-Water-Moderated and Cooled Reactors. The energy efficiency of the uran-235-based fuel rods is only 1.5–5%. Their recycling yields plutonium needed for nuclear bombs, the reason why this reactor type was pushed by the US military. On the other hand, can the later recovery of used fuel rods from the storage site of radioactive waste become a significant source of energy for future generations? Now 60 reactors of higher energy efficiency are being built or are planned on being built, with the example of the European Pressure-Water Reactor being built in Finland.

The risk for life and health of the nuclear energy is much smaller than the risks of fossil energy and of renewable energy taking into account the direct fatalities and the after-effects from air pollution from burning fossil fuel [3] and from the role of CO_2 for climate change. The new generation of safe type III and type IV generators including thorium reactors will have high energy efficiency, cause significantly less radioactive waste and shorten the required storage time for radioactive waste [4]. Until these modern reactors are fully developed, mankind should learn from experiences of the two nuclear accidents in Chernobyl and Fukushima with respect to optimized planning of the safe site of the reactor including its safety infrastructure, considering the worst-case scenario of all possible risks. The following discussion of the Fukushima problems may help in case one of the existing nuclear reactors should have an accident although the probability is extremely small. After the Fukushima incident, the existing nuclear reactors in Japan should be checked with respect to the worst-case scenario of earthquake and flooding risks. Also, the risks of extremely complex technologies should be considered. One could discuss whether all reactors worldwide should be checked by an international specialist team, possibly under guidance from the International Atomic Energy Agency (IAEA) in Vienna taking into account the national nuclear safety organizations.

2. Critical planning phase of the Fukushima Daiichi plant

The start of a nuclear power plant requires the study of all potential risks like earthquakes, landslides, aviation routes, the risks of flooding from mountain sides and from seaside and extreme weather. Also, the groundwater situation has to be considered. The primary

http://dx.doi.org/10.5772/intechopen.77726

responsibility is with the owner of the plant and its planning team. The government and its ministries have the main control function, and the International Atomic Energy Agency (IAEA) in Vienna has the obligation to supervise the safety aspects especially in view of preventing proliferation of nuclear material.

In case of the Fukushima Daiichi plant, the owner company did not consider the worst-case scenario for financial reasons [5]: Despite the in-house study which revealed the possibility of 10 m high tsunami waves, the company's headquarters declared such a risk as unrealistic. Also, warnings from the Research Institute of Earthquake and Volcano Geology of the Geological Survey of Japan and of the US Nuclear Regulatory Commission were not followed by the company and by the responsible safety agency of Japan. This agency had a conflict of interest and was replaced in September 2012 by the Nuclear Regulation Authority under the Ministry of the Environment [6].

In order to protect the Fukushima coast against tsunami with the miss-judged low heights of the waves, seawalls of about 10 m height were erected, see **Figure 1**. This photo was taken after the accident and also shows the tanks with radioactive contaminated water. The north seawall shows the remaining low height (probably caused by the tsunami) and the two seawalls of the remaining height of claimed 10 m.

The plant owner failed to arrange safe electric backup generators and a reliable emergency cooling system which resulted in the primary cause of the Fukushima accident.

Earthquakes above magnitude 7.0 were of concern for the IAEA due to large earthquakes earlier. However, the March 11, 2011, earthquake with magnitude 9 did not damage the Fukushima plant [5], it caused the correct shutdown of all reactors.

Figure 1. Top view of Fukushima power plant Dezember 2015 with lateral and height dimensions.

The failures of the planning phase and the actual causes and sequences of the Fukushima disaster have been analyzed by an independent commission which was appointed by the Japanese Government and which delivered the report July 5, 2012. The conclusion was that the accident could have been prevented and that it was man-made. Furthermore, the evacuation conditions were criticized as they caused 1600 fatalities due to stress from the hectic exaggerated evacuation, whereas radiation did not cause direct death [5].

The Fukushima accident has demonstrated the interaction of neighbor reactors: the meltdown problem of reactor 1 effected meltdown and hydrogen explosions in reactors 3 and 4. As consequence, a minimum distance between reactors of say 50 m should be demanded in future and all reactors provided with individual emergency power supplies, pumps and other safety equipment. In existing rows of reactors, they should be separated, for instance, by steel plates and have individual safety equipment, all with at least three-fold redundancy.

3. Effects of the March 11, 2011, earthquake and tsunami

Japan is situated on the Pacific Ring of Fire with active plate tectonics where the Pacific Plate is subducting the Eurasian Plate and thus causes frequent earthquakes. The country has spent remarkable efforts to reduce the risks of collapsing buildings. When earthquakes of magnitude larger than 6.5 occur in the sea, they may cause tsunami depending on the displacement of the seafloor actually caused [7]. Such tsunami can lead to flooding on the coast and cause numerous fatalities: in case of the 2011 tsunami, 19,000 fatalities and large damages. However, such tsunami catastrophes are not so frequent so that protection measures have been realized only in a few areas. Frequently, classical breakwaters are constructed by placing heavy caissons onto rubble mounts or foundations which have a slope on the seaside [8]. The typical failures of such breakwaters consist of sliding or tilting of the caissons [9]. One example is the harbor city Kamaishi north of Sendai at the Honshu/Japan coast where, after experiencing the 1896 tsunami catastrophe, the world's largest breakwater was built in 31 years at the cost of 1.3 billion US dollar. Only 6 months after celebrating the world record for Guinness Book of Records, the Tohoku tsunami of March 11, 2011, destroyed most of the breakwater and part of the Kamaishi harbor region and caused 1000 fatalities. Details of the construction of the combined breakwater and of the damages have been described [10]. Recently it was shown that this breakwater had been built on the wrong site with a non-optimal technology [11] and that a submerged barrier, with vertical wall toward the sea, at the entrance of Kamaishi bay would have prevented the local tsunami catastrophe.

The tsunami pressure (impulse) waves travel from the earthquake area at a high speed of typically 700 km/hour at an ocean depth of 4 km in all directions. The velocity c is given by

$$c = \sqrt{(g \times h)} \tag{1}$$

with g the gravitational acceleration and h the water depth. By the law of energy conservation, the kinetic energy of the pressure waves is transformed to potential energy when the wave approaches the coast with decreasing water depth according to

$$A^2 \times c = \text{constant} \tag{2}$$

where, A is the amplitude or wave height. With a starting wave height between 0.3 and 1 m in the deep sea, the wave height will increase at the coast to 3 and 10 m and can rise in narrowing bays to values up to 38 m as observed 2011 with the Tohoku tsunami [11]. As a consequence, the seaside of submerged buildings in the sea should not have slopes, should always be vertical walls.

In order to prevent the tsunami flooding catastrophes, the concept of a submerged vertical barrier (wall) has been developed which reflects the tsunami impulse waves and also the storm surges from a typhoon so that these Tsunami-Flooding-Barriers (TFB) would have prevented the Fukushima disaster [11].

In the case of the Fukushima plant, three classical breakwaters (seawalls) have been built as shown in **Figure 2**.

The northern breakwater in the Google photo, taken after the accident, shows a low height and flat surface indicating that the caissons on top of the rubble mound foundations may have slit down. The western and southern breakwaters showed a height between 10 m and 13 m and thus were still intact.

The tsunami pressure wave, which arrived from the north-eastern direction, is indicated in **Figure 2** by the red arrow. The wave height was increased at the slope of the northern breakwater. Then the tsunami energy was focused by the two remaining breakwaters toward south-west explaining that the southern Reactor 1 with its emergency auxiliary equipment was damaged, whereas the northern reactors 5 and 6 were not affected from the tsunami.

The height of the tsunami water front was estimated as 13—15 m, but in view of the concentration effect, it may have been locally significantly higher when approaching the southern reactors 1– 4 and their emergency equipment.

The following description of events is a concentrated summary of reports detailed in [5].

From the six reactors, the units 4–6 had been shut down for a normal-scheduled inspection. The reactors 1–3 had been operating and were immediately switched off when the earthquake struck. Therefore, the reactors did not produce electricity and could not use their own power. The available emergency diesel generators were disabled from the floods; also, the switching stations for the diesel generators at higher position were flooded. Furthermore, the attempts to connect the water pumps to portable generators failed. Due to lack of sufficient cooling, the fuel rods with zircaloy mantle reached temperatures above 1000°C where the exothermic reaction $Zr + 2\ H_2O > > ZrO_2 + 2H_2$ produced explosive hydrogen. This then caused in the following days successive explosions in reactors 1, 3 and 4 destroying the roofs and tops of

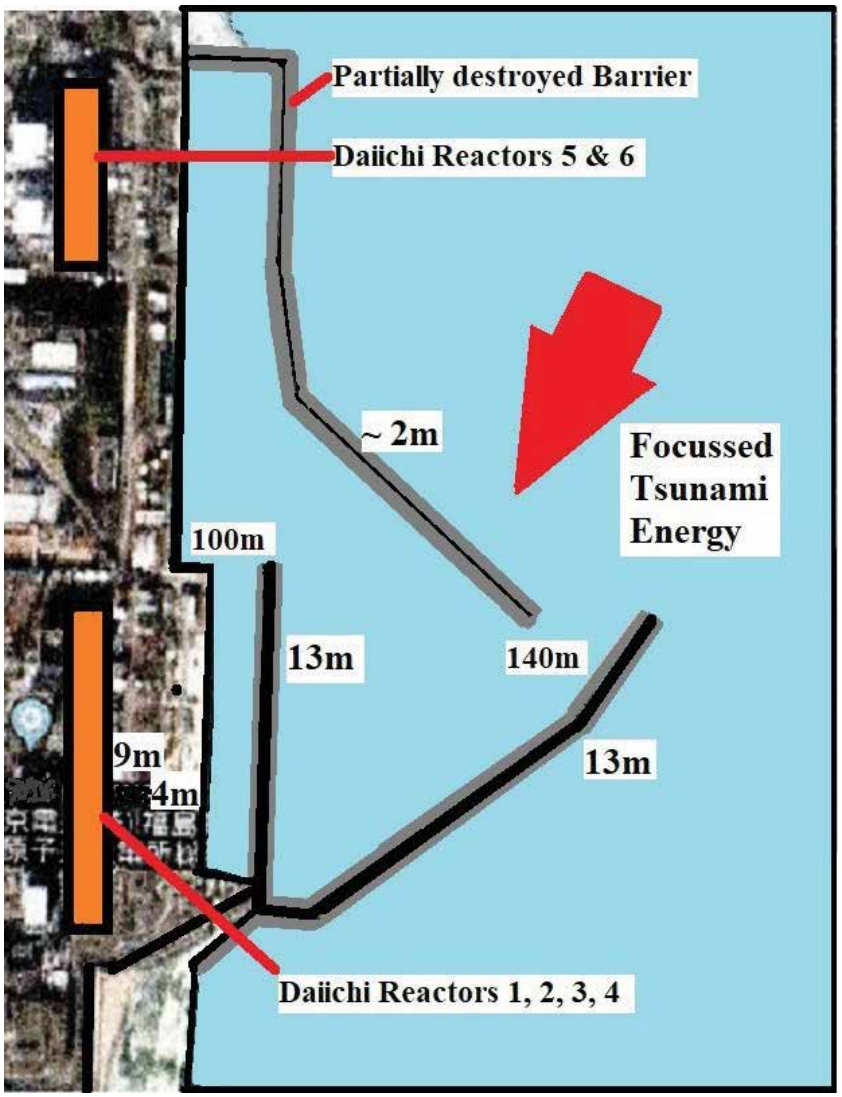

Figure 2. Top view of Fukushima Daiichi Reactors with two intact sea walls and one remnant wall. The two walls focused the tsunami energy and led to increased secondary tsunami water wave.

the reactor buildings. Cooling the fuel rods was essential even when the reactors had been switched off. The helplessness of the owner's management became obvious when on TV one could observe helicopters dropping water onto the reactor ruins and ships which directed water guns toward the reactors. Insufficient cooling therefore could not prevent the melt-down of the fuel which then fused through to the bottom of the reactor pressure vessel and partially went through to the primary containment vessel of concrete 7.6 m thick where it is assumed to have stopped.

Attempts to investigate the situation inside the reactors by muon scanning and by a remote-controlled camera have proven the meltdown of the fuel and its lowering to the concrete containment vessel.

A large amount of radioactive materials of 130 petabequerels has been released into the air from March 11 to April 5, 2011, which corresponds to 11% of the Chernobyl emissions. Accordingly, the heavily contaminated area around Fukushima corresponded to 10–12% of the Chernobyl area. The sea was contaminated by about 84 kg of cesium-137 corresponding to 27 petabequerels whereby 82% flowed into the sea before April 8, 2011. This contamination consisted of controlled and uncontrolled release of contaminated water, of surface water flowing over contaminated soil and of airborne radioactive particles that entered the sea by rain. The attempts of the owner's company to stop the flow of contaminated water to the sea by a 30 m-deep wall in the ground and by an underground ice wall have been only partially successful. On September 10, 2015, the typhoon Etau caused an uncontrolled flow of contaminated water into the ocean.

Studies have shown that contamination of the ocean as measured would not have long-term effects on health due to the powerful Kuroshio current and the dilution in the wide Pacific. The contamination through the air into the ground requires the collection of radioactive soil in millions of plastic bags in order to facilitate the return of the evacuated people to their homes.

The World Health Organization (WHO) and other institutions and organizations evaluated the health risks which are expected to be small for most of the population due to the estimated small amount of received radiation [12]. The main health effects have been observed with the evacuated people of which 1600 died from stress and suicide, not from cancer. The main cause of these fatalities is due to the accident and the hectic exaggerated evacuation, but a certain responsibility have the green-political parties, organizations and media with excessive reports about the accident and risks. The extremely low personal value of 1 millisievert (mSv) per year from artificial radiation in Japan is in contrast to international annual doses of 20 mSv as accepted by the International Commission on Radiological Protection (ICRP), the United Nations Scientific Committee on the Effects of Atomic Radiation (UNSCEAR) and the World Health Organization (WHO). Due to the low received radiation, no significant health effects are expected for the population of cities within the 20-mile zone around the Fukushima plant. The March 2015 thyroid gland investigation of 300,000 children effectively showed no noticeable cases.

There are enormous costs for the owner company and for Japanese taxpayers for compensation, decontamination, dismantling the reactors and radioactive waste storage, exceeding 187 billion US dollars. The main consideration will be Japan's energy future in view of lack of resources and resistance from the population. In view of the crucial importance of nuclear energy for Japan's future, as a personal responsibility, opponents of nuclear energy could consider reducing their electricity consumption during periods of electricity shortage.

Emergency actions and consequences for reducing the aftereffects in case of a future, most-improbable nuclear accident are discussed later.

4. Discussion on the possible management problems after March 11, 2011

4.1. Missed chances to reduce the contamination level

The nuclear accidents in Chernobyl and in Fukushima have caused huge contamination of cities, villages and land and had necessitated the evacuation of ten-thousands of people a fraction of which in case of Chernobyl had received hazardous radiation.

In case of a such nuclear accident, there are two aspects which require immediate action:

1. Can the fission rate and the development of uncontrolled heating of the fuel rods be stopped from the control room or by remote actions to lift the fuel rods or by introducing neutron-absorbing elements or compounds based on boron, silver, cadmium and indium combined with intensive cooling, decisions to be made immediately by an experienced reactor engineer.
2. In case of fire or escaping flames and clouds, the collateral damage by widespreading of radioactivity has to be minimized by very intense water spraying using any water resources, be it from nearby lake or river or sea and using water pumps and high-power water guns powered from pre-installed and mobile diesel generators. When a natural water source cannot be reached, then the installation of a nearby pond of sufficient volume should be arranged near all reactors. Contamination of the sea is less harmful than contamination of cities, villages and landscapes. The optimum would be sea reservoirs built with the Tsunami-Flooding Barriers [11]. With visible installations for the water guns outside the reactor building, with watering exercises and with proper information, people can be assured that evacuation will not be required in the future, even in case of an accident.

If a long-lasting fire occurs as in Chernobyl, where the graphite moderator burnt and sent radioactive clouds very high so that contamination spread over large distances or in case of Fukushima, where the cloud left the reactor building and was carried by wind, intensive suction should be considered. **Figure 3** schematically shows the reactor building with attached large-diameter steel pipes which collect the cloud by a powerful ventilator of at least 5000 m^3 per hour depending on tube diameter. A sprinkler system condenses the radioactive vapors and particles, and this contaminated water should then flow into the sea reservoir or into a basin. In case of Fukushima, this contaminated water should in the first phase have been transported by long pipes to the Kuroshio current where it is diluted. In the second phase, the gaps of 100 and 140 m between the existing seawalls/breakwaters could have been closed and water could have been pumped out to the basins where it could be collected and stored for later treatment. The intense spraying followed by the suction activity would have reduced the extended radioactive spreading and thus the evacuation requirements. Such suction systems could also be useful in case of accidents and fires in chemical factories and in oil refineries.

Reactor surrounding should always be covered by a thick concrete layer with a slope of 2–3° in the direction of the sea or the basin, so that all water is controlled and collected and the soil cannot be contaminated.

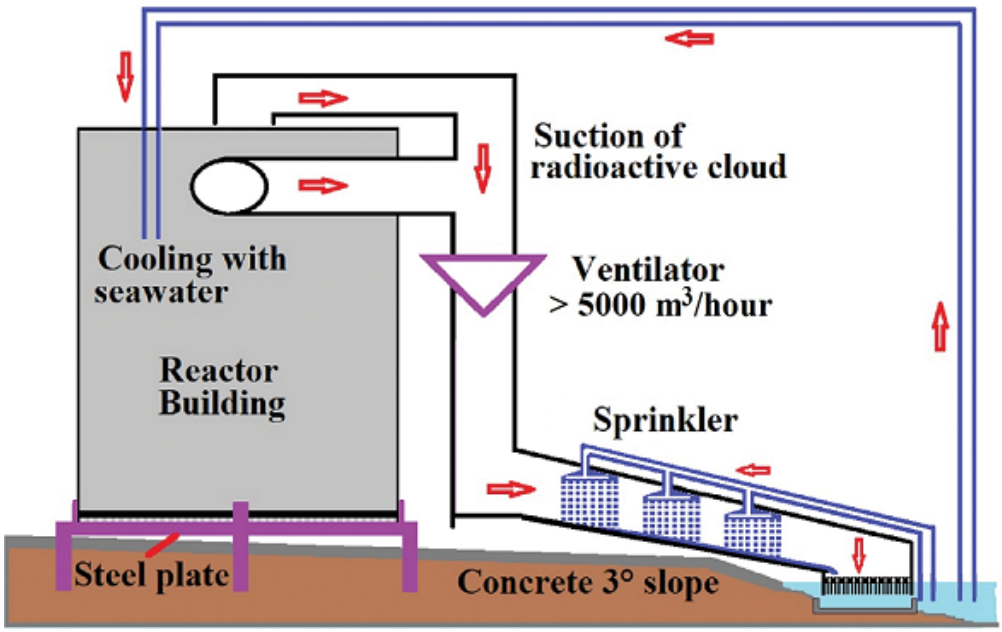

Figure 3. Schematic view of suction of radioactive cloud and sprinkling with seawater.

The groundwater should never become a problem for the reactor by installing deep water-tight barriers around the reactor area, before the reactor starts to work.

The successive hydrogen explosions, which destroyed a part of the reactors and their roofs, should have been prevented by hydrogen detectors, which raise an alarm and which activate valves for high-pressure injection of nitrogen or CO_2. Hydrogen concentration should always be kept below the explosion level of 4% in air, this value depending on humidity and other factors. The alternative of Passive Autocatalytic (Hydrogen) Recombiners (PAR) [13] does not require electricity to operate and has been installed in some reactors worldwide. PAR had been applied in the Three-Mile-Island accident (March 28, 1979) to reduce the hydrogen content in a hydrogen bubble inside the reactor chamber to prevent a large explosion. Hydrogen removal works even in the presence of CO which is frequently formed in fires [14].

4.2. The contaminated water problem

After the initial weeks following the accident, large amounts of cooling water had been pumped into the reactors, for example, 300 metric tons per day, which initially was further diluted with 400 m^3 groundwater. Despite large efforts taken to reduce the influx of groundwater, it could not be stopped. Half of the water returning from reactor cooling was filtered and partially decontaminated and returned for cooling, and the other half of 200 m^3 was collected daily in large storage tanks in the plant surroundings for later treatment. A fraction of this tank collection is shown in **Figure 4**.

Decontamination of water was problematic. Equipment from France, USA and Japan had been applied using reverse osmosis, adsorption by zeolites or evaporation of salt water.

Figure 4. Fraction of tanks with >300,000 m3 contaminated water at Fukushima power plant.

Problems have been errors in handling of valves, repeated leakages of connections and pipes and stopped pumps which could not be re-activated. Reference [15] gives some details of the dramatic water contamination problems. From outside it looks like small-scale attempts to solve large-scale problems.

With the existence of the three seawalls in front of the coast of Fukushima plants, there is the possibility to connect the ends of these seawalls by new walls of 100 and 140 m length to form three basins as shown in **Figure 5**.

To construct these barriers by conventional technology with rubble mound foundations and top caissons [8] or to build concrete walls would be a lengthy process and not provide highest safety. Recently, two methods have been developed which allow efficient construction of submerged barriers at reduced costs [11, 16]. In a first step, deep "beds" are dredged into the bottom of the sea with the depth depending on the sea ground (rocks, gravel, sand, mud). In the double-pontoon technology, two separated pontoons start from a ramp road at the coast and allow to move trucks. The first truck inserts a stainless steel (316L, 316LN, 1.4429) fence outside the pontoons into the sea, for instance, stable fence of Geobrugg, Romanshorn, Switzerland. The next truck inserts alternating rocks and concrete in the gap between the pontoons into the sea. Distance holders allow to erect a stable vertical wall of 6 –20 m width. These central pontoons hang on steel beams between assisting pontoons in order to carry the heavy weights. The second technology uses long tall cylinders of more than 100 m length fabricated in the harbor and floated to the site where they are inserted into the sea bed and filled with rocks, sand, and so on. These walls named Tsunami-Flooding-Barriers (TFB) are vertical toward the sea and thus reflect the impulse waves of tsunami. They extend about 10 m above sea level and carry a service road on top which is protected against storm waves by replaceable surge stoppers (parapets) [11].

Hydrodynamic modeling [17] of the action of TFB barriers by coupling the far-field depth-averaged Boussinesq-type model pCOULWAVE of Lynett et al. [18] with a near-field

http://dx.doi.org/10.5772/intechopen.77726

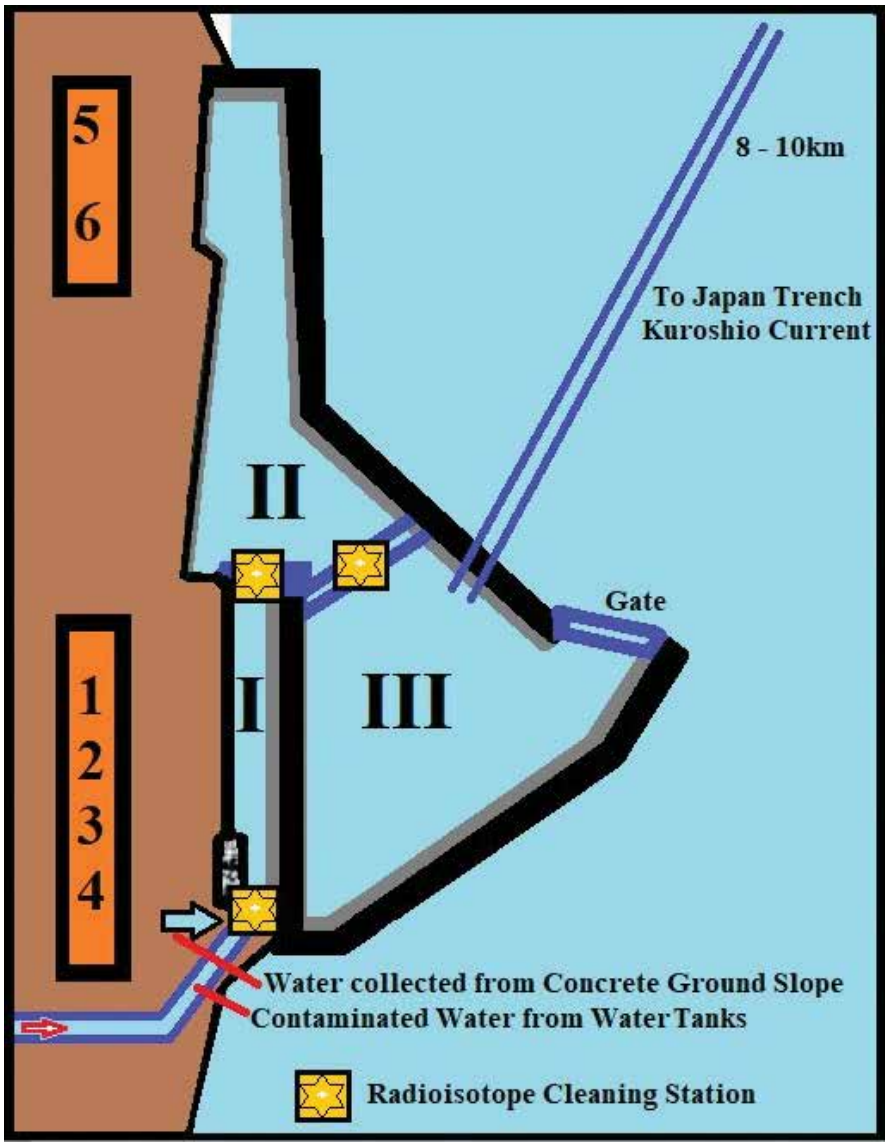

Figure 5. De-contamination of water and release to the sea, schematic top view.

Navier–Stokes Computational Fluid Dynamics CFD model [19] allowed a more accurate simulation of the fluid–structure interaction. The high efficiency of the TFB to reflect the tsunami impulse waves and the storm-wave reflection of the surge stopper (parapet) is confirmed. Furthermore, the loading onto the vertical walls has been estimated [17].

The TFB concept could find wide application as it protects coastal cities and industries, but also beaches against tsunami and against flooding from tropical storms like hurricanes and typhoons. Also, flora and fauna could be saved in case of an oil-spill. In the past 20 years, these natural

catastrophes have caused a quarter of a million fatalities and damages exceeding 500 billion US dollars mainly in Japan, Indonesia, Malaysia, Philippines, Sri Lanka, India and at the east coast of USA. In Japan, the TFB would have prevented in 2011 the 19,000 tsunami fatalities and 300 billion US dollars damages with destroyed houses and, of course, it would have prevented the Fukushima catastrophe. For the countries with risk of storm and tsunami flooding, such a large project would stimulate the building, transport and steel industries and would occupy thousands of workers and thus would have a significant impact on the economic development.

Now Japan started a large project to build tall concrete walls, with height up to 14 m and width up to 46 m, along the coast of Honshu. The estimated costs are higher than building the TFB walls submerged in the sea at large distances from the coast, thereby not disturbing the view of the ocean for coastal citizens and for tourists. Fishermen would keep access to the sea. The population has formed a large resistance against the Japanese great wall of which only partial protection can be expected in case of a large tsunami which on March 11, 2011, had a reported maximum height of 38 m. The 500 km great wall along Honshu coast would consume 23 million m^2 land area plus land surface for the required construction and service roads.

The water from the three basins (shown in **Figure 5**) is pumped out before their bottom is covered with a thick concrete layer. Contaminated water from reactor cooling, from the collecting point of the sloped concrete ground and from the storage tanks flows into basin I. After passing through the first decontamination stage, it enters basin II and then through the next decontamination step to basin III. After checking the low residual radioactivity from cesium-134, cesium-137 and Sr-90, the remaining radioactivity will be from tritium. This has a short half-life time of 12.3 years and anyhow occurs naturally in seawater, formed by cosmic rays, in extremely low concentrations of hydrogen(10^{-18}). Therefore, there is no risk if this tritium-containing water of basin III is transported through long pipes into the Kuroshio current near the Japan trench which has a depth of 10 km. The short half-life time and the dilution effect will prevent the detection of tritium supply from Fukushima.

In view of the large quantity of contaminated water in the 1000 m^3 tanks, a pre-decontamination step could be to introduce by stirring an isotope-adsorbing agent (e.g. zeolite) into the tank and letting it settle by gravity for sufficient time so that the deposit mud on the tank bottom can be sucked by slowly sweeping long tubes and then compacted by a drying process. An alternative could be salting-out and precipitate cesium-137 compounds. This would reduce the contamination level of the collected water and facilitate the final treatment.

4.3. Storage of radioactive waste

The storage of radioactive waste consisting of used fuel rods, of cut pieces of the reactor chambers, of rubble from the reactor foundation and building and from contaminated soil collected from the reactor surrounding is a technological challenge but mainly a political problem. Therefore, a site near the reactor ruins could find minimum resistance from the public. Large amounts of concentrated radioactive waste were collected and transported to the temporary storage facility.

After solving the water problem, the three sea basins with the thick concrete bottom are pumped empty and used as a dump for radioactive waste with the final goal of reclaiming

new land. The rubble caused by the reactor explosions, the drums with sludge from the decontamination process, all the plastic bags with collected contaminated soil and all contaminated material presently stored in Interim Storage Facilities will be transported to this dump. Finally, the debris from scrapping the destroyed reactors 1–4 could be deposited in these basins. The concrete debris could partially be milled and used for new concrete buildings.

The schematic cross-section view (**Figure 6**) of this "Fukushima dump" shows the original reactor before dismantling as well as the dump in the basin which is protected against flooding with the Tsunami-Flooding-Barrier. In view of keeping radiation and the elevated temperature, the molten fuel rods, after sufficient cooling in 30–80 years, should be enclosed in tubes of a metal which is relatively stable against oxidation at ambient oxygen pressure and temperature and limited humidity. Theoretically, the best materials for encapsulation would be the noble metals silver, gold and platinum but their high value would make them too attractive and thus cause a risk for the storage site for radioactive waste. **Figure 7** shows the temperature dependence of the thermodynamic stability of oxides of metals which could be applied as container for radioactive material. This Ellingham-type diagram [20], extended for CO–CO_2 and for H_2–H_2O gas ratios by Richardson and Jeffes [21], is discussed in [22]. Practical values for temperature can be obtained by a straight line passing from one of the three points (O, H, C) on the left margin to the oxygen partial pressure or the gas ratios on the scales on the right side of the diagram and hitting the stability line of the specific metal. Iron-nickel-chromium alloys (stainless steel) and lead could be considered, and copper is foreseen for enclosing radioactive material in Sweden.

Depending on the shape of molten fuel rods within their surrounding they could be cut to pieces and enclosed in capsules or in thin tubes of one of the suitable metals and then sealed. In any case, the fuel-rod-material should be safely stored in a site from which it can be recovered by future generations to use the significant energy remaining in the fuel rods.

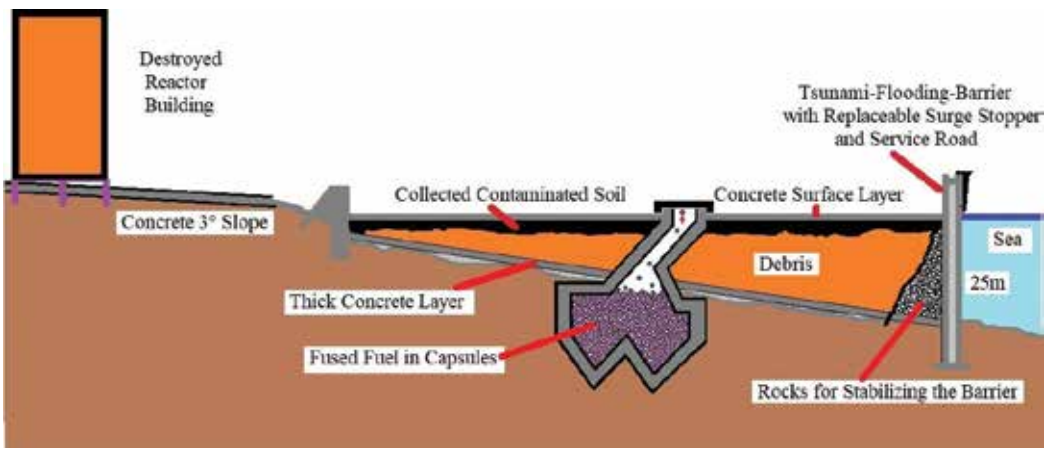

Figure 6. Storage of the rubble of the dismantled reactor building and of the collected contaminated soil in basin I which before had been emptied and covered with a thick concrete layer. After sufficient cooling the fused fuel is encapsulated and inserted into the cavity. Finally, with concrete cover on top new land is generated. The Tsunami-Flooding-Barrier protects against future tsunami and against flooding from typhoon. (Schematic cross section).

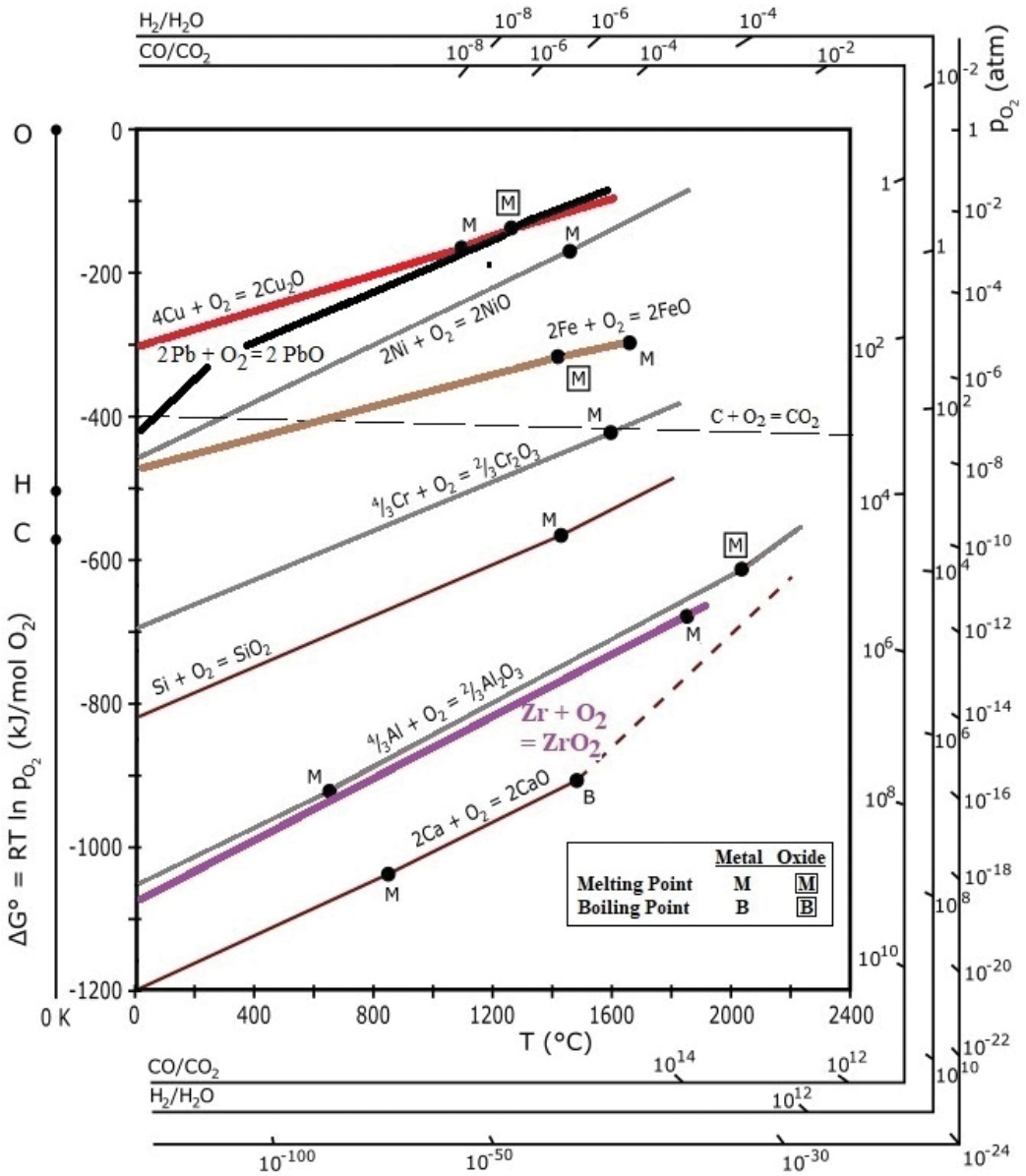

Figure 7. Standard free energy of formation of metal oxides as a function of temperature.

These tubes and capsules are then introduced through an opening shown in **Figure 6** into a barium-concrete chamber prepared below the bottom of the dump. Leakage to the ocean will be excluded when the material with highest radioactivity is stored in basin I and basins II and III also have been emptied, provided with a thick concrete layer, and used as dry dump for less-contaminated waste.

The original sea walls with seaside slopes will be complemented with Tsunami-Flooding-Barriers [11, 16] with the vertical wall on the seaside so that future tsunami and typhoons cannot harm the deposit development. Protection against heavy rain by a cover and against storm waves by a large floating fence in front of the TFB barriers [23] will prevent disturbance of the dump activities. With proper planning the sequence and the locality of the radioactive waste, the final radioactivity on top of the dump will not be higher than the natural value in Japan.

With this procedure the total costs for dismantling the reactors, for decontamination, for interim storage and for final storage of about 100 billion US dollars can be significantly reduced.

5. Conclusions and outlook

The Fukushima accident (and also the former Three-Mile-Island and Chernobyl catastrophes) has demonstrated that no engineer and manager with wide experiences and deciding power have been on site. In the case of Fukushima, urgent actions for very intense water spraying the fire and the cloud, for suction of the cloud, for manually opening the valve of the passive cooling system and for covering the ground with a thick concrete layer with slope of 2–3° depended on decisions of the owner's headquarters in Tokyo. This was concentrated on the internal problems of the reactors, on political and publicity pressure and anyhow was under enormous stress and was not aware of the consequences for the local population and of the following national and international consequences. The experiences from the Three-Mile-Island accident and the recommendations have been summarized in Ref. [24].

Competent reactor engineers should be educated who learn, besides nuclear technology, about all possible chemical reactions, corrosion and electro-corrosion, properties of the involved materials, failure of materials and components, aero-and hydrodynamics, meteorology, and so on.-.

Another question is about the possibility for emergency interruption of nuclear fission by cadmium-indium alloys inside thin silver tubes and boron carbide/boron nitride/boron oxide composite tubes, whether such tubes can be inserted into Type-II generators until the safe generation III/III+ and IV reactors with a four-fold redundancy of emergency equipment will be developed.

It has become clear that the Fukushima accident could have been prevented if in the planning stage the worst-case scenario would have been considered by the plant owner and by the responsible ministry. Even after the accident caused by the unexpected tsunami, the collateral damages could have been mitigated if a competent foresighted management had timely initiated the described procedures. An international emergency team of top engineers with multidisciplinary and industry experience could assist worldwide in case of heavy nuclear, chemical, fire and other catastrophes.

Anyhow, with the development of the safe generation III and IV reactors the nuclear energy will become more dominating and increasingly replace the fossil energy in view of limited resources, of the CO_2 climate problem and of overall safety concerns. The new high-temperature reactors and fast breeders will have a significantly higher efficiency, consume less fuel and produce less radioactive waste. The renewable wind and solar energy is faced with the electricity storage problem, so that nuclear energy is more and more needed as reliable band energy. Frequently, the storage of radioactive waste is regarded as a problem with concern of the population regarding the site for a deep geological deposit. Recently the concept of a safe deposit the waste in a lonely mountain site has been developed which will be economic and faces less political resistance [25].

The common features of the three nuclear accidents (Three-Mile-Island 1979, Chernobyl 1986 and Fukushima 2011) are the combination of personnel error and mistakes, deficiencies in reactor and safety component design, and component failures. Charles Perrow has formulated the "Normal Accident Theory" that in processes of huge complexity, accidents are due to "unanticipated interaction of multiple failures in a complex system" [26–28]. Thus, for nuclear reactors with their enormous complexity all possible failure combinations should be analyzed and precautions with sufficient redundancy found before the plant is switched on. Of great importance is also multidisciplinary high-level education of reactor engineers and reactor managers and adequate training of operators to reduce accidents and their consequences.

It is hoped that the described experiences will assist in planning future reactors and in reducing collateral damage in case of a future accident which, however, hopefully will not occur.

Acknowledgements

The author is thankful to friends in universities and industries for arranging many visits to fascinating Japan and for support of his research. He was shocked by the 2011 earthquake and tsunami and their aftereffects which stimulated him for the present study.

Author details

Hans J. Scheel

Address all correspondence to: hans.scheel@bluewin.ch

General Protection Engineering GmbH, Goldswil b. Interlaken, Switzerland

References

[1] Schirane L, Pellitteri F. Energy policies and sustainable management of energy sources. Sustainability. 2017;**9**:2321-2324. DOI: 10, 3390/su9122321

[2] Schaffers K et al. Advanced material development for inertial fusion energy(IFE). In: Capper P, Rudolph P, editors. Crystal Growth Technology, Semiconductors and Dielectrics. Weinheim: Wiley-VCH; 2010. pp. 229-248. ISBN: 978-3-527-32593-1.ch13

[3] Burgherr P, Hirschberg S. Comparative risk assessment of severe accidents in the energy sector. Energy Policy. 2014;**74**:545-556. http://dx.doi.org/10.1016/j.enpol.2014.01.035

[4] Hirschberg S et al. Neue erneuerbare Energien und neue Nuklearanlagen: Potenziale und Kosten. PSI Bericht. Vol. 05-04. 2005. Available from: http://gabe.web.psi.ch/projects/bfe/index.html. ISSN 1019-0643

[5] https://wikipedia.org/wiki/Fukushima_Daiichi_nuclear-disaster [Accessed: Feb 9, 2018]

[6] https://en.wikipedia.org/wiki/Nuclear_and_Industrial_Safety_Agency [Accessed: Feb 22, 2018]

[7] Bryant E. Tsunami, the Underrated Hazard. 2nd ed. Chichester: Springer; 2008. p. 330. ISBN 978-3-540-74273-9

[8] Takahashi S. Design of vertical breakwaters, short course of hydraulic response and vertical walls. In: Proceedings 28th International Conference on Coastal Engineering Cardiff. Wales, UK; July 7, 2002

[9] Takahashi S, Shimosaki K, Kimura K, Suzuki A. Typical failures of composite breakwaters in Japan. In: Proceedings 27th International Conference on Coastal Engineering. ASCE. 2000. pp. 1885-1898

[10] Arikawa T, Sato M, Shimosako K, Hasegawa I, Yeom G-S, Tomita T. Failure mechanism of Kamaishi breakwaters due to the great East Japan Earthquake Tsunami. In: Coastal Engineering Proceedings; 2012

[11] Scheel HJ. Novel tsunami barriers and their applications for hydroelectric energy storage, fish farming, and for land reclamation. Science of Tsunami Hazards, Journal of Tsunami Society International. 2014;**33**(3):170-192

[12] http://www.nuklearforum.ch/de/aktuell/e-bulletin/fukushima-fünf-jahre-nach-dem-unfall-statusbericht [Accessed: Mar 31, 2016]

[13] Bachellerie E, Arnoud F, Auglaire M, de Boeck B, Braillard O, Eckardt B, Ferroni F, Moffett R. Generic approach for designing and implementing a passive autocatalytic recombiner PAR-system in nuclear power plant containments. Nuclear Engineering and Design. 2003;**221**(1-3):151-165. DOI: 10.1016/S0029-5493(02)00330-8

[14] Klauck M, Reinicke E-A, Kelm S, Meynet N, Bentaib A, Allelein H-J. Passive auto-catalytic recombiners operation in the presence of hydrogen and carbon monoxide: Experimental study and model development. Nuclear Engineering and Design. 2014;**266**:137-147. DOI: 10.1016/j.nucengdes.2013.10.021

[15] https://en.wikipedia.org/wiki/Fukushima_disaster-cleanup [Accessed: Aug 31, 2016]

[16] Scheel HJ. Protection against Storm Surges and Tsunami by Novel Submerged and Vertical Reflecting Barrier. 2018. Available from: www.general-protection-engineering.ch (Project 3 & 4. Brochure)

[17] Elsafti H, Oumeraci H, Scheel HJ. Hydrodynamic efficiency and loading of a tsunami-flooding barrier (TFB). In: Coastal Engineering Proceedings. Vol. 35. 2016. pp. 1-12. DOI: https://doi.org/10.9753/ice.v35.structures.23

[18] Lynett PJ, Liu PL-F, Sitanggang KI, Kim DH. Modeling wave generation, evolution, and interaction with depth-integrated dispersive wave equations COULWAVE code manual. Cornell University Long and Intermediate Wave Modeling Package. 2008. p. 90

[19] Elsafti H. Modelling and analysis wave-structure-foundation interaction for monolithic breakwaters [PhD thesis]. Leichtweiss-Institute for Hydraulic Engineering and Water Resources, Germany: TU Braunschweig; 2015. Available form: http://www.digibib.tu-bs.de/?docid=00060996

[20] Ellingham HJT. Transactions and Communications. London: Journal of the Society of Chemical Industry. 1944;**63**:125-133. DOI: 10.1002/jctb.5000630501

[21] Richardson FD, Jeffes JHE. The thermodynamics of substances of interest in iron and steel making from 0°C to 2400°C. The Journal of the Iron and Steel Institute. 1948;**160**:261-273

[22] Darken LS, Gurry RW. Physical Chemistry of Metals. Tokyo: McGraw-Hill; 1953. p. 535. Library of Congress Catalog Number 52-8315

[23] Scheel HJ. Tidal energy and large-scale fish farming, benefits of novel tsunami and flooding barriers. International Journal of Environmental Science and Development. 2014;**5**(5):484-490. DOI: 10.7763/IJESD.2014.V5.532

[24] United States Nuclear Regulatory Commission NRC. Backgrounder on the Three Mile Island Accident. February 2013. Available form: https://www.nrc.gov/reading-m/doc-collections/fact-sheets/3mile-isle.html [Accessed: March 6, 2018]

[25] Scheel HJ. Realisierbare Endlager für radioaktive Abfälle. 2018. Available form: Project 2 in www.general-protection-engineering.ch

[26] Perrow C. The President's commission and the normal accident. In: Sils D, Wolf C, Shelanski V, editors. Accident at Three Mile Island: The Human Dimensions. Boulder: Westview. pp. 173-184

[27] Perrow C. Normal Accidents: Living with High-Risk Technologies. New York: Basic Books; 1984

[28] Whitney DE. Normal Accidents by Charles Perrow. Cambridge, Massachusetts, USA: Massachusetts Institute of Technology; 2003. Available from: http://esd.mit.edu/WPS/wplit-2003-01.pdf

Edited by Florin-Constantin Mihai and Adrian Grozavu

Environmental risks are a multi- and interdisciplinary topic with a great interest in current society. This book examines the issues of natural hazards (e.g., typhoons, landslides, wildfires), anthropogenic activities (construction of artificial dams, the operation of nuclear power plants), and their potential risks to the environment and/or quality of life at various scales, from local to regional and even at a global level. The book intends to discuss concepts, methods, and techniques to address environmental risks and vulnerabilities, revealing the complex interactions between nature and human communities and activities. Policies and practices for disaster risk management should be based on the best state-of-the-art methods and techniques, integration between natural and/or social approaches, interdisciplinary research, and multilevel cooperation.

Published in London, UK

IntechOpen

ISBN 978-1-78984-223-4